THE UNIVERSITY *of* EDINBURGH

Investigating type I interferon signalling regulation in the context of human Mendelian autoinflammatory disease

Gaofeng Zhu

THE UNIVERSITY *of* EDINBURGH

Thesis submitted for the degree of

Doctor of Philosophy

The University of Edinburgh

2024

Table of contents

Contents

Declaration

I declare that this thesis is an original report of my research, has been written by me and has not been submitted for any previous degree. The experimental work is almost entirely my own work. Due references have been provided on all supporting literature and resources. The collaborative contributions are acknowledged in the following:

1. Whole-genome sequencing for patient AGS2258 was performed by the Commissariat à l'énergie atomique et aux énergies alternatives (CEA), as part of a collaboration between CEA-IBFJ/CNRGH, Institut Imagine, INSERM and Université Paris Descartes. In-house exome sequencing was undertaken at the Institut Imagine (Paris, France). Targeted Sanger sequencing to identify *PTPN1* variants in patients and their parents was performed jointly by Luis Seabra and myself.

2. Panel qPCR and NanoString interferon-stimulated gene expression data for all the patients reported in this study were derived by Dr. Gillian I. Rice (Division of Evolution, Infection and Genomics, The University of Manchester, Manchester, UK). Data were plotted using GraphPad Prism10 by myself.

3. Protein structure modelling in Fig. 7c and Fig. 13 was performed by Dr. Mihaly Badonyi (MRC Human Genetics Unit, The University of Edinburgh, Edinburgh, UK).

4. Immunoblotting and qPCR analyses on primary dermal fibroblasts in Fig. 19a and Fig. 19b were performed jointly by Blaise Didry-Barca, Moncef Touimy (both of whom are affiliated with Institut Imagine, Paris, France), and myself.

5. Graphs for *PTPN1* capture RNA sequencing with RNA derived from primary fibroblasts and whole-blood in Fig. 19b-d were kindly provided by Dr. Alice Lepelley (Institut Imagine, Paris, France).

6. Neuro-radiological imaging was performed by the physicians responsible for the patients.

7. Chapter 2 is based on my first-author publication titled ‘‘Type I Interferonopathy due to a Homozygous Loss-of-Inhibitory Function Mutation in STAT2’’ published in *Journal of Clinical Immunology* (PMID: 36753016), with minimal modifications including numbering of figures, style of references, and an extended Summary and discussion section

List of figures

List of tables

Abbreviations

A

ADAR1: adenosine deaminase acting on RNA

AGS: Aicardi-Goutières syndrome

AIRE: autoimmune regulator

B

BAF: barrier-to-autointegration factor

BCAR1: breast cancer anti-oestrogen resistance protein 1

BCG: Bacillus Calmette-Guérin

BCL6: B cell lymphoma transcription factor 6

BCR: B cell receptor

BDNF: brain-derived neurotrophic factor

BMDM: bone-marrow-derived macrophage

C

CARD: caspase activation and recruitment domain

CCD: coiled-coil domain

cGAMP: cyclic guanosine monophosphate-adenosine monophosphate

cGAS: cyclic guanosine monophosphate-adenosine monophosphate synthase

cGMP: 2',3'-cyclic guanosine monophosphate

CNS: central nervous system

COPA: coatomer protein subunit alpha

COPI: coatomer protein complex I

COVID-19: coronavirus disease 2019

CRL5: cullin-RING ubiquitin ligase 5

CSF: cerebrospinal fluid

CTLA4: cytotoxic T-lymphocyte associated protein 4

CVID: common variable immunodeficiency

CXCL10: C-X-C motif chemokine ligand 10

D

DC: dendritic cell

DDX41: DEAD-box helicase 41

diABZI: di-amidobenzimidazole

DM: diabetes mellitus

dsDNA: double stranded DNA

dsRNA: double stranded RNA

E

EGFR: epidermal growth factor receptor

eIF2α: eukaryotic initiation factor 2α

EMT: epithelial–mesenchymal transition

ER: endoplasmic reticulum

ERGIC: endoplasmic-reticulum–Golgi intermediate compartment

ERK: extracellular signal-regulated kinase

F

FOXP3: forkhead box P3

G

GAS: gamma-activated sequence

GOF: gain-of-function

GSEA: gene set enrichment analysis

GWAS: genome-wide association study

H

HEK: human embryonic kidney

HL: Hodgkin lymphoma

HLH: haemophagocytic lymphohistiocytosis

HSE: herpes simplex encephalitis

HSV-1: herpes simplex virus 1

I

IAV: influenza virus A

IFI16: interferon-gamma inducible factor 16

IFIH1: interferon induced with helicase C domain 1

IFN: interferon

IFNAR: interferon alpha and beta receptor subunit

IgG: immunoglobulin G

IKK: IκB kinase

IL: interleukin

ILD: interstitial lung disease

iPSC: induced pluripotent stem cell

IR: insulin receptor

IRAK: interleukin-1 receptor associated kinase

IRF: interferon regulatory factor

IRF-E: interferon regulatory factor-element

IRS: insulin receptor substrate

ISG: interferon-stimulated gene

ISGF3: interferon-stimulated gene factor 3

ISRE: interferon-stimulated response element

IκB: inhibitor of kappa B

J

JAK: Janus kinase

JNK: c-Jun N-terminal kinase

K

KI: knock-in

KO: knock-out

L

LAV: live-attenuated viral vaccine

LEPR: leptin receptor

LGP2: laboratory of genetics and physiology 2

LMO4: LIM domain only 4

LOF: loss-of-function

LPS: lipopolysaccharide

LSM11: U7 snRNA-associated Sm-like protein LSm11

M

MAPK: mitogen-activated protein kinase

MAVS: mitochondrial antiviral signalling

MDA5: melanoma differentiation-associated protein 5

MEF: murine embryonic fibroblast

MERS: Middle East respiratory syndrome

miR: microRNA

MMR: measles, mumps, and rubella

MSMD: Mendelian susceptibility to mycobacterial disease

mTOR: mammalian target of rapamycin

mTORC2: mammalian target of rapamycin complex 2

MX1: MX dynamin like GTPase 1

MyD88: myeloid differentiation primary response 88

N

NDV: Newcastle disease virus

NEMO: nuclear factor kappa B essential modulator

NF-κB: nuclear factor kappa B

NLS: nuclear localisation signal

NMD: nonsense-mediated decay

NO: nitric oxide

O

OAS: 2-5 oligoadenylate synthetase

ODN: oligodeoxynucleotide

OVA: ovalbumin

P

PAMP: pathogen-associated molecular pattern

PBMC: peripheral blood mononuclear cell

pDC: plasmacytoid dendritic cell

PDK-1: 3-phosphoinositide dependent protein kinase 1

PI3K: phosphoinositide 3 kinase

PIP3: phosphatidylinositol-3,4,5-trisphosphate

PKC: protein kinase C

PKR: dsRNA-dependent protein kinase R

PLCγ: phospholipase Cγ1

PMBCL: primary mediastinal B cell lymphoma

Poly I:C: polyinosinic-polycytidylic acid

PRAAS: proteasome-associated autoinflammatory syndrome

PRR: pattern recognition receptor

PTM: post-translational modification

PTP1B: protein tyrosine phosphatase 1B

PTPN1: protein tyrosine phosphatase non-receptor type 1

Q

qPCR: quantitative polymerase chain reaction

R

RA: rheumatoid arthritis

RAG1/2: recombination activating 1/2

Ras: rat sarcoma

RIG-I: retinoic acid-inducible gene I

RLR: RIG-I like receptor

RNS: reactive nitrogen species

RNU7-1: RNA, U7 small nuclear 1

ROS: reactive oxygen species

RPE: retinal pigment epithelial

S

SAMHD1: SAM and HD domain containing deoxynucleoside triphosphate triphosphohydrolase 1

SAVI: STING-associated vasculopathy with onset in infancy

SeV: Sendai virus

SLE: systemic lupus erythematosus

SMS: Singleton-Merten syndrome

SOCS: suppressor of cytokine signalling

Sp1: specificity protein 1

SPF: specific-pathogen free

SPSB3: spIA/ryanodine receptor domain and SOCS box containing 3

ssDNA: single stranded DNA

ssRNA: single stranded RNA

STAT: signal transducer and activator of transcription

STING: stimulator of interferon genes

T

T1I: type I interferonopathy

TAK1: transforming growth factor-β-associated kinase 1

TBK1: TANK-binding kinase 1

TCPTP: T cell protein tyrosine phosphatase

TCR: T cell receptor

TIR: Toll-interleukin-1 receptor

TLR: Toll like receptor

TNF: tumour necrosis factor

TRAF: tumour necrosis factor receptor-associated factor

Treg: regulatory T cell

TREX1: 3’ repair exonuclease

TRIF: Toll-interleukin-1 receptor-domain-containing adaptor-inducing IFN-β

TrkB: tropomyosin receptor kinase B

TYK2: tyrosine kinase 2

U

UNC93B1: uncoordinated 93 homolog B1

USP18: ubiquitin-specific protease 18

V

VACV: vaccinia virus

W

WGS: whole-genome sequencing

WT: wild-type

Lay summary

Viruses are tiny organisms that are everywhere. In order to make more copies of themselves viruses, infect the cells of other organisms, including humans. Being able to fight off viruses is absolutely necessary for our survival; simply put, if a person cannot do so, they will die.

How do our cells realise that they are being infected by a virus? It turns out that the way we do this is by sensing the presence of viral genetic material (referred to as DNA and RNA) as the virus enters the cell. Much as a dog might bark to wake up the owner when a burglar breaks into a house, our cells ‘raise the alarm’ when they sense viral DNA and RNA by producing a very powerful chemical called interferon. Interferon acts as a kind of cellular disinfectant and is very good at killing virus. However, like a disinfectant, too much interferon can be dangerous, so that it is important that interferon is used carefully, and only when needed.

In my thesis, I have studied diseases that result in the body producing too much interferon. These diseases are referred to as ‘type I interferonopathies’. In particular, I have studied diseases where there is a failure of turning off a type I interferon ‘anti-viral’ response. By allowing for a genetic diagnosis to be made, this work is important for the patients and families affected. It might also be important for the future treatment of their problems, and for the treatment of other diseases also associated with ‘too much interferon’.

Abstract

Type I interferons (IFN-Is) are primary antiviral cytokines. Homeostasis of IFN-I signalling is under tight regulation, with too little or too much IFN-I activity resulting in significant pathology. While impaired IFN-I signalling is characterised by immunodeficiency, inappropriate upregulation of IFN-I signalling results in a set of autoinflammatory states termed the type I interferonopathies. In this work, through the study of real-world patients, distinct but related regulatory mechanisms important for homeostatic IFN-I signalling were investigated.

In the first part of the thesis, I studied a patient presenting with features consistent with a type I interferonopathy, who we identified to carry a rare homozygous missense variant p.(A219V) in STAT2. Through in vitro testing, I showed that while STAT2 p.(A219V) maintained the ability to transduce an IFN-I signal, its negative regulatory function was impaired due to defective binding of USP18.

In the second part of this study, I report a novel cohort of patients with a highly stereotyped clinical phenotype comprising normal early development followed by the onset of subacute neuro-regression, with increased IFN-stimulated gene (ISG) expression in whole-blood and raised neopterin levels in cerebrospinal fluid. We found these patients to harbour rare heterozygous variants in *PTPN1* resulting in loss of mRNA and/or protein expression, suggesting that haploinsufficiency of *PTPN1* leads to upregulated IFN-I signalling. Indeed, cells deficient in *PTPN1* demonstrate an upregulation of ISG expression at baseline, and 'hypersensitivity' to stimulation with IFNα2b and the STING agonist diABZI. Underlying mechanisms could involve enhanced STING signalling, as evidenced by an overexpression of *IFNB1* upon diABZI stimulation, and/or enhanced IFN-I signalling, where higher levels of STAT1 phosphorylation upon IFNα2b stimulation result in overproduction of ISGs.

Overall, this thesis describes the study of IFN-I mediated autoinflammation, with a particular focus on IFN signalling downstream of the IFN-I receptor. This work thus contributes new knowledge relevant to the physiological regulation of IFN-I signalling in humans, with potentially important implications for clinical testing and treatment.

Chapter 1: Introduction

The human body encounters numerous pathogens daily, posing a threat to physiological homeostasis. Hence, the immune system has evolved, and continues to develop, molecular, cellular, and structural strategies to limit or prevent pathogen invasion and restrict their growth. Constituting the very first line of defence, the physical and anatomical barriers of the human body, such as skin, mucosa, lung cilia, and bodily fluids, ‘‘passively’’ prevent pathogen entry into the internal environment. However, once there is a breach in these barriers, the innate immune system is engaged – not through the recognition of specific characteristics of a particular pathogen, but, rather, through the identification of features common across different pathogen species. These features, known as pathogen-associated molecular patterns (PAMPs), include conserved nucleic acid, lipid, protein, or polysaccharide ‘‘motifs’’, which typically do not exist in a normal human cell. To sense these PAMPs, human cells employ a series of receptors (pattern recognition receptors, PRRs) that recognise and bind to PAMPs, triggering downstream cellular signalling cascades to combat infection. With the help of adaptor proteins and sometimes second messengers, danger signals detected at the cell surface or within intracellular membrane compartments are propagated through the cytosol. Via the action of transcriptional activators, cells actively reprogram their transcriptional network to express cytokines such as interferons (IFNs) and interleukins (ILs) with inherent anti-pathogen properties. Once secreted, cytokines bind to surface receptors to exert a broad spectrum of functions, including the restriction of pathogen replication, the regulation of cell proliferation and death, and the modification of the innate and adaptive immune state. Essentially, all of these activities are triggered following the recognition of ‘‘non-self’’ biological material, with the detection of foreign nucleic acid playing a particularly important role in the antiviral response.

1.1 Nucleic acid sensing

1.1.1 DNA sensing

cGAS-STING

The appreciation of cGAS-STING (cyclic guanosine monophosphate-adenosine monophosphate (cGAMP) synthase-stimulator of interferon genes) signalling as a major intracellular DNA sensing pathway was initiated by the discovery of STING.[1] In a study to characterise critical molecular determinants facilitating an effective innate antiviral response, the laboratory of Glen N. Barber identified a novel adaptor protein, deficiency of which impaired efficient type I IFN (IFN-I) production against several viruses and a failure to restrict viral growth, not involving the TLR (Toll-like receptor) signalling pathway.[1] Further, overexpression of this protein in HEK 293T cells significantly activated the IFNβ promoter, the IRF3 (IFN regulatory factor 3) responsive promoters, and the NF-κB (nuclear factor kappa B) responsive promoter, indicating that it can activate both IRF3 and NF-κB transcription pathways to confer an antiviral state.[1] This newly discovered protein was termed STING. Immunofluorescence experiments with overexpression of HA-tagged STING in HEK 293T cells demonstrated STING to exhibit a predominant ER (endoplasmic reticulum)-localisation, which was further confirmed by subcellular fractionation experiments.[1]

In a follow-up study, the researchers of the same group used STING-deficient mice, as well as MEFs (murine embryonic fibroblasts), BMDMs (bone-marrow-derived macrophages) and DCs (dendritic cells) from these mice, to demonstrate that STING plays a non-redundant role in mediating an effective innate response against intracellular DNA challenge, such as infection with HSV-1 (herpes simplex virus 1).[2] Evidence regarding STING's role in adaptive immunity was also obtained. Thus, after immunisation with plasmid DNA encoding OVA (ovalbumin), STING KO (knock-out) mice displayed significantly less antigen-specific (in this case OVA) IgG (immunoglobulin G) in the serum, compared to WT (wild-type) mice.[2] Furthermore, the percentage of cytotoxic $CD8^+$ T cells in the spleen of STING KO mice was significantly less than that in the spleen of WT mice, with decreased IFNγ secretion, indicating a less potent adaptive immune reaction following DNA immunisation.[2] On the other hand, STING KO mice displayed similar B and T cell subsets compared to WT animals, and a normal

Ig response to OVA antigen peptide.[2] These data strongly suggested that DNA adjuvant elicited a STING-dependent innate immune response that also influenced adaptive immunity.

STING plays an essential role in mediating DNA-dependent innate signalling, best exemplified by the cellular immune response to DNA viruses. However, STING itself does not recognise DNA species. The missing link between DNA and STING was uncovered by Zhijian J. Chen and colleagues in 2012 in two ground-breaking papers in the field,[3,4] both of which derived from an integrated programme of work. Through elaborate (bio)chemical and structural studies, and with the help of high-resolution, high-accuracy mass spectrometry, these researchers determined cGAMP as a second messenger, which directly binds to and activates STING to initiate IRF3 dimerisation and IFNβ production.[3] Further, Chen and colleagues purified and characterised the enzyme responsible for cGAMP synthesis from human as well as mouse cell lines, and termed it cGAS.[4] They also showed that cGAS works upstream of STING as a DNA sensor, and is absolutely necessary for efficient IFN-I induction in a DNA-dependent, RNA-independent manner.[4] For this remarkable achievement, Zhijian J. Chen was awarded the 2024 Albert Lasker Basic Medical Research Award (https://laskerfoundation.org/winners/cgas-enzyme-that-senses-self-and-foreign-dna/).

To summarise, the presence of spatially and/or temporally aberrant double-stranded DNA (dsDNA) in the cytosol, such as occurs in the context of infection or cellular stress,[5,6] is recognised by cGAS, which leads to cGAS dimerisation and assembly along the DNA strand.[7,8] Activated cGAS catalyses the synthesis of cGAMP from cytosolic ATP and GTP substrates,[3] which in turn diffuses into the cytosol to bind STING in the ER, resulting in significant conformational changes and the oligomerisation of STING.[9-11] STING oligomers dissociate from the ER, interact with trafficking proteins, and incorporate into COPII vesicles.[12] COPII vesicles containing STING pass through the Golgi apparatus where STING recruits TBK1. Through autophosphorylation, TBK1 then becomes activated and phosphorylates STING at Ser366.[13] IRF3 and NF-κB are subsequently recruited by the STING-TBK1 complex for phosphorylation,[13] and activated IRF3 and NF-κB translocate into the nucleus to initiate

the transcription of IFN-I genes and pro-inflammatory cytokines, respectively.[13] Later, STING can either go through the autophagy-lysosome degradation pathway or be sorted into COPI vesicles for retrograde Golgi-ER trafficking,[14-18] thereby effectively turning off the signalling cascade. An illustration of cGAS-STING pathway is presented in Fig. 1. (Fig. 1 was created by Decout et al., *Nature Reviews Immunology*, 2021.[19])

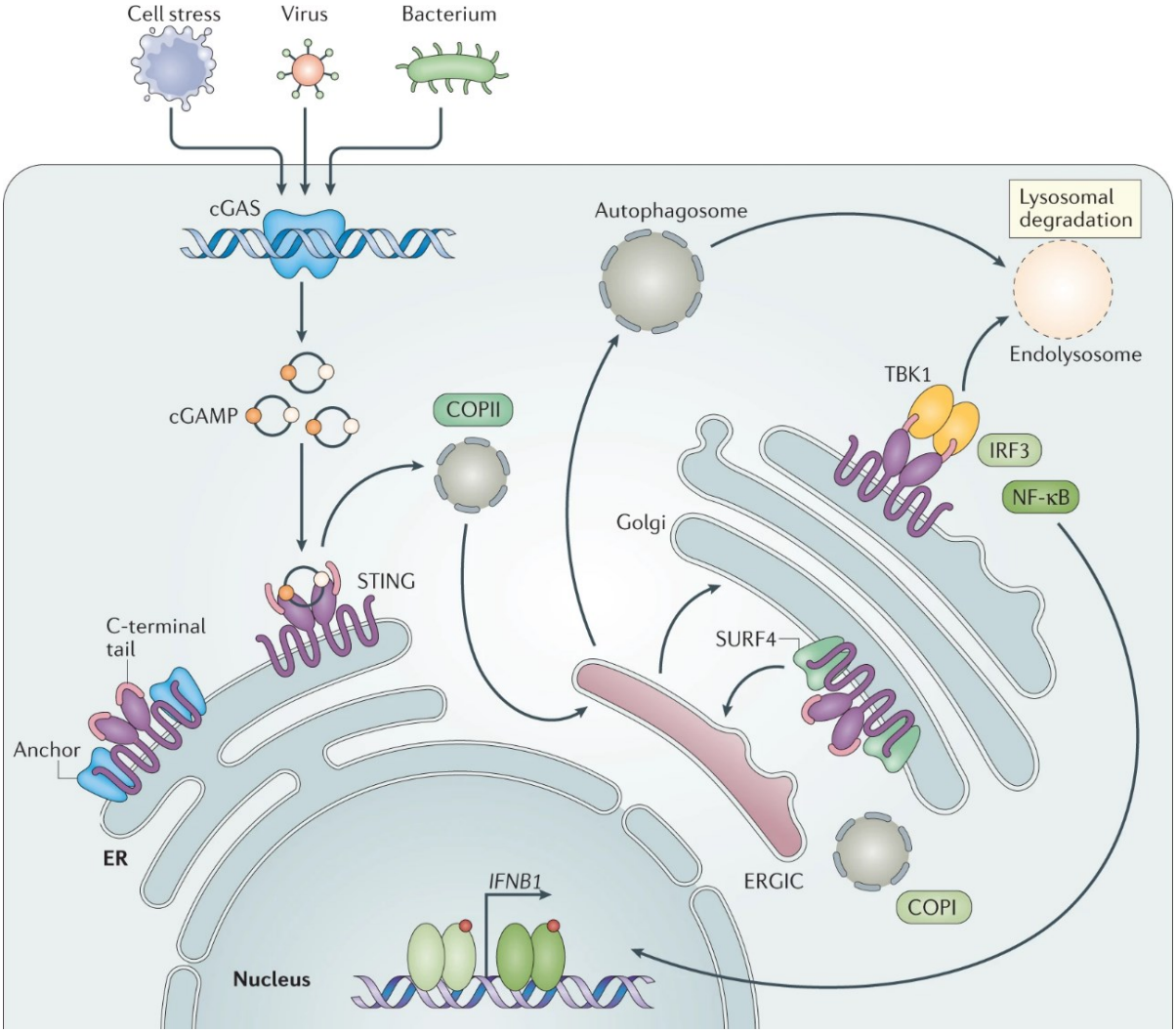

Fig. 1. Illustration of cGAS-STING pathway. Intracellular DNA sensor cGAS can recognise spatially/temporally abnormal dsDNA generated through cell stress or infection, leading to the production of the second messenger cGAMP. cGAMP binds to the ER-localised adaptor protein STING, which then undergoes conformational changes and dimerisation/oligomerisation. Activated STING is incorporated into COPII vesicles and trafficked to the ERGIC and the Golgi compartment, where it recruits TBK1. TBK1 in turn phosphorylates STING and further recruits and activates IRF3 and NF-κB, both of which translocate into the nucleus to initiate the transcription of IFN-I genes (such as *IFNB1*) and pro-inflammatory cytokines (not shown here). After signalling, STING is either sorted into autophagosome-endolysosome for degradation, or is incorporated into COPI vesicles for Golgi-ER retrograde trafficking. cGAS, cyclic guanosine monophosphate-adenosine monophosphate synthase. cGAMP, cyclic guanosine monophosphate-adenosine monophosphate. STING, stimulator of interferon genes. ER, endoplasmic reticulum. COP, coat protein complex. ERGIC, endoplasmic-reticulum–Golgi intermediate compartment. TBK1, TANK-binding kinase 1. IRF3, interferon regulatory factor 3. NF-κB, nuclear factor kappa B. SURF4, surfeit 4.

In general terms, cellular antiviral innate sensing should be as sensitive as possible to ensure the effective detection of pathogens, whilst avoiding inappropriate activation due to mis-identification of ‘‘self’’ as ‘‘non-self’’. For most PRRs, this does not pose a risk in that the PAMPs they recognise do not usually exist in a normal (human) cell (e.g. TLR4 recognising LPS (lipopolysaccharide), and TLR5 recognising bacterial flagellin). However, this is not the case for cGAS, whose recognition of dsDNA does not require a particular sequence motif; rather, detailed molecular and structural biology work has demonstrated that cGAS signalling can only be initiated in the presence of longer stretches of dsDNA.[8] In this scenario, cGAS rearranges itself into phase-separated ladder-like structures along the dsDNA strand,[7] with a length-dependent threshold critical to the triggering of cGAS activity.

Initially, cGAS was determined to largely localise in the cytosol.[4] However, a comprehensive immunofluorescence microscopy study by Daniel B. Stetson and colleagues, using numerous commercially available antibodies against human and mouse cGAS, showed that cGAS resides predominantly in the nucleus, tightly tethered to chromatin.[20] More direct evidence of this observation was obtained shortly after from structural biology studies using cryo-electron microscopy.[21-26] The presence of cGAS in the nucleus poses another risk of mis-activation through contact with nuclear genomic DNA. Recent years have seen an expansion of studies relating to the regulation of nuclear cGAS activity. It is now established that nuclear cGAS has a much higher affinity for nucleosomes compared to naked DNA, specifically binding to the H2A-H2B acidic patch region, thereby preventing the oligomerisation and activation of cGAS.[21-26] Possibly in line with this notion, a disturbance of linker histone stoichiometry due to mutations in *LSM11* (U7 snRNA-associated Sm-like protein LSm11) and *RNU7-1* (RNA, U7 small nuclear 1) possibly underlies an abnormal distribution of cGAS on chromatin and its subsequent activation in patients with Aicardi–Goutières syndrome (AGS), leading to upregulation of IFN-I signalling.[27] Further, work performed by the laboratory of Andrea Ablasser showed that transient DNA-cGAS contact due to acute nuclear rupture or enhanced cGAS nuclear localisation is prevented by BAF (barrier-to-autointegration factor) through

competitive binding,[28] a mechanism distinct from the physical separation of cGAS and nuclear DNA through inhibition by nucleosomes. A more recent study from the same group demonstrated that cGAS harbours a C-terminus Asn-Asn minimal degron motif, which recruits SPSB3 (splA/ryanodine receptor domain and SOCS box containing 3) for ubiquitination and proteasomal degradation in the presence of CRL5 (cullin–RING ubiquitin ligase 5), thus providing another safeguarding mechanism to prevent cGAS activation in cycling cells.[29] On a similar note, cGAS has been shown, during mitosis, to be hyperphosphorylated at the N terminus by mitotic kinases such as Aurora kinase B, which inhibits nuclear DNA sensing. Additionally, cGAS is tethered to the chromatin during cell division, and is prevented from oligomerisation and activation.[30]

TLR9, DDX41 and IFI16

Another well-studied intracellular DNA sensor is TLR9 (a member of the TLR family), identified in 2000 by Shizuo Akira and colleagues.[31] Endosomal TLR9 senses unmethylated CpG dinucleotides typically present in bacteria and certain viruses,[31,32] as well as synthetic CpG oligodeoxynucleotides.[33] Newly synthesised TLR9 is chaperoned by UNC93B1 (Unc-93 homolog B1) for ER-endosome trafficking through the classical secretory pathway.[34,35] TLR9 and DNA have a binding ratio of 2:2, and dimerised TLR9-CpG-DNA promotes intracellular signalling via MyD88 (myeloid differentiation primary response 88).[36] Binding of TLR9 to MyD88 activates IRAK4 (interleukin-1 receptor-associated kinase 4), which in turn transmits the signal to IRAK1. IRAK1 recruits TRAF6 (tumour necrosis factor receptor-associated factor 6), with the latter further activating TAK1 (transforming growth factor-β-associated kinase 1). TAK1 phosphorylates IKK (IκB kinase) and IRF7 to promote NF-κB signalling and to activate the transcription of IFN-I genes, respectively.[36] Additionally, TLR9 signalling can activate the MAPK (mitogen-activated protein kinase) pathway, which cooperates with NF-κB signalling for efficient transcription of pro-inflammatory cytokines. A summary of TLR9 signalling is given in Fig. 2, created by Dongye et al.[36]

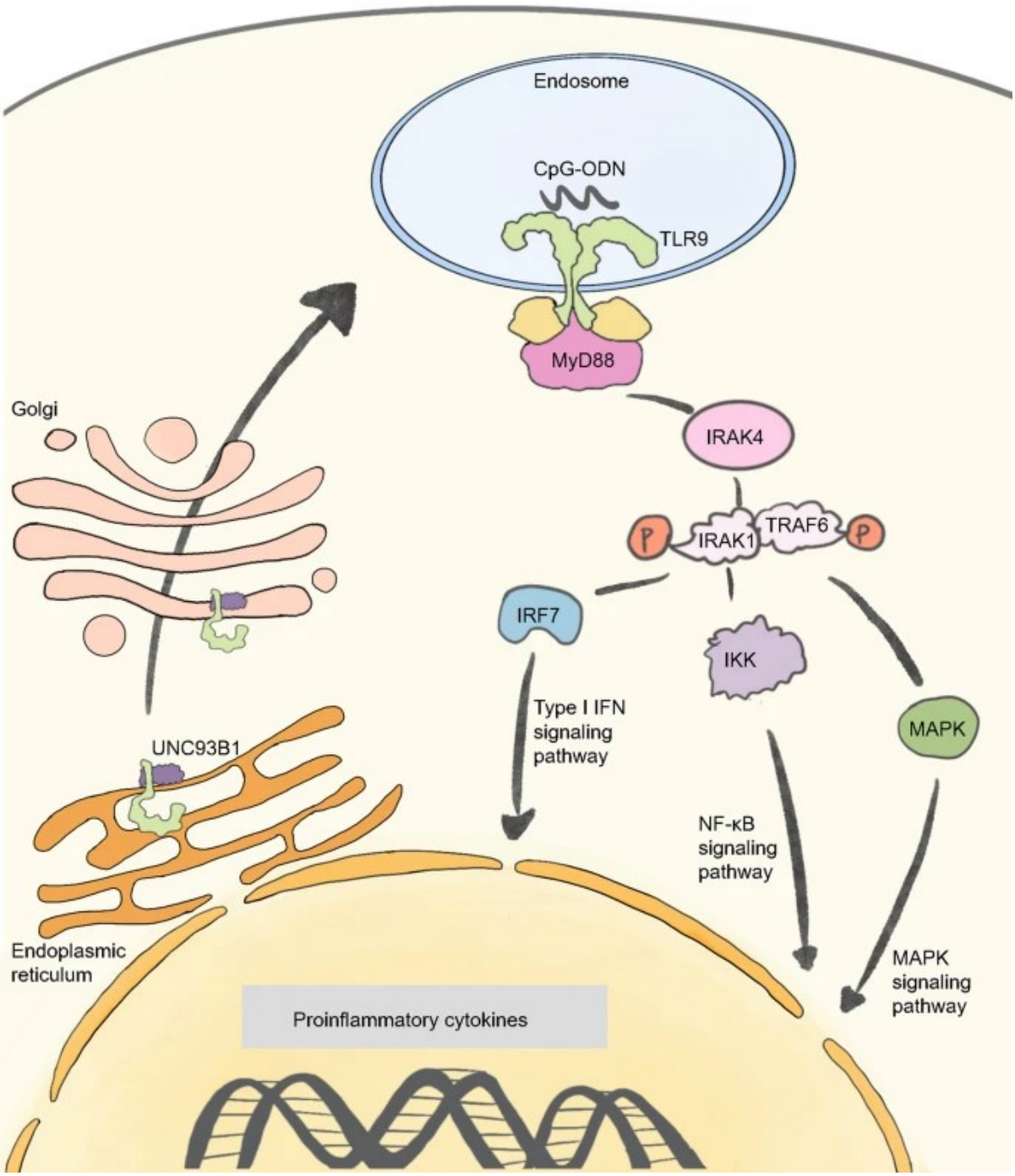

Fig. 2. TLR9 signalling pathway. TLR9 is chaperoned by UNC93B1 to re-localise from the ER, via the Golgi apparatus, to the endosome, where it recognises endocytosed DNA with CpG motifs. MyD88 is then recruited by the TLR9-DNA complex and further activates IRAK4. IRAK4 interacts with IRAK1 and the latter recruits TRAF6, which in turn activates TAK1 kinase (not shown). TAK1 phosphorylates IRF7 and IKK to promote IFN-I and pro-inflammatory cytokine expression. The MAPK pathway is also activated by TLR9 signalling and contributes to an optimal transcriptional response. UNC93B1, Unc-93 homolog B1. CpG, cytosine-phosphate-guanine. ODN, oligodinucleotide. TLR9, Toll-like receptor 9. MyD88, myeloid differentiation primary response 88. IRAK, interleukin-1 receptor-associated kinase. TRAF6, tumour necrosis factor receptor-associated factor 6. IRF7, interferon regulatory factor 7. IKK, IκB kinase. NF-κB, nuclear factor kappa B. MAPK, mitogen-activated protein kinase.

Other less well-characterised DNA sensors have also been shown to play a role in IFN-I

induction upon DNA challenge. For example, in DCs, DDX41 (DEAD-box helicase 41) deficiency impaired IFN-I expression following DNA virus infection, while overexpression potentiated the IFN-I response.[37] Moreover, DDX41 binds DNA and STING in the cytosol, suggesting that DDX41 is another DNA sensor dependent on STING, besides cGAS.[37] A further study hinted that DDX41 is essential for the full activation of cGAS-STING signalling.[38] DDX41 exhibits both DNA unwinding capacity and DNA annealing activity. A particular separation-of-function mutation p.(R525H) of DDX41, that specifically affects the unwinding capacity while maintaining a normal annealing activity, was identified in patients with myelodysplastic syndromes and acute myeloid leukemia.[38] This mutant leads to an unbalanced distribution of dsDNA over single-stranded DNA (ssDNA) following DNA binding, which favours cGAS activation. Cells harbouring DDX41 p.(R525H) produce higher amounts of IFN-I in response to DNA stimulation.[38] Along the same lines, in monocytes, IFI16 (interferon-gamma inducible factor 16) deficiency inhibits the activation of IRF3 and NF-κB, and the expression of IFNβ, after DNA, but not RNA, viral infection.[39] It was shown that IFI16 directly binds to transfected dsDNA and recruits STING.[39] Further, IFI16 deletion in macrophages was demonstrated to decrease cGAMP production upon DNA stimulation, while IFI16 overexpression enhanced cGAS activity.[40,41] Additionally, IFI16 facilitates STING dimerisation and phosphorylation, as well as recruiting TBK1 to STING for downstream signalling.[40,41]

1.1.2 RNA sensing

RIG-I/MDA5-MAVS

In 2004, MDA5 (melanoma differentiation-associated protein 5, encoded by *IFIH1*, interferon induced with helicase C domain 1) was discovered as an IFN-I inducible factor promoting apoptosis.[42] Shortly thereafter, overexpression of MDA5 was shown by Richard E. Randall's group to upregulate IFNβ promoter activity in response to intracellular dsRNA stimulation.[43] In the same year, through studies combining functional screens and characterisation assays, RIG-I (retinoic acid-inducible gene I) was identified as a novel sensor for cytosolic viral RNA

by Takashi Fujita et al..[44] Comparative structural and functional research has demonstrated that RIG-I and MDA5 share two CARD (caspase activation and recruitment domain) domains and an RNA helicase domain,[45] with the CARD domains mediating downstream signalling. RIG-I and MDA5, (together with LGP2 (laboratory of genetics and physiology 2)),[46] are members of the RLR (RIG-I-like receptor) family. RIG-I preferentially binds to short dsRNA with 5'-triphosphate groups, while MDA5 favours longer dsRNA[47] – as demonstrated by the selective activation by transfected short and long synthetic agonist poly I:C (polyinosinic-polycytidylic acid), respectively.[48]

MAVS (mitochondrial antiviral signalling protein, also called VISA, IPS-1, CARDIF) was discovered in 2005 by several groups as the adaptor protein for RIG-I and MDA5 mediated innate sensing.[49-52] As the name suggests, MAVS is predominantly localised on the outer membrane of mitochondria through its C-terminal transmembrane domain, and is essential to the cellular antiviral response against RNA viruses.[49] Some studies also showed that MAVS can be found in peroxisomes and mitochondria-associated ER membranes in different viral and cellular contexts.[53,54]

After activation by (viral) dsRNA, RIG-I/MDA5 induces the polymerisation and activation of MAVS on the mitochondria, which in turn recruits E3 ligase TRAF proteins (TRAF2/5/6).[55] TRAFs initiate the synthesis of polyubiquitin chains that can be recognised by NEMO (NF-κB essential modulator) via its ubiquitin-binding domain.[56] NEMO further recruits IKK and TBK1, and these kinases phosphorylate IκBα and IRF3, respectively, to promote the transcription of pro-inflammatory cytokines and IFN-I.[55] RIG-I/MDA5-MAVS signalling is summarised in Fig. 3, created by Wu et al..[57]

TLR3/7/8, OAS-RNase L and PKR

Certain TLRs can also sense foreign intracellular RNA upon viral and bacterial infections. Specifically, like the CpG DNA sensor TLR9, TLR3, TLR7, and TLR8 are all localised in endosomes.[58] TLR3 recognises pathogen-derived dsRNA as well as naked synthetic poly I:C,[59] while TLR7 and TLR8 bind to ssRNA usually derived during infection.[60] Of note, human

gain-of-function (GOF) mutations in TLR7 underlie a systemic and neuroinflammatory state including systemic lupus erythematosus (SLE) due to its heightened sensitivity towards guanosine and 2',3'-cGMP (2',3'-cyclic guanosine monophosphate),[61] indicating that an inappropriate recognition of self nucleic acids by TLR7 can drive autoinflammation/autoimmunity.[61-63] Unlike TLR7 and TLR8 that utilise MyD88 as an adaptor protein to transduce signalling,[64] TLR3 recruits TRIF (Toll-interleukin-1 receptor-domain-containing adaptor-inducing IFNβ) to mediate downstream events.[65] After MyD88 is activated by TLR7/8, IRAKs are recruited to the TLR-MyD88 complex, which further recruits E3 ligase TRAF6, and through the synthesis of polyubiquitin chains, IKK and IRF7 are activated, inducing NF-κB signalling and IFN-I transcription.[66] For TLR3, after TRIF engagement, TRAF3 and TRAF6 are recruited to initiate the activation of IKK and TBK1, which later promotes the transcription of pro-inflammatory cytokines and IFN-I, respectively.[67] Through compartmentalisation, the endosomal localisation of TLR3/7/8, as well as the previously mentioned TLR9, represents an intrinsic protection mechanism to avoid mis-recognition of self RNA/DNA as foreign. Indeed, an engineered chimeric TLR9 mutant that relocates to the cell surface is able to sense self, but not viral, DNA.[68] This work suggests that the localisation of TLR9 is not required for nucleic acid sensing per se, but is critical to avoiding recognition of host DNA. Along similar lines, UNC93B1 is known to negatively regulate TLR7 signalling by controlling its ER-to-endolysosome trafficking.[34,69,70] Specific mutations in UN93B1 confer a gain of TLR7/8 activity and promote lupus pathogenesis.[71-74]

Pathogen-derived RNA can also be detected in the cytosol by the OAS (2'-5' oligoadenylate synthetase) family, and by PKR (dsRNA-dependent protein kinase R). Here, despite these molecules being induced by IFN-I stimulation (i.e. they are IFN-stimulated genes (ISGs) or ISG-like), their antiviral effect is not directly linked to the production of IFN-I. Rather, in the presence of viral dsRNA, OAS proteins catalyse the synthesis of 2'-5'oligoadenylates as a second messenger, which activates dormant RNase L in the cytosol. RNase L in turn digests both cellular RNA and viral RNA to restrict pathogen replication and trigger the apoptosis of

infected cells.[75] In the case of the kinase PKR, the molecule undergoes dimerisation and autophosphorylation upon recognition of viral dsRNA.[76] Activated PKR phosphorylates eIF2α (eukaryotic initiation factor 2α) that halts global protein translation, inhibits cell growth, and thereby restricts pathogen propagation.[76] RNA sensing via OAS-RNase L and PKR is illustrated in Fig. 3,[57] and TLR3/7/8 signalling in Fig. 4.[77]

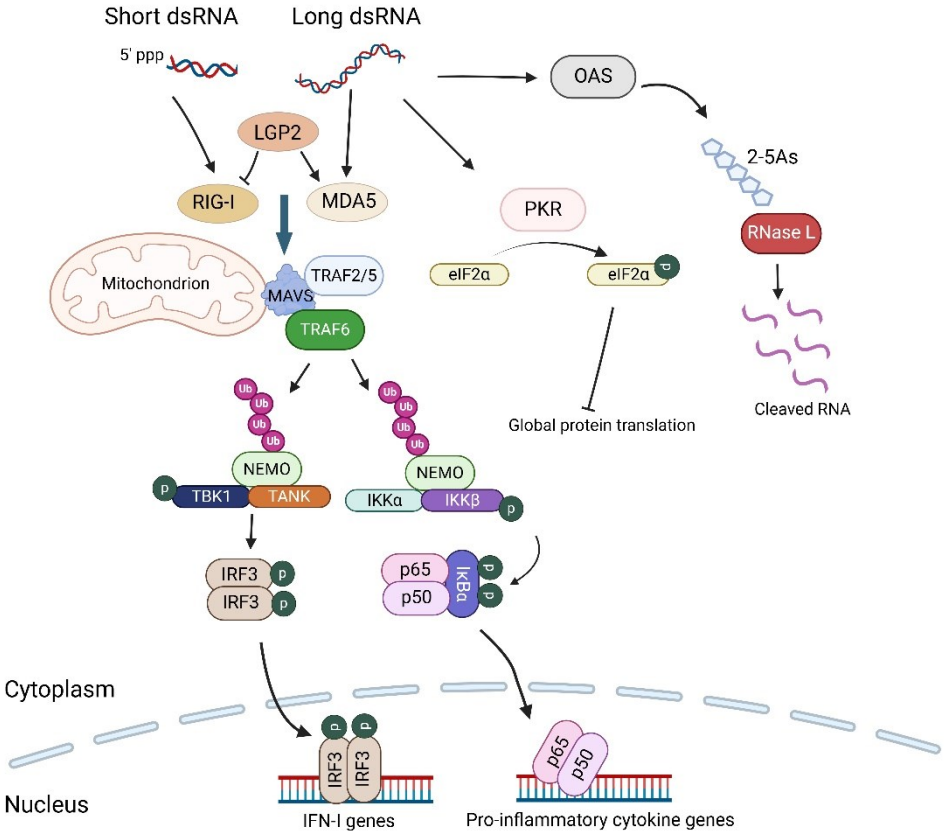

Fig. 3. Intracellular RNA sensing via RIG-I/MDA5-MAVS, OAS-RNase L and PKR. RIG-I and MDA5 recognise short 5'-triphosphate RNA and long dsRNA, respectively, and their activation induces the polymerisation of MAVS, which in turn recruits TRAF proteins to catalyse the polyubiquitin chains sensed by NEMO. NEMO recruits TBK1 and IKK kinases to the MAVS polymer to further phosphorylate IRF3 and NF-κB, which promote the transcription of IFN-I and pro-inflammatory cytokine genes. LGP2, another member of the RLR (RIG-I-like receptor) family, may function as a regulator of RIG-I and MDA5 activity. Additionally, (viral) dsRNA can be sensed by OAS, which catalyses the synthesis of 2'-5'oligoadenylates (2-5As) as a second messenger. 2-5As then activate RNase L to degrade both viral and cellular RNA, leading to inhibition of pathogen propagation and induction of cell apoptosis. In contrast, PKR, undergoes dimerisation and autophosphorylation upon recognition of foreign dsRNA, which leads to the activation of PKR and the subsequent phosphorylation of eIF2α, thus inhibiting global protein translation, cell growth and pathogen replication. RIG-I, retinoic acid-inducible gene I. MDA5, melanoma differentiation-associated protein 5. LGP2, laboratory of genetics and physiology 2. MAVS, mitochondrial antiviral signalling protein. TRAF, tumour necrosis factor receptor-associated factor. NEMO, NF-κB essential modulator. TBK1, TANK-binding kinase 1. IKK, IκB kinase. IRF3, interferon regulatory factor 3. OAS, oligoadenylate synthetase. PKR, protein kinase R. eIF2α, eukaryotic initiation factor 2α. Figure is adapted from Wu & Chen, *Annu Rev Immunol* 2014 and created in Biorender.

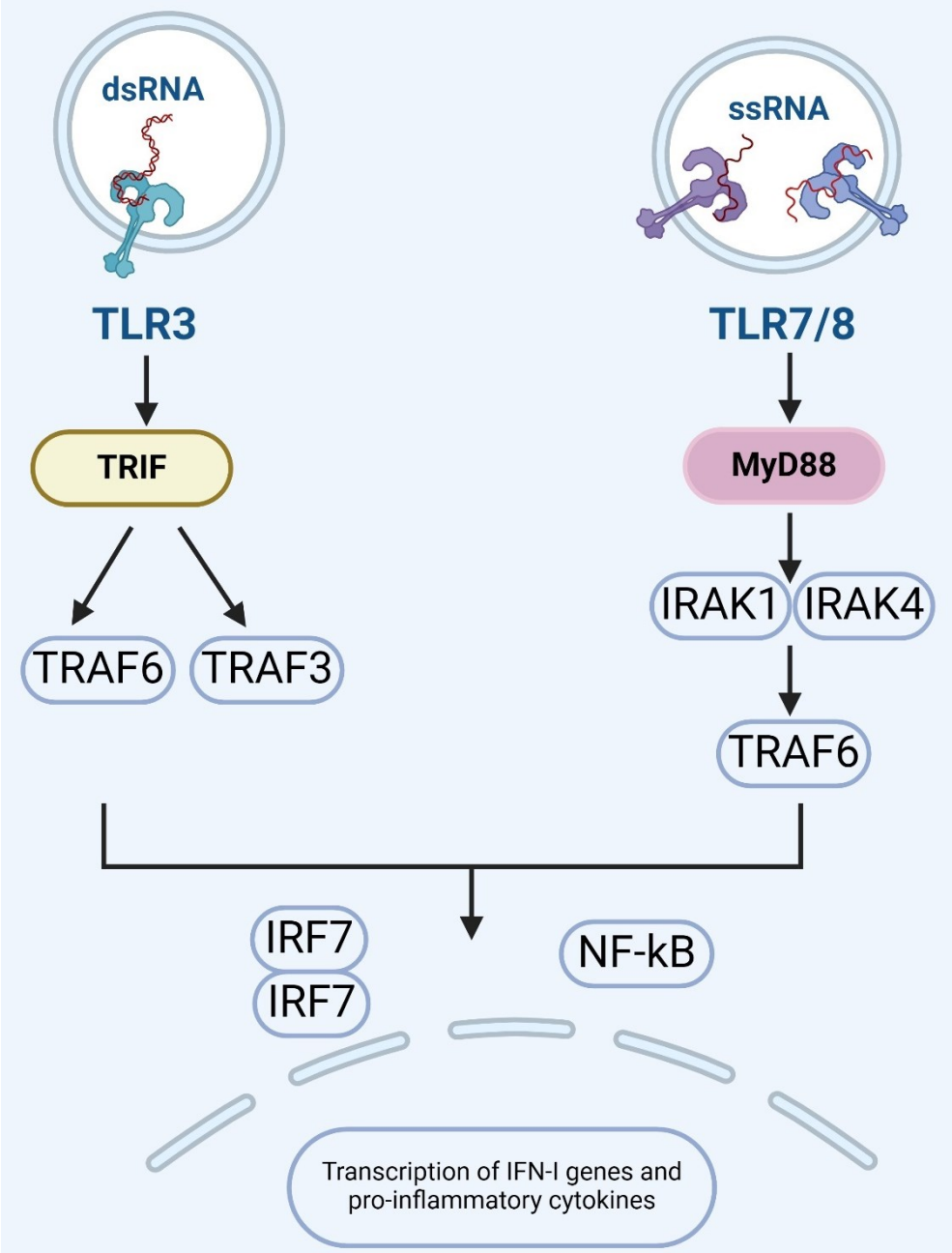

Fig. 4. Intracellular RNA sensing via TLR3/7/8. RNA viruses are endocytosed into endosomes where the viral RNA is recognised by TLR3/7/8. TLR3 uses TRIF as an adaptor protein to transduce signalling to TRAFs, which further activate IRF7 and NF-κB for downstream gene transcription of IFN-I and pro-inflammatory cytokines. TLR7/8 signal through MyD88, which activates IRAKs. IRAKs further recruit TRAFs to promote IRF7 and NF-κB signalling. TLR, Toll-like receptor. TRIF, Toll-interleukin-1 receptor-domain-containing adaptor-inducing IFN-β. MyD88, myeloid differentiation primary response 88. IRAK, interleukin-1 receptor-associated kinase. TRAF, tumour necrosis factor receptor-associated factor. NF-κB, nuclear factor kappa B. IRF7, interferon regulatory factor 7. Figure is adapted from Nair, P., Sapre, S.U. (2020). Significance of RNA Sensors in Activating Immune System in Emerging Viral Diseases. In: Bramhachari, P. (eds) Dynamics of Immune Activation in Viral Diseases. Springer, Singapore. and created in Biorender (https://www.biorender.com).

1.2 Type I interferon (IFN-I) signalling

1.2.1 Discovery of IFN-I

The first description of IFN was from the research by Alick Isaacs and Jean Lindenmann in 1957,[78,79] in which the authors studied the interference generated by heat-inactivated influenza virus A (IAV) in chick chorioallantoic membrane. A certain product was released by the membrane some time (a lag phase) after heated virus inoculation; and after incubation with fresh membranes, this product could confer protective qualities against live virus infection. The interference activity was measured by the titre of hemagglutinin generated by IAV compared to control conditions. Hence, the authors termed this product as ‘‘interferon’’, and showed that the protective qualities of IFN depended on the time and temperature of incubation, that IFN displayed some degree of instability, and that the amount of IFN produced positively correlated with the amount of heated virus inoculated.[78] Further studies revealed certain properties of IFN in more detail. Most strikingly, IFN was shown to inhibit the activity of several viruses including SeV (Sendai virus), NDV (Newcastle disease virus), VACV (vaccinia virus) as well as IAV. Moreover, IFN was stable at 2 °C for two weeks, while significant inactivation was observed after incubation for one hour at 60 °C. Efforts to purify IFN were carried out through high-speed centrifugation, filtration, and dialysis. The supernatant remaining after centrifugation at 20,000 g for two hours, or 100,000 g for half an hour, still retained the interfering activity against viruses, suggesting that IFN molecules were rather small. A series of filtration attempts using gradocol membranes with varying pore sizes demonstrated that the interfering activity was completely held back by the 0.6 micron membrane. Dialysis of IFN solution for 48 hours at 2 °C did not alter IFN activity, while incubation of IFN preparations at 60 °C completely abolished interference against viral replication. Electron microscopy failed to reveal any virus-like particles in IFN preparations. Further, serological studies revealed that anti-IAV rabbit serum was not able to neutralise the activity of IFN obtained from heated IAV inoculation. Collectively, these data indicated that IFN was not identical to the original heated virus; nor was it a ribonuclease, a heat-resistant molecule previously characterised to display interference to viral infectivity. Follow-up

standard biochemical experiments revealed that IFN was resistant to acidic environments up to a pH of 2. Additionally, IFN could be precipitated by ammonium sulphate, destroyed by ether, and digested by trypsin, all of which are common traits of proteins.[80]

The following decades saw an explosion of IFN-I research. IFN-I was first demonstrated to display anti-tumour activity in mice in 1969,[81] expanding the original conception that IFN-I mainly functioned as a cellular antiviral molecule. In 1975, distinct types of IFN-I (IFNα and IFNβ) were described, a conclusion initially drawn from the observation that the IFNs obtained from human fibroblasts and leukocytes were antigenically distinct.[82] Between 1979 and 1980, cDNAs for IFNα and IFNβ were cloned,[83,84] and shortly thereafter, their respective encoded proteins were purified,[85,86] paving the way for future clinical therapy. The first recombinant IFN clinical trials were conducted in cancer patients in 1981.[87] The first ISG, *OAS*, was cloned in 1983.[88] In 1985, Richard L. Friedman and George R. Stark reported the existence of a consensus sequence in IFN-induced genes through the study of *HLA*, *MT2A*, and *OAS*, and this consensus sequence was later termed the ISRE (IFN-stimulated response element) by Darnell et al..[89] By 1998, hundreds of ISGs had been identified using oligonucleotide arrays, many without any previously recognised function.[90]

Now it is widely accepted that different subtypes of human IFN-I exist, that the genes encoding these proteins cluster on chromosome 9, and that they characteristically lack introns.[91] In total, 17 genes encode human IFN-Is, including 13 subtypes of IFNα (1, 2, 4, 5, 6, 7, 8, 10, 13, 14, 16, 17, and 21), and single subtypes for IFNβ, IFNω, IFNε and IFNκ.[92] The amino acid sequences for mature IFNα1 and IFNα13 are identical. Thus, 13 IFNα genes encode 12 IFNα proteins.[93,94] Likely all cells can express some amount of IFN-I under certain stimuli, with plasmacytoid DCs (pDCs) being the IFN-I producing powerhouse.[95] Cells also exhibit variability in the expression profile (timing and magnitude) of different IFN-I subtypes. Certain IFN-I subtypes have a more restricted expression pattern. For example, IFNκ is almost exclusively expressed in keratinocytes,[96] while IFNε is usually found in mucosal tissues.[97]

1.2.2 Discovery of IFN-I signalling pathway components

It was already appreciated early on in IFN-I research that secreted extracellular IFN-I exerts antiviral/anti-tumour activity through the actions of ISGs expressed by cells following stimulation, whose diverse functions play essential roles in restricting pathogen growth, limiting cellular proliferation, and modifying innate and adaptive immunity.[98] However, the missing link between IFN-I and ISG induction was only gradually revealed starting from 1990, when Georges Lutfalla and colleagues cloned and expressed the human IFN-I receptor gene (now known as *IFNAR1*) in mouse cells.[99] Later that year, the Darnell laboratory identified ISGF3 (IFN-stimulated gene factor 3), a multimeric complex that directly binds the ISRE sequence of ISGs shortly after IFN-I stimulation.[100] In a follow-up study, the same group purified the protein components of ISGF3 and cloned the corresponding cDNA sequences,[101] which are now known as IRF9, STAT1 (signal transducer and activator of transcription 1) and STAT2. Roughly around the same time, several other teams were also actively looking for components essential to IFN-I signalling. Andrew F. Wilks and Stuart A. Aaronson cloned cDNA sequences for JAKs (Janus kinases 1/2/3), utilising PCR-based methods and reduced stringency hybridisation, respectively.[102-104] The last member of the JAK family, TYK2, was discovered by Sandra Pellegrini and colleagues using chemical selection and mutagenesis, through which different mutant cell lines unresponsive to IFN were established. By complementation assays, the critical role for TYK2 in mediating IFN-I signalling was identified.[105] Curiously, even though the existence of more than one subunit of IFN-I receptor was suggested based on several observations since the discovery of IFNAR1,[106-108] it was only in 1994 that Menachem Rubinstein et al. first described the characterisation and cloning of *IFNAR2*.[109] Thus, at this point, the core machinery for functional IFN-I signalling had been identified and the signal transduction pathway established.

1.2.3 IFN-I signalling pathway

Detailed biochemical, molecular and structural work has shed light on the signalling cascade engaged following IFN-I stimulation, with features specific to cell types and the nature of the

stimulatory signal continuing to be revealed (Fig. 5, created in Biorender). In general, IFNAR1 and IFNAR2 are localised separately on the cell surface in steady state. Only after high affinity IFN-I molecule binding to IFNAR2, does IFNAR1, whose affinity for IFN-I is 1000-fold weaker than that of IFNAR2, migrate to the IFN-I-IFNAR2 complex.[110] The ternary complex comprises IFNAR1-IFN-I-IFNAR2 in a ratio of 1:1:1.[110] Ligand biding results in receptor conformational changes, thus bringing receptor associated TYK2 and JAK1 into closer proximity.[111] Through auto- and trans-phosphorylation of tyrosine residues (Y1054/Y1055 for TYK2 and Y1034/Y1035 for JAK1),[112] TYK2 and JAK1 become activated and, in turn, phosphorylate IFNARs.[111] Phosphorylated receptors and JAK kinases further recruit latent intracellular STAT1 and STAT2, which, through tyrosine-phosphorylation at Y701 and Y690, respectively, become activated.[113,114] Phosphorylated STAT1 and STAT2 dimerise and translocate into the nucleus, where they further recruit IRF9, thus forming the trimeric ISGF3.[115] As a transcriptional activator, ISGF3 binds to genes with an ISRE sequence in their promoter region, thereby initiating the transcriptional cascade of hundreds of ISGs.[115]

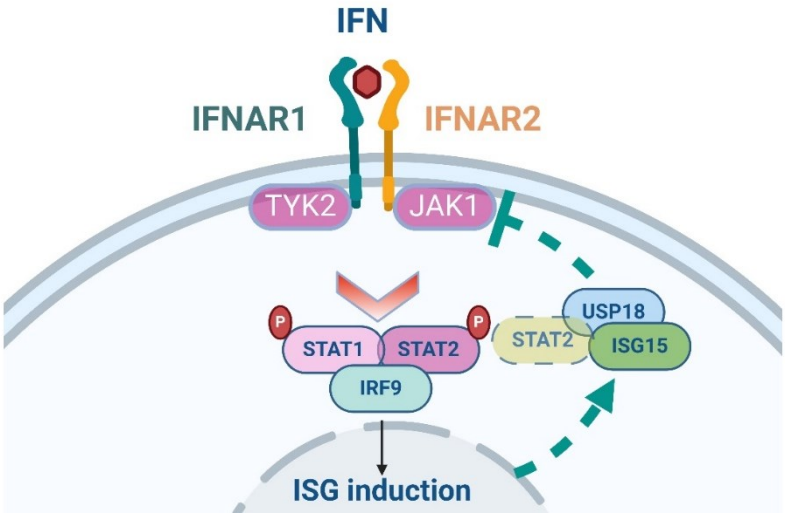

Fig. 5. Type I interferon signalling pathway. After interferon (IFN) molecules bind to their cognate cell surface receptor subunit 2 (IFNAR2) with high affinity, IFNAR1 binding also occurs, thus forming the ternary IFNAR1-IFN-IFNAR2 complex. The receptor-associated Janus kinases (TYK2 (tyrosine kinase 2) and JAK1) are brought into proximity for auto/trans-phosphorylation. Activated JAK kinases then phosphorylate the receptors as well as STAT proteins. STATs translocate into the nucleus to bind IRF9, thus forming a trimeric complex ISGF3 (IFN-stimulated gene factor 3), which acts as a transcriptional activator to bind genes with an ISRE (IFN-stimulated response element) motif, initiating the transcriptional cascade of ISGs (IFN-stimulated genes). In the later stages of IFN-I signalling, USP18 and STAT2 form a duplex to displace JAK1 from IFNAR2, thus turning off excessive signalling. IFNAR, IFN alpha and beta receptor. STAT, signal transducer and activator of transcription. IRF9, IFN regulatory factor 9. USP18, ubiquitin-specific protease 18. ISG15, IFN-stimulated gene 15.

The above-described pathway represents the best-understood and predominant signalling event driven by IFN-I in most, if not all, cells. However, alternative signalling pathways mediated by other STATs can also be induced in different cell types and in the presence of additional ligands other than IFN-I.[116] For example, IFN-I stimulation can lead to the dimerisation of tyrosine-phosphorylated STAT1 alone, which, without a third IRF protein, directly translocates into the nucleus, binding to genes with a GAS (gamma-activated sequence) element and promoting the expression of a largely overlapping subset of ISGs.[117] Additionally, ISG transcription has been observed in cells with upregulation of unphosphorylated STAT1/2 and IRF9 protein levels persisting long after the IFN-I stimulant is removed and JAK phosphorylation is diminished, suggesting that the unphosphorylated ISGF3 complex drives a sustained expression network of some ISGs, particularly important in maintaining an antiviral state.[118] Other reports also indicate that phosphorylated STAT2 can homodimerise with a weak DNA-binding capacity; but in the presence of IRF9, this non-canonical transcriptional complex can directly bind some genes with an ISRE sequence, a phenomenon implicated in cellular antiviral responses induced by DENV (Dengue virus).[119]

Besides STAT1/2, IFN-I signalling can also drive the activation of other STAT proteins, resulting in various downstream effects in a number of cell types of both lymphoid and myeloid lineages, an observation that can be partially explained by the relative abundance of STATs in specific cell types and according to differentiation/development stage.[120] For instance, STAT6 can form a dimer with STAT2, and together, the STAT2-STAT6 complex activates Sp1 (specificity protein 1) and inhibits BCL6 (B cell lymphoma transcription factor 6) to promote the antiproliferative effects of IFN-I in a human B-lymphoblastoid cell line.[121] On the other hand, in $CD8^+$ T cells, STAT4 can counteract the STAT1-dependent antiproliferative effects following IFN-I stimulation, promoting the expansion of antigen-specific cytotoxic T cells for pathogen clearance.[122] Further, STAT3 is suggested to promote an anti-inflammatory phenotype in IFN-I activated monocytes. In this case, STAT3 activation following IFN-I signalling does not induce STAT1 phosphorylation or nuclear translocation. Rather, STAT3 sequesters STAT1 and

impairs its dimerisation, providing a parallel regulation mechanism preventing overactivation of IFN-I signalling.[123]

Non-canonical signalling cascades can also be initiated via IFN-I binding to IFNARs, followed by TYK2/JAK1 activation. The most well-studied non-canonical signalling cascade is perhaps the MAPK pathway involving the activation of JNK (c-Jun N-terminal kinase), ERK (extracellular signal-regulated kinase) and/or p38,[116,124] contributing to the optimal transcription and translation of ISGs.[125] Another non-canonical signalling pathway is PI3K-mTOR (phosphoinositide 3 kinase-mammalian target of rapamycin), which controls cell proliferation and, in a dysregulated context, promotes tumourigenesis.[126] It has been shown that IFNβ promotes STAT1-STAT3 activation and glucose metabolism via mTOR signalling to enhance the immunomodulatory effects of mesenchymal stromal cells.[127]

1.2.4 IFN-I signalling regulation

Positive regulation

As an indispensable cellular signalling pathway with diverse downstream effects, it can be expected that various non-redundant regulatory mechanisms exist to fine-tune (both positively and negatively as required) the dynamics and magnitude of IFN-I signalling so as to maintain homeostasis, and in response to diseased states.

Several members of the IRF family exhibit positive regulatory roles towards IFN-I induction and/or signalling, and with many of them being ISGs, participate in a feedforward loop to amplify IFN-I activity. IRF3 and IRF7 are the major transcriptional activators of IFN-I genes following viral infection, induced by various PRRs such as TLRs, RLRs and cGAS.[128] IRF3 is critical to the initial signalling following viral nucleic acid sensing, resulting in a rapid expression of IFNβ while enhancing the expression of IRF7. IRF7, in turn, drives the expression of the many IFNα subtypes to further consolidate the cellular antiviral state.[129,130] Of note, pDCs constitutively express relatively high amounts of IRF7, consistent with their role as the primary IFNα producing cells upon infection.[95,131,132] IRF9, as the only IRF member able to bind STAT2

to form the ISGF3 complex with STAT1, is essential for the transcriptional cascade of a large number of ISGs.[133] Further, IRF1, IRF3 and IRF7 have all been shown to induce expression of some ISGs in an IFN-I-independent manner by directly binding to targets genes with an IRF-E (IRF-element) sequence motif.[134,135]

Another positive regulator involved in the amplification of IFN-I signalling is STAT1, which is absolutely required for initial downstream ISG induction. As an ISG itself, STAT1 is upregulated within minutes to hours, depending on the cell type, following IFN-I stimulation; and cells deficient for STAT1 are significantly limited in the ability to transduce an IFN-I signal.[136,137] Further, several innate sensors themselves are ISGs, such as RIG-I, MDA5, and IFI16, participating in positive regulation of antiviral response.[138-140]

Negative regulation

Because a persistent and/or abnormally enhanced IFN-I activity can underly severe inflammatory disease,[141] and noting that IFN-I therapy can sometimes induce adverse effects,[142] appropriate negative regulation strategies are employed by cells to restrict excessive IFN-I signalling and avoid pathological consequences. USP18 (ubiquitin-specific protease 18) is arguably the most important player in this regard. In the later stages of IFN-I signalling, USP18, itself an ISG, forms a dimer with STAT2, and displaces JAK1 from IFNAR2, effectively restricting unwarranted signalling (Fig. 5).[143] Cells deficient for USP18 display hyperactive IFN-I signalling, leading to persistent STAT1 phosphorylation and unrestrained ISG upregulation.[144] ISG15, a ubiquitin-like ISG that is able to stabilise the structure of USP18, contributes to USP18-mediated negative regulation of IFN-I signalling via altering the abundance of available USP18 protein in the cytosol.[145,146] Interestingly, in addition to what the name suggests, USP18 also catalyses the removal of ISG15 from conjugated proteins, a process termed deISGylation.[147] A notable feature of STAT2 is its role in regulating opposing signalling effects, one in transducing a positive signal to downstream effectors, and the other in restricting overt signals in the same pathway. Given this insight, one might expect that different functional domains exist within STAT2 to mediate these two capabilities, with

mutations specifically affecting one function not necessarily impairing the other, thus conferring distinct molecular and cellular outcomes.

SOCS (suppressor of cytokine signalling) proteins are also important negative regulators in a number of signalling pathways including IFN-I, TCR (T cell receptor), TLR, and IL signalling.[148] Specifically relating to IFN-I, SOCS1 and SOCS3 are implicated in at least two major ways to dampen down signalling. First, SOCS1 and SOCS3 can induce the polyubiquitination and subsequent proteasomal degradation of some innate sensing pathway components such as IRAK1 and TBK1, ultimately leading to the downregulation of IFN-I gene transcription. Second, SOCS1 and SOCS3 can also directly bind TYK2 and JAK1, respectively, resulting in reduced phosphorylation of STAT1.[117]

Signalling activation of the IFN-I pathway can be summarised as a series of tyrosine phosphorylation events. Unsurprisingly, pathway components can be targets of tyrosine phosphatases – well recognised regulators of multiple cellular signalling programmes. Indeed, PTP1B and PTPN2,[117] the two prototype members of the non-receptor protein tyrosine phosphatase family, participate in the dephosphorylation of JAKs, potentially regulating not only IFN-I signalling, but also many other JAK-STAT pathways such as IFN-II, IFN-III, IL and EGFR (epidermal growth factor receptor).[149] Further, SHP1 (src homology 2 domain-containing tyrosine phosphatase 1) and SHP2 can dephosphorylate JAK1 as well as STATs, thereby restricting downstream signalling.[150,151] Ubiquitination of several pathway components is known to negatively regulate signalling. For example, nuclear RNF2 (ring finger protein 2) was shown to promote the K33-linked polyubiquitination of STAT1 at K379 residue following IFN-I stimulation, leading to its dissociation from DNA and the inhibition of ISG transcription.[152]

Some IRFs can negatively regulate IFN-I signalling through a variety of mechanisms. IRF2 displays significant sequence homology with IRF1, and both can bind to a similar subset of genes. As a result, IRF2 is appreciated as an antagonist of IRF1.[153] Moreover, IRF2 is found to associate with STAT1 and NF-κB, preventing their translocation into the nucleus for gene transcription.[154,155] IRF2-deficient mice demonstrate enhanced ISGF3 activity-dependent skin

autoinflammation with an upregulation of ISG expression.[156] Along the same lines, IRF4 is able to antagonise IRF5 through competitive binding with MyD88 and similar target genes, thus limiting the magnitude of TLR signalling.[157,158]

Certain non-coding microRNA (miR) species have been shown to directly downregulate IFN-I transcripts. Thus, miR-466l binds to the 3' UTR region of several IFNα subtypes,[159] while a number of miRNAs target IFNβ, including miR-26a, miR-34a, miR-145 and let7b.[160] Besides IFN-I transcripts, ISGF3 can also be targeted by miRNA. For example, miR-221 and miR-222 antagonise STAT1/2,[161] and IRF9 is recognised and bound by miR-302d.[162]

1.2.5 Human inherited diseases due to unbalanced IFN-I signalling

Mendelian deficiency in IFN-I activity

IFN-I induction and activity has been implicated in a number of human diseases, including infection, cancer, autoimmunity and neurodegeneration.[163-166] The current study has focused on human monogenic disorders resulting in unbalanced IFN-I signalling, with a particular interest in the uncontrolled upregulation of IFN-I. To provide an overview of the topic, this thesis also introduces Mendelian deficiencies of IFN-I signalling.

Germline defective IFN-I signalling can underly severe (viral) infections frequently affecting the nervous and the respiratory systems, and sometimes also conferring susceptibility to live-attenuated viral vaccines (LAVs) against measles and yellow fever in otherwise healthy patients.[93] In general, defects in the signalling pathways leading to an impaired antiviral state include: deficits in IFN-I producing pathways, deficits in IFN-I signalling, and deficits in particular IFN-I proteins or ISGs.[93]

Insufficient IFN-I production upon viral infection can arise due to compromised innate sensing pathways. For example, MDA5 (encoded by *IFIH1*) recognises intracellular viral dsRNA and initiates a signalling cascade driving IFN-I expression. Loss-of-function (LOF) mutations in MDA5 predispose to recurrent viral infections in the upper and lower respiratory tract, and encephalitis induced by enteroviruses.[167-169] TLR3 is an intracellular dsRNA sensor localised

to the endosome, and LOF mutations in TLR3 were found in some patients with HSE (herpes simplex encephalitis), severe influenza, and critical COVID-19 pneumonia.[170-172] Many of the TLRs utilise MyD88 as adaptor protein to transduce signalling to downstream effectors. Certain patients with critical COVID-19 have been shown to be deficient for MyD88, but other than that, are not prone to other viral infections.[173] It has also been reported that children with autosomal recessive MyD88 and IRAK4 deficiency suffer from recurrent life-threatening bacterial infections.[174,175]

A priori, impaired IFN-I signalling might result from a deficiency of any components of a relevant viral signalling pathway. For example, particular *IFNAR1* LOF mutations have a relatively high prevalence in the Polynesian population.[176] Individuals carrying these *IFNAR1* mutations display higher susceptibility to certain viral infections (RSV (respiratory syncytial virus), HHV6 (human herpesvirus 6), enterovirus, rhinovirus, parainfluenza, and bocavirus) as well as severe side effects following LAV such as MMR (measles, mumps, and rubella). Cells from these patients are completely unresponsive to IFN-I stimulation.[176] Similarly, IFNAR2 deficiency is observed at a high frequency in the Arctic region.[177] Patients suffer from life-threatening influenza, COVID-19 and disseminated disease following LAV.[177] These reports indicate that rare genetic mutations affecting the IFN-I system can be fairly common in some remote geographical regions, highlighting the possible importance of genetic screening in these populations. It is of note that defective IFN-I signalling confers susceptibility to only a narrow range of viral infections in humans (HSV-1 encephalitis, severe respiratory infections caused by influenza and SARS-CoV2, and disseminated disease following yellow fever and measles LAV), a surprising observation given the ubiquitous expression profile of IFN-Is and their pleiotropic actions against most viruses. This finding might be, at least partially, explained by redundancy of IFN-I and IFN-III against certain viral infections in the lung and central nervous system (CNS), a notion potentially supported by the fact that no human patients with inherited IFN-III signalling deficiency have been reported to date.

Finally, although specific mutations in IFN-I genes have not been identified to date, neutralising autoantibodies against some IFN-I subtypes in the circulating blood have been described in patients with critical COVID-19, MERS (Middle East respiratory syndrome), and influenza pneumonia,[178-180] where the autoantibody titre, and the number of IFN-I subtypes they neutralise, correlate well with disease severity.[181] Multiple factors could contribute to the production of autoantibodies, such as acute infections, genetic variation, age, sex, and environmental triggers.[182] The genetic basis for the presence of autoantibodies against IFN-I is elusive. Speculation has been made in relation to the association of such autoantibodies with LOF mutations in *AIRE* (autoimmune regulator), *FOXP3* (forkhead box P3), *RAG1/2* (recombination activating 1/2) and *CTLA4* (cytotoxic T-lymphocyte associated protein 4), among others.[182] On a different note, defects in four (*USP18*, *ISG15*, *OAS1*, and *OAS2*) of the six known Mendelian genetic defects directly involving ISGs underlie autoinflammation rather than susceptibility to virus.[144,183,184] STAT2 deficiency leads to critical viral disease as well as inflammation due to the dual functions of STAT2.[185,186] Patients develop recurrent viral infections including COVID-19, HSE and LAV-associated adverse effects.[185] Interestingly, these patients also demonstrate manifestations related to hyperinflammation.[186] The most recently identified Mendelian disease involving mutations in a canonical ISG relates to mutations in MX1 (MX dynamin like GTPase 1), LOF of which underlies severe H7N9 swine influenza cases.[187] It is unclear if these patients also display a higher susceptibility to other respiratory infections.

Type I interferonopathies

In another aspect of dysregulated IFN-I signalling, persistent enhancement of IFN-I activity has been associated with a group of Mendelian autoinflammatory diseases termed the type I interferonopathies (T1Is).[93,188] Since its conception, 52 known discrete genotypes belonging to this categorisation have been described, with the largest group pertaining to a disturbance of nucleic acid metabolism or sensing.[93] A further subgroup involves genes playing a role in the regulation of IFN-I signalling per se – particularly, negative regulators of this pathway.[93]

Aicardi–Goutières syndrome (AGS), mentioned earlier in the context of mutations in *LSM11* and *RNU7-1* conferring a disturbance of linker histone stoichiometry,[27] was the first described T1I; with a clinical report published in 1984 by French physicians Jean Aicardi and Françoise Goutières. Here, eight infants were described with severe microcephaly, mild yet persistent CSF lymphocytosis, and basal ganglia calcification. Aicardi and Goutières suspected that this disorder could be genetic, but also highlighted that ‘‘some features, especially the pleocytosis, may erroneously suggest an inflammatory condition’’.[189] About two decades later, the first gene identification studies in AGS were reported by Yanick J. Crow and Andrew P. Jackson, which illustrated a subset of AGS patients to harbour LOF mutations in either TREX1 or any of the three components of the RNase H2 complex (composed of A/B/C subunits).[190,191] TREX1 is a 3'-5' DNA exonuclease that digests and prevents the accumulation of both ss- and dsDNA in the cytosol, limiting the activation of the cGAS-STING signalling pathway and IFN-I production.[192,193] On the other hand, the RNase H2 complex can degrade the RNA strand in RNA-DNA hybrids, with defective RNase H2 activity also resulting in hyperactive cGAS-STING signalling.[194,195] Since that time, the Crow group has identified five further genes, mutations in any of which can result in a phenotype consistent with AGS. Specifically, SAMHD1 (SAM and HD domain containing deoxynucleoside triphosphate triphosphohydrolase 1) is a negative regulator of cellular dNTP pool and a 3’ exonuclease for ssRNA,[196-198] LOF mutations in which lead to an accumulation of cytosolic DNA, and possibly RNA, species. ADAR1 (adenosine deaminase acting on RNA) catalyses adenosine (A) to inosine (I) editing of dsRNA, especially in transcripts containing Alu-repeat elements.[199,200] LOF mutations in ADAR1 are thought to be associated with the accumulation of cytosolic dsRNA, triggering MDA5-MAVS pathway activation and overproduction of IFN-I.[201] *IFIH1*, encoding MDA5, is an intracellular dsRNA sensor essential to the antiviral response against RNA viruses.[202,203] GOF mutations in *IFIH1* lower its activation threshold, thereby increasing its sensitivity to self RNA.[204] LSM11 and *RNU7-1* are involved in histone pre-mRNA processing as part of the U7–snRNP complex, and LOF mutations in either result in abnormal histone

stochiometry.[27] Remarkably, all of these genes encode products playing a role in the metabolism or sensing of nucleic acids, albeit indirectly in the case of LSM11 and *RNU-7*. The end result is the over/mis-activation of innate sensing pathways leading to enhanced IFN-I signalling, which is thought to be both a hallmark characteristic of these diseases and a direct driver of pathogenesis.[93,188]

Mutations involving the STING pathway have been reported to drive a distinct subset of T1Is. SAVI (STING-associated vasculopathy with onset in infancy) patients display early-onset systemic inflammation with particular involvement of the skin (vasculopathy) and lung (ILD, interstitial lung disease).[205] GOF mutations in *STING1* lead to constitutive activation of STING, increased levels of IFNα protein and, in turn, ISG expression.[205] On a similar note, LOF mutations in components of the STING trafficking pathway have also been identified in patients demonstrating an overlapping clinical phenotype with SAVI. In particular, COPA syndrome is characterised by chronic diffuse alveolar haemorrhage in the lung, as well as renal and joint involvement.[206] Lepelley et al., and several other groups, reported that heterozygous missense mutations in *COPA* are associated with impaired Golgi-ER retrograde trafficking of STING, leading to STING Golgi-retention and IFN-I overproduction.[18,207-209]

T1Is can also be caused by an overactive IFN-I signalling pathway per se. Thus, STAT1 GOF has been reported in patients with diverse clinical features, likely explained by the protein's involvement in multiple signalling pathways not limited to IFN-I, but also including IFN-II, IFN-III, and other cytokine-mediated signalling events. Patients can demonstrate chronic mucocutaneous candidiasis,[210] severe early-onset combined immunodeficiency,[211] and autoimmunity.[212] To date, no convincing GOF defects in the IFNAR1/2 genes themselves have been documented (while Degos disease has been described due to an activating mutation of IFNAR1, the report concerns a single patient, with definitive proof of causality lacking).[213] However, studies of trisomy 21 (also known as Down syndrome) have linked this disorder with upregulated IFN-I activity due to the extra copy of IFNAR1/2. Autoimmunity, immunodeficiency, and intracranial calcification have been described in individuals with Down syndrome.[214-218]

IFN-I signalling is controlled at many levels, so as to confer efficient protection against virus while minimising the risk of autoinflammation. Therefore, it is unsurprising that a disturbance of these mechanisms could result in an interferonopathy state. A failure in the negative regulation of IFN-I signalling resulting in autoinflammation represents the core study of this thesis, with detailed examples presented in the chapters which follow. Certain cases of USP18 deficiency represent the most severe examples of a T1I described to date, with eight of the ten patients reported with complete or partial USP18 deficiency dying in the perinatal period.[144,219-221] As an inbuilt safeguarding mechanism against the potential risk of unrestrained IFN-I signalling, USP18 interacts with STAT2 to displace JAK1 from IFNAR2. Unsurprisingly then, an absence of USP18 leads to chronic upregulation of ISG expression. Haploinsufficiency in another master negative regulator of IFN-I signalling, SOCS1, has also been described. SOCS1 is known to bind TYK2 in the IFN-I pathway, decreasing STAT1 phosphorylation. Patients display early-onset autoimmune clinical features encompassing cytopenia, SLE and organ-specific autoimmunity. This broad phenotype, beyond that of the more 'classical' T1Is, is likely explained by the involvement of SOCS1 in multiple JAK-STAT signalling pathways critical in immune homeostasis.[222-224]

Mutations in the ubiquitin-proteasome degradation machinery have also been reported to enhance IFN-I signalling,[93,225,226] with Davidson et al. describing PKR activation by cytosolic IL-24 in cell models with decreased proteasome function, as well as in cells derived from patients with proteasome-associated autoinflammatory syndrome (PRAAS).[227] Higher amounts of phosphorylated PKR and eIF2α were observed in PRAAS patient cells compared to healthy controls, which corresponded to overexpression of IL-24. Genetic ablation or pharmacological inhibition of PKR decreased the inflammatory phenotype observed in proteosome deficiency, thus providing a possible explanation linking proteotoxic stress and inflammatory disease in PRAAS.[227]

A summary of the above-described genetic disorders conferring a T1I state is given in Table 1, adapted from Yanick J. Crow and Jean-Laurent Casanova, *Science Immunology*, 2024.[93]

An increasingly recognised feature in T1I research, as well as in the broader discipline of inborn errors of immunity, is incomplete penetrance.[188,228-230] That is, these disorders can exhibit imperfect segregation of mutations with clinical phenotype. To put it more plainly, if all carriers of a particular mutant genotype demonstrate a disease trait by a certain age, a genotype is considered fully penetrant. In contrast, the term ‘‘incomplete penetrance’’ is used to describe the situation where the genotype does not manifest in certain individuals despite the presence of the mutation. Penetrance is considered to be a binary phenomenon, although clinically asymptomatic individuals might demonstrate a phenotype at a cellular or molecular level; for example, while Rice et al. found 13.5% of carriers of a heterozygous GOF mutation in MDA5 to be clinically unaffected, almost all of these individuals demonstrated an upregulation of ISG expression in blood.[231] Of note, the term “expression” refers to variability in the way in which a mutant genotype manifests clinically (e.g. some patients with STING GOF mutations might experience both lung and skin disease, while others might manifest only one or the other). Disease penetrance is not necessarily easy to assess, a point of particular note where asymptomatic relatives of an affected proband are not tested. Mutations causing T1Is, inherited as either dominant or recessive traits, have been described to display incomplete penetrance.[18,231,232] The factors contributing to incomplete penetrance likely relate to the following: environmental factors (perhaps most obviously infections and vaccinations in the context of inborn errors of immunity); other genetic variants acting as protective or susceptibility alleles ; epigenetic modifiers affecting gene expression; and somatic mosaicism, where only a proportion of an individual’s cells carry the putative gene mutation.[228] Other mechanisms might also be relevant, including preferential allelic expression, genetic compensation of a homologue, and repeat expansion of a WT allele.[230] Specific examples will be further discussed later in this thesis.

Table 1. Examples of known type I interferonopathies.

Protein/RNA (gene)	Function	Link to IFN-I signalling	LOF/GOF	Clinical phenotypes
Defective cytosolic nucleic acid sensing				
ADAR1	Deaminase (A-I editing in dsRNA)	Cytosolic dsRNA	LOF	AGS, BSN, SP, DSH
MDA5 (*IFIH1*)	dsRNA sensor	Cytosolic dsRNA	GOF	AGS, SP, SMS, DA
RNASEH2A	Ribonuclease	Cytosolic RNA-DNA hybrids, micronuclear DNA	LOF	AGS
RNASEH2B	Ribonuclease	Cytosolic RNA-DNA hybrids, micronuclear DNA	LOF	AGS, SP
RNASEH2C	Ribonuclease	Cytosolic RNA-DNA hybrids, micronuclear DNA	LOF	AGS
SAMHD1	Negative regulator of dNTP pool/ssRNA 3' exonuclease	Cytosolic DNA/RNA	LOF	AGS, CL, CVD
TREX1	Deoxyribonuclease	Cytosolic DNA	LOF	AGS, CL, SLE
Inappropriate nuclear DNA sensing				
LSM11	RDH pre-mRNA processing	Histone stoichiometry	LOF	AGS
U7 (*RNU7-1*)	RDH pre-mRNA processing	Histone stoichiometry	LOF	AGS
Aberrant STING signalling/trafficking				
COPA	Golgi to ER vesicular transport	STING trafficking	LOF	COPA syndrome
STING (*STING1*)	Adaptor for cytosolic DNA sensing	dsDNA-dependent signalling	GOF	SAVI, CL
Impaired IFN-I signalling and regulation				
ISG15	Inhibition of IFNAR signalling	IFNAR2 negative regulation	LOF	ICC, MSMD, SL
SOCS1	JAK inhibition	TYK2/JAK1 inhibition	LOF	AIHA, ITP, MIS
STAT1	Cytokine signalling	ISG signalling	GOF	CMC, ID, AI, ICC,
STAT2	Regulation of ISG expression	IFNAR2 negative regulation	LOF	AGS-like
Trisomy 21	Trisomy of chromosome 21	Triplication of IFNAR1/2	GOF	Down syndrome, ID, ICC
USP18	Inhibition of IFNAR signalling	IFNAR2 negative regulation	LOF	AGS-like
Deficient proteasome function				
PSMA3	Proteasome	PKR activation	LOF	PRAAS
PSMB4	Proteasome	PKR activation	LOF	PRAAS
PSMB8	Proteasome	PKR activation	LOF	PRAAS
PSMB9	Proteasome	PKR activation	LOF	PRAAS
PSMC3	Proteasome	PKR activation	LOF	PRAAS

Table 1. AGS: Aicardi-Goutières syndrome; AI: autoimmunity; AIHA: autoimmune haemolytic anaemia; BSN: bilateral striatal necrosis; CL: chilblain lupus; CMC: chronic mucocutaneous candidiasis; CVD: cerebrovascular disease; DA: deforming arthropathy; DSH: dyschromatosis symmetrica hereditaria; ER: endoplasmic reticulum; GOF: gain-of-function; ICC: intracranial calcification; ID: immunodeficiency; ISG(s): interferon stimulated gene(s); ITP: immune thrombocytopaenia; LOF: loss-of-function; MIS: multisystem inflammatory syndrome; MSMD: Mendelian susceptibility to mycobacterial disease; PRAAS: proteasome associated autoinflammatory syndrome; SAVI: STING-associated vasculopathy with onset in infancy; SL: skin lesion; SLE: systemic lupus erythematosus; SMS: Singleton-Merten syndrome; SP: spastic paraparesis.

Chapter 2: A loss-of-inhibitory-function mutation in STAT2 causes a severe type I interferonopathy

2.1 Introduction

Type I interferon (IFN-I) signalling drives a complex downstream transcriptional network crucial to host defence against invading pathogens.[233] Almost all cells in the human body can express some amount of IFN-I upon appropriate stimulation.[234] After production, type I IFNs are secreted and, in an autocrine or paracrine manner, bind to IFN-I receptors (IFNARs). IFNARs consist of two subunits, namely, IFNAR1 and IFNAR2, which are phosphorylated upon ligand binding, leading to the activation of the receptor-associated Janus kinase (JAK) family members tyrosine kinase 2 (TYK2) and JAK1, respectively.[235] In turn, TYK2 and JAK1 recruit and activate signal transducer and activator of transcription 1 (STAT1) and STAT2 through phosphorylation. Phosphorylated STAT1 and STAT2, together with IFN regulatory factor 9 (IRF9), form a complex, named IFN-stimulated gene factor 3 (ISGF3), which translocates to the nucleus and acts as a transcriptional activator by binding to IFN-sensitive response elements (ISREs) within a broad repertoire of so-called IFN-stimulated genes (ISGs). ISG proteins play diverse roles in modifying the innate and adaptive immune systems, restricting pathogen survival and growth, and regulating cell proliferation, survival and death.

IFN-I production and signalling require tight regulation, with a failure of such regulation having severe consequences. As examples, IFNAR2 deficiency results in potentially fatal MMR vaccination-related encephalitis,[236] while deficiency of USP18, a known negative regulator of IFN-I signalling, is associated with a T1I state, where patients can exhibit congenital microcephaly, thrombocytopenia, hepatic dysfunction, and hepatosplenomegaly.[144] In mice, Usp18 negatively regulates Stat1 activation and the downstream IFN-I response by interaction with Ifnar2, and mice lacking Usp18 in microglia display brain disease due to uncontrolled IFN-I signalling.[237]

Here, in a patient with clinical features of a T1I, we describe the identification of a homozygous single nucleotide transition in STAT2 (c.656C > T) which results in an alanine 219 to valine 219 substitution (p.(A219V)) in STAT2.

A role for STAT2 as an effector of IFN-I signalling was reported more than 30 years ago.[238] In 2017, another role of STAT2 was uncovered by Arimoto et al.:[143] specifically, in the later stages of IFN-I signalling, STAT2 was shown to bind to USP18, leading to a displacement of phosphorylated JAK1 from IFNAR2 and a shutdown of the IFN-I induced signalling cascade. Duncan et al. subsequently described two patients from the same family with a homozygous STAT2 mutation specifically affecting this negative feedback regulatory role of STAT2[239]. In their study, STAT2 p.(R148W) lost the ability to bind USP18, so that IFN-I signalling was abnormally activated. These patients demonstrated intracranial calcification, systemic inflammation, and multiorgan dysfunction. Shortly thereafter, Gruber et al. identified another patient with a mutation involving the same amino acid residue of STAT2.[240] In this case, the mutation, p.(R148Q), retained USP18-binding capacity, but the STAT2-USP18 dimer could not traffic to IFNAR2 (so as to displace JAK1), also resulting in enhanced IFN-I signalling. This patient shared some of the same clinical features observed in the two patients described by Duncan et al..

2.2 Results

Severe neurological disease and systemic inflammation associated with excessive IFN-I signalling in blood

We evaluated a male patient (AGS2258) born to first cousin consanguineous Turkish parents (Fig. 6a). Briefly, he presented with fever and deranged liver function at age 5 months. Cranial MRI and CT at age 8 months revealed intracranial calcification and cerebral atrophy (Fig. 6b). He began to walk at 18 months of age, and talk at age 3 years. Subsequently, he was recognized to demonstrate a progressive spastic paraparesis. Several stroke-like episodes of acute hemiparesis occurred between 2 and 3 years of age, sometimes apparently associated

temporally with fever in the context of viral infection. Later, at age 3.5 years, he experienced a pontine haemorrhage, followed by a pseudobulbar palsy and spastic dystonic tetraparesis. His head circumference at age 19 years was 49.5 cm (− 5 SD), height 150 cm (− 4 SD), and weight 40 kg (< < 1 centile). The patient is currently alive at age 23 years, with very little language ability although he can still communicate. He demonstrates a spastic dystonia and is able to walk a few steps with help but normally uses a wheelchair. The patient has not experienced any unusual susceptibility to infection, has received a full program of vaccinations (Pentavalent vaccine, MMR, BCG) without untoward effect, and does not currently manifest any overt inflammatory features. He is on no regular medication beyond trihexyphenidyl and baclofen for his neurological dysfunction.

This clinical phenotype is consistent with a severe T1I. In line with this, at age 18 years, we measured whole-blood mRNA levels of 6 ISGs by quantitative polymerase chain reaction (qPCR) (Fig. 6c).[241] Compared to the composite data derived from 29 healthy donor controls, the expression of all 6 ISGs was elevated in the patient. Further, NanoString analysis, a technique to measure individual RNA molecules, assessed at age 20 years, showed a similar up-regulation of the expression of a larger panel of 24 ISGs (Fig. 6c), indicating a persistent IFN-mediated inflammatory state.

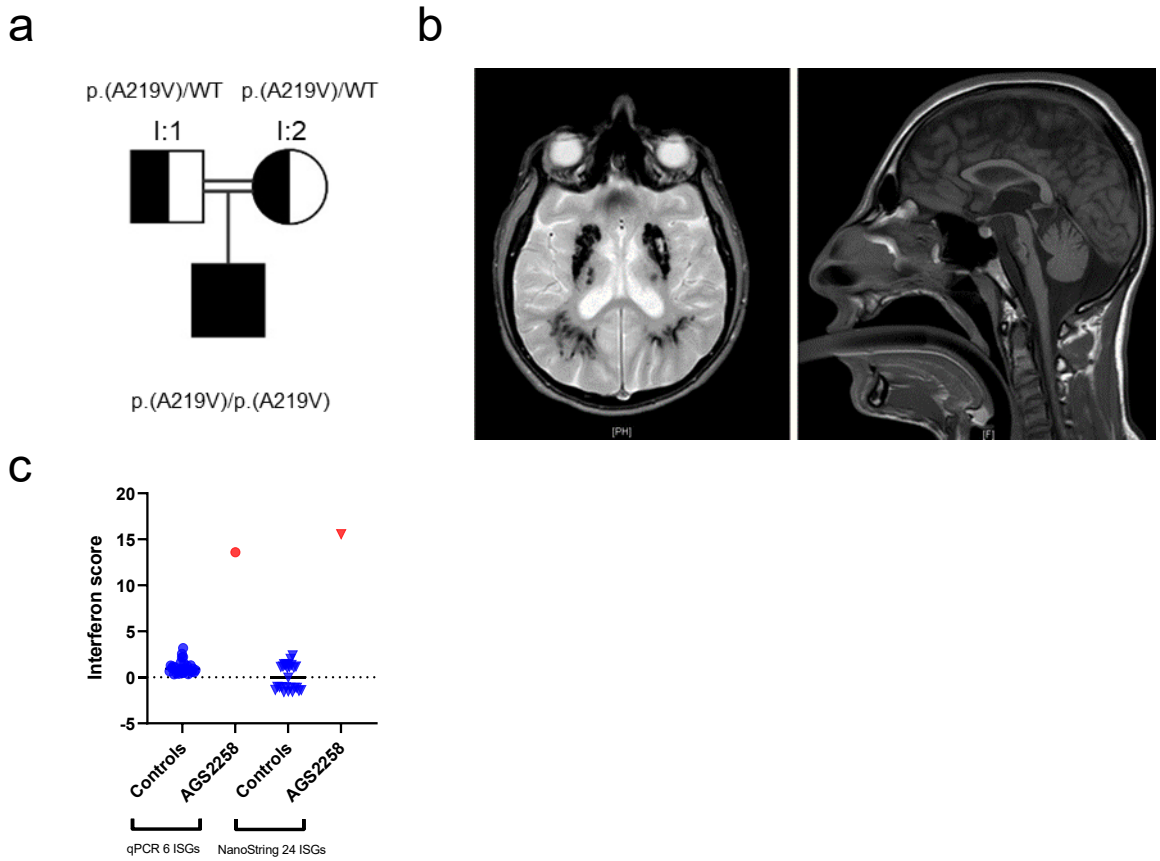

Fig. 6. Identification of a patient (AGS2258) presenting with neurological abnormalities and enhanced interferon (IFN) signalling in blood. a. Pedigree. Filled symbol indicates the affected patient, half-filled symbols indicate unaffected heterozygous parents, squares indicate males, circle indicates female, and the double line indicates consanguinity. WT, wild type. p.(A219V) and WT refer to STAT2 genotypes. b. Neuroimaging showing intracranial calcification (dark signal voids) (left: axial GE) and microcephaly, small pons and cerebellar hemispheres (right: sagittal T1). c. qPCR and NanoString analyses of IFN-stimulated genes (ISGs) in whole blood RNA isolated from the patient and healthy controls.

Homozygous missense substitution in STAT2 identified through whole-genome sequencing (WGS)

Taking a candidate gene approach to the WGS data, and concentrating on homozygous variants given the recorded parental consanguinity, we noted a very rare STAT2 variant in the homozygous state in our patient, where a single nucleotide transition c.656C > T (transcript: NM_005419.4) results in an alanine to valine substitution at residue 219. The patient's asymptomatic parents were heterozygous for this variant, which is present only once on gnomAD and is not present in the Greater Middle East Variome database. In silico analysis using SIFT and Polyphen predicted this STAT2 p.(A219V) substitution as "Deleterious" and "Possibly damaging" (score 0.698), with a CADD score of 17.81. STAT2 protein sequence

alignment across different species showed that the A219 residue is well conserved (Fig. 7a). The affected amino acid residue A219 is located in the coiled-coil domain (CCD) of STAT2 (Fig. 7b), which is essential for USP18 binding and thus restricting excessive IFN-I signalling.[143] Notably, the two previously reported homozygous STAT2 mutations affect the same R148 residue that is also in this domain.[239,240] 3D modelling of the STAT2-USP18 heterodimer showed both the amino acid residues, A219 and R148, to localize to the interface between STAT2 and USP18 (Fig. 7c), suggesting that the A219, like the R148, residue might play an essential role in mediating a STAT2-USP18 protein interaction.

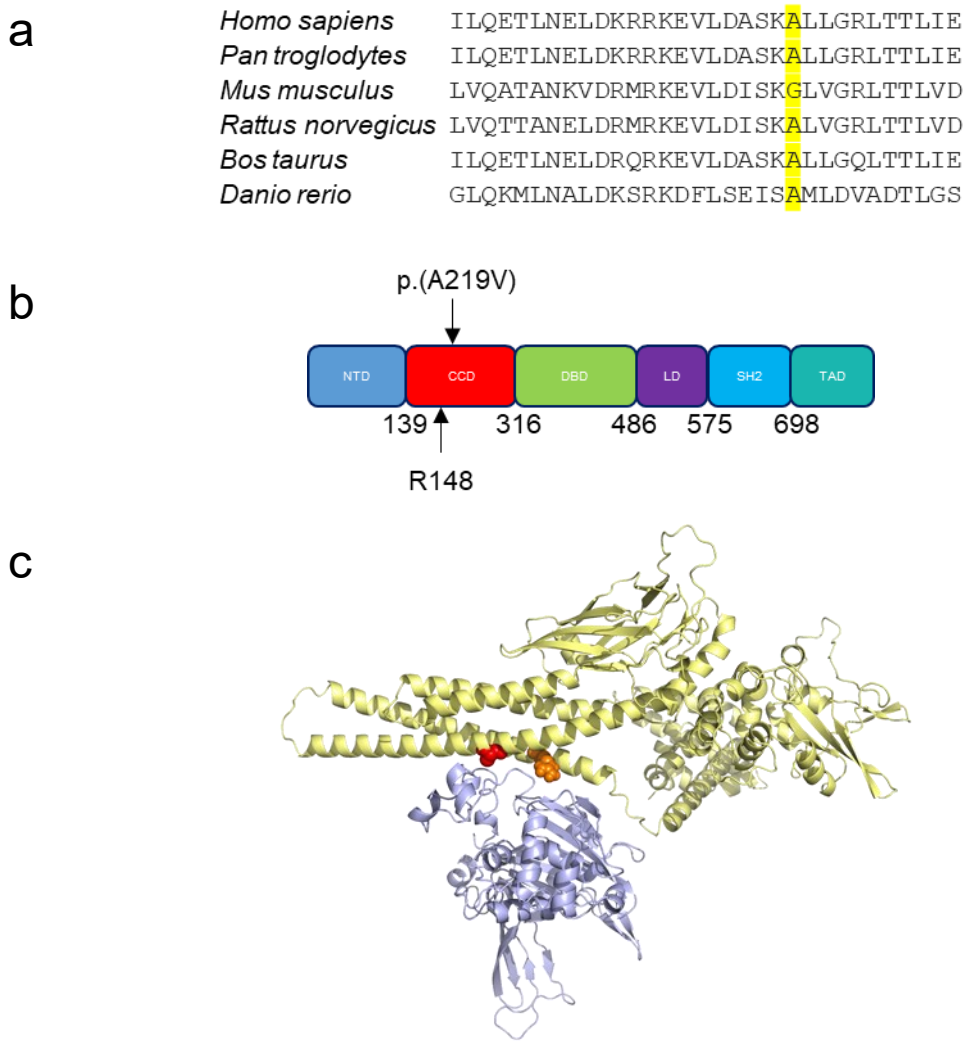

Fig. 7. STAT2 protein. a. STAT2 A219 is conserved across species, except in mouse. b. Cartoon of the protein structure of STAT2. The p.(A219V) substitution identified in AGS2258 and the R148 amino acid residue mutated in the patients described by Duncan et al. and Gruber et al. are indicated. NTD, N-terminal domain; CCD, coiled-coil domain; DBD, DNA-binding domain; LD, linker domain; SH2, Src homology 2 domain; TAD, trans-activation domain. c. Structural model showing interaction of STAT2 (yellow) and USP18 (pale blue). Alanine 219 is depicted in red and arginine 148 in orange.

STAT2 p.(A219V) leads to prolonged activation and elevated ISG expression upon IFNα2b stimulation in vitro

In order to functionally characterize the cellular and molecular consequences of the p.(A219V) substitution, and in the absence of patient material, particularly dermal fibroblasts, we performed stable lentiviral transduction of STAT2-deficient U6A human fibrosarcoma cells with STAT2 WT and mutant (p.(A219V); p.(R148W)) constructs.[242,243] Assessing the STAT2 protein level in transduced cells by western blot, all 3 transduced clones demonstrated stable STAT2 expression, with no significant difference between WT and p.(A219V) and WT and p.(R148W) (Fig. 8a, b).

Next, we performed stimulation experiments with different concentrations of IFNα2b for 30 min in cells transduced with STAT2 WT or p.(A219V). At a concentration of 250 IU/mL, STAT2 p.(A219V) showed higher phosphorylation levels compared to WT (Fig. 9a, b), indicating that the p.(A219V) mutant protein was able to transduce an IFN-I stimulus, and which was enhanced. We then performed qPCR analysis in transduced cells stimulated with 250 IU/mL IFNα2b for 16 h (Fig. 8c; Fig. 10a). It is notable that at baseline, i.e., without IFNα2b stimulation, no difference in ISG transcripts was observed between cells transduced with STAT2 WT, p.(A219V) (Fig. 8c) or the previously described mutant p.(R148W) (Fig. 10a). However, compared to cells transduced with STAT2 WT, cells transduced with p.(A219V) displayed elevated levels of IFI27, IFIT1, ISG15, MX1, RSAD2, and USP18 transcripts after IFNα2b stimulation (Fig. 8c). Similarly, in agreement with the findings of Duncan et al.,[239] cells transduced with p.(R148W) showed elevated ISG transcript expression after IFNα2b stimulation (Fig. 10a).

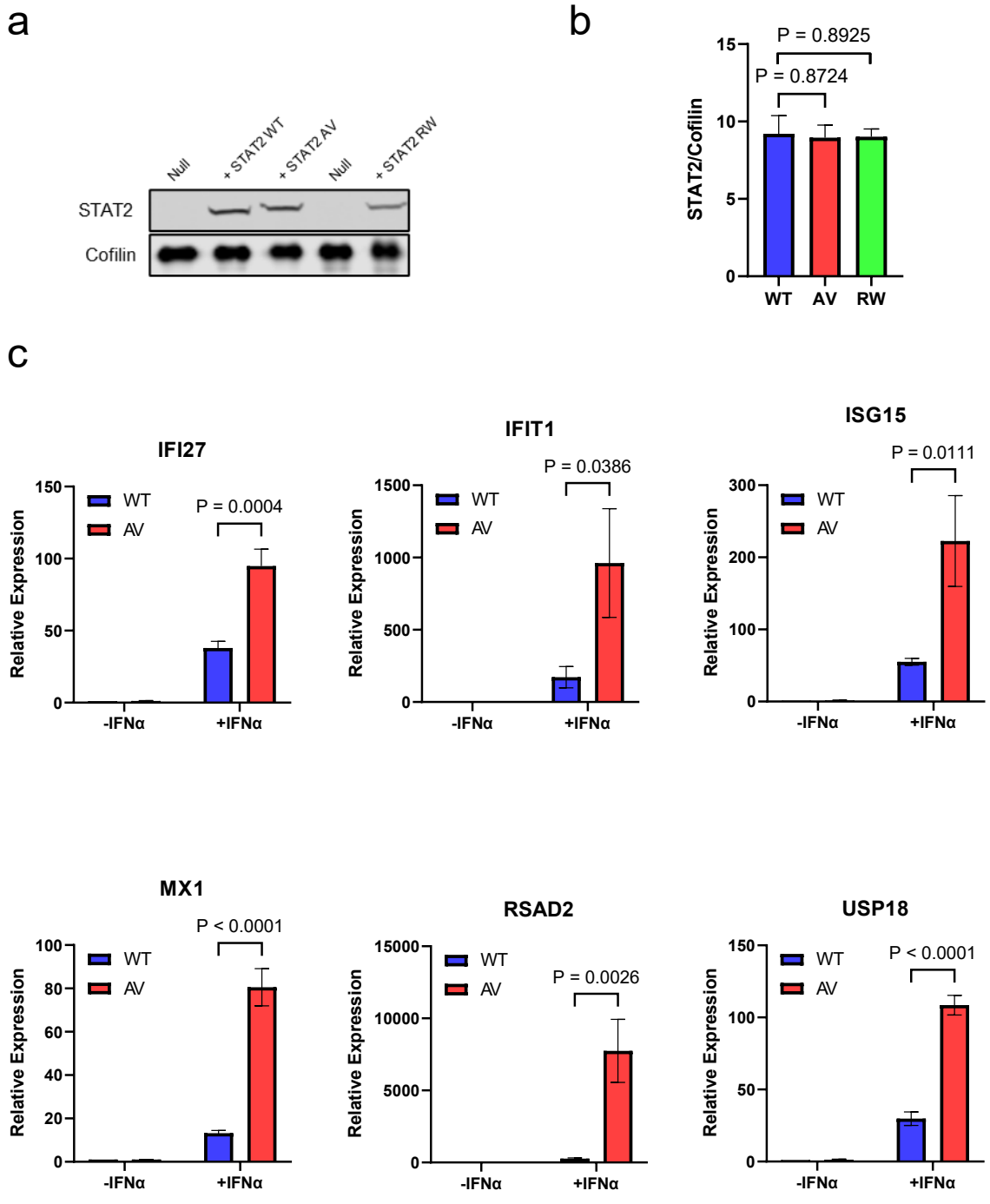

Fig. 8. Cells transduced with the STAT2 p.(A219V) substitution display heightened sensitivity to IFN stimulation. a. Immunoblotting analysis of U6A cells stably transduced with STAT2 WT, p.(A219V) ("AV") or p.(R148W) ("RW"). b. Densitometry quantification as in a. n = 3; unpaired t test. c. qPCR analysis of ISG transcription in U6A cells stably transduced with either STAT2 WT or p.(A219V) and stimulated for 16 h with 250 IU/mL IFNα2b. n = 3; two-way ANOVA with Sidak's multiple comparisons test. d. ISG expression in time-course following 250 IU/mL IFNα2b stimulation. e. Densitometry quantification as in d. MX1, n = 4; USP18, n = 4; ISG15, n = 2; unpaired t test. f. Immunofluorescence analysis of cells transduced with STAT2 WT or p.(A219V) and stimulated with 250 IU/m IFNα2b for 24 h. Blue, DAPI; red, STAT2. Scale bar represents 20 micrometers g. Fluorescence signal intensity quantification as in f. n = 2; a total of 346 cells were quantified; two-way ANOVA with Sidak's multiple comparisons test.

d

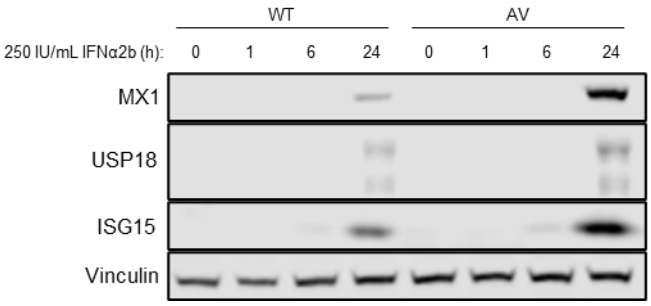
WT
AV
250 IU/mL IFNα2b (h):
0 1 6 24 0 1 6 24
MX1
USP18
ISG15
Vinculin

e

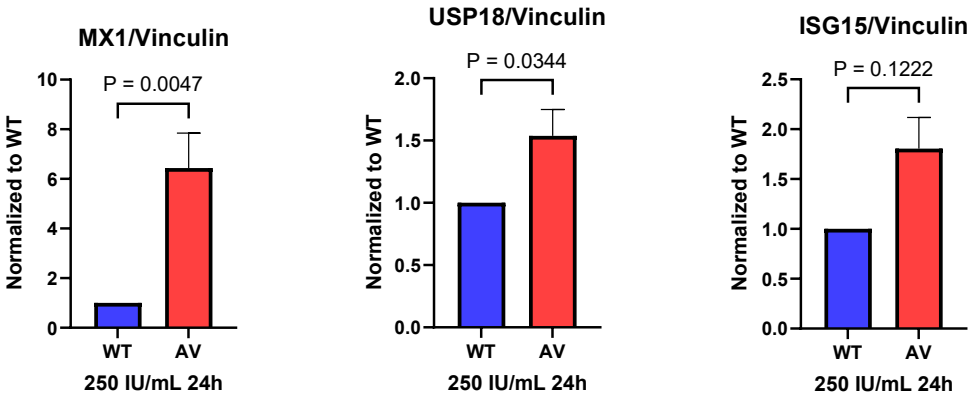
MX1/Vinculin
P = 0.0047
Normalized to WT
WT AV
250 IU/mL 24h
USP18/Vinculin
P = 0.0344
Normalized to WT
WT AV
250 IU/mL 24h
ISG15/Vinculin
P = 0.1222
Normalized to WT
WT AV
250 IU/mL 24h

f

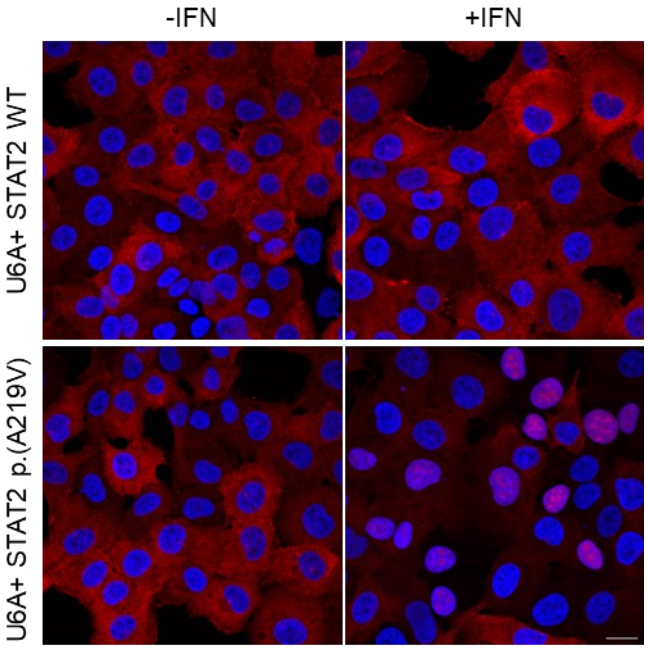
-IFN
+IFN
U6A+ STAT2 WT
U6A+ STAT2 p.(A219V)

g

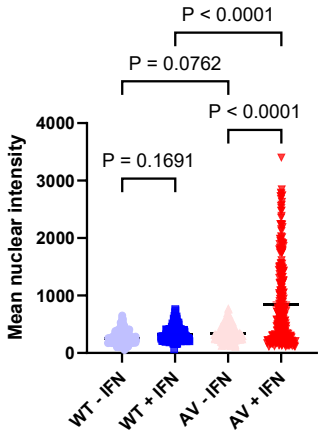
P < 0.0001
P = 0.0762
P < 0.0001
P = 0.1691
Mean nuclear intensity
WT - IFN
WT + IFN
AV - IFN
AV + IFN

Next, we carried out a time-course experiment following stimulation with 250 IU/mL IFNα2b in WT and p.(A219V) cells (Fig. 8d). In line with the qPCR results, in western blot analysis, at the 24-h time point, p.(A219V) cells expressed higher amounts of MX1, USP18, and ISG15 proteins compared to STAT2 WT cells (Fig. 8e).

ISG transcription and expression are driven by the nuclear translocation of ISGF3, a hetero-trimer complex composed of p-STAT1, p-STAT2, and IRF9. To further assess if enhanced ISG expression in p.(A219V) cells was caused by prolonged STAT2 activation, we performed immunofluorescence in WT and p.(A219V) cells stimulated with 250 IU/mL IFNα2b for 24 h (Fig. 8f, g). In these experiments, STAT2 WT cells showed a STAT2 cytoplasmic staining. In contrast, cells with STAT2 p.(A219V) showed both cytoplasmic and nuclear STAT2 staining, suggesting prolonged IFNα2b signalling activation.

In summary, the above data indicate that the p.(A219V) mutation is able to transduce an IFN-I stimulus, of which the response is heightened and prolonged compared to STAT2 WT.

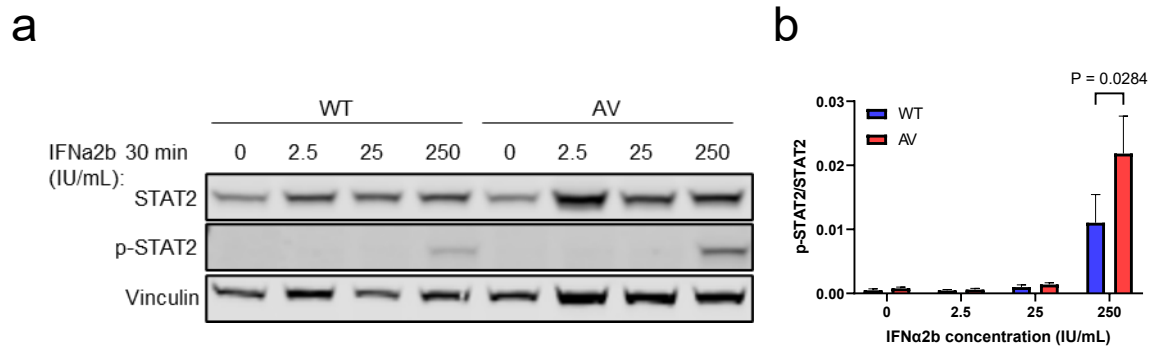

Fig. 9. STAT2 p.(A219V) demonstrates heightened proximal activation upon a short-time IFN stimulation. a. Immunoblotting analysis of cells stably transduced with STAT2 WT or p.(A219V) (‘‘AV’’) and stimulated with 0, 2.5, 25, or 250 IU/mL IFNα2b for 30 min. b. Densitometry quantification as in a. n=3; two-way Anova with Sidak’s multiple comparisons test.

STAT2 p.(A219V) fails to induce IFNAR2-mediated negative feedback due to defective USP18 binding

STAT2 p.(A219V) retains the ability to transduce IFN-I signalling, associated with a prolonged and enhanced response to an IFN-I stimulus compared to STAT2 WT. We hypothesized the cause of this disturbance to be an impairment of the role of STAT2 p.(A219V) in negative feedback signalling. To explore this possibility, a priming experiment was designed (Fig. 11a). Here, we first primed WT and p.(A219V) cells with 250 IU/mL IFNα2b for 12 h, washed them extensively, and let the cells rest for 36 h. Then, we re-stimulated the cells with a second dose of 250 IU/mL IFNα2b for 1 h. In these experiments, IFNα2b-induced p-STAT1 and p-STAT2 did not increase following a second stimulation in WT cells. In contrast, in p.(A219V) cells, phosphorylation of STAT1 and STAT2 was as high as in unprimed cells (Fig. 11b, c), indicating that STAT2 p.(A219V) failed to induce IFNAR2 desensitization. In keeping with this, MX1 and ISG15 expression remained elevated in p.(A219V) cells compared to WT cells, even 36 h after the first IFNα2b stimulation was removed (Fig. 11b, lane 3 and lane 7; 11c). Similarly, cells with the previously described p.(R148W) mutant also showed persistent STAT1 and STAT2 phosphorylation, and elevated MX1 and ISG15 protein expression (Fig. 10b, c), upon a second IFNα2b stimulation.

To explore the basis of this impaired negative feedback response, we investigated the role of USP18. USP18 is a negative regulator in IFN-I signalling, mediating IFNAR2 desensitization in combination with STAT2.[143] Since USP18, itself an ISG product, was induced in p.(A219V) cells to a higher amount (Fig. 8d, e), we reasoned that it was a defective STAT2-USP18 binding, rather than a lack of USP18, that was responsible for the excessive IFN-I signalling. To investigate this possibility, we performed co-immunoprecipitation in human embryonic kidney (HEK) 293FT cells transiently transfected with STAT2 WT or p.(A219V), together with USP18 (Fig. 11d). These experiments showed a more than 50% decrease in USP18 pulled

down by STAT2 p.(A219V) compared to WT (Fig. 11e), indicating defective binding of STAT2 p.(A219V) to USP18.

a

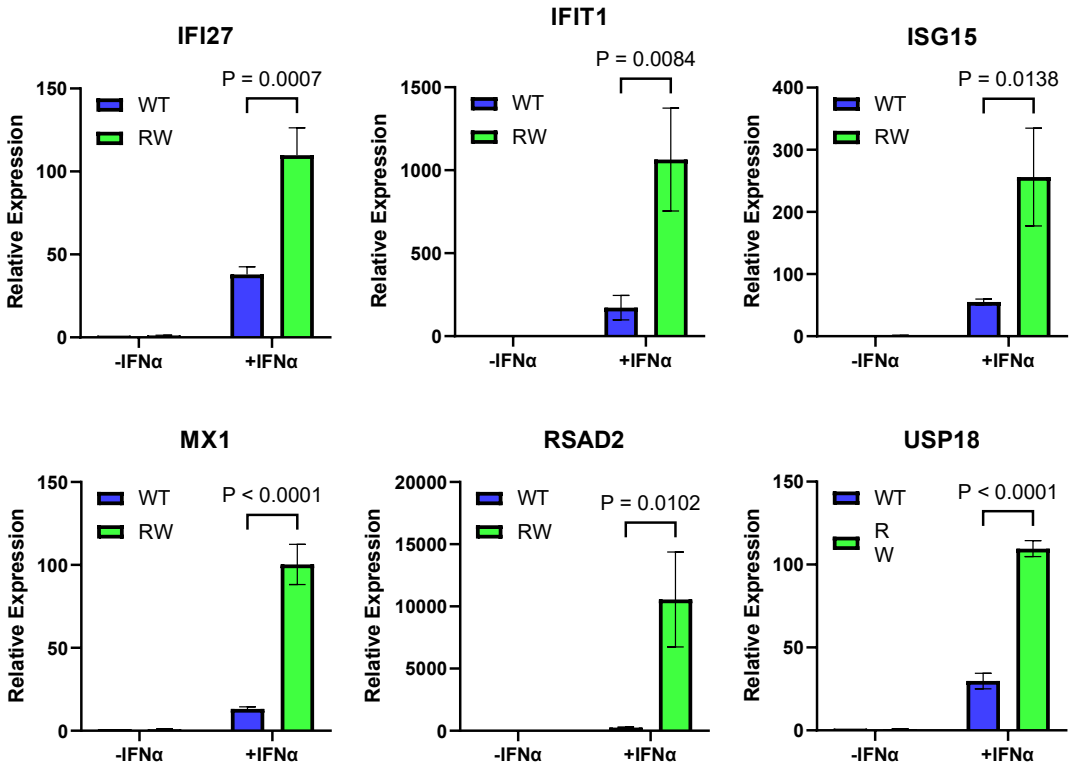

b

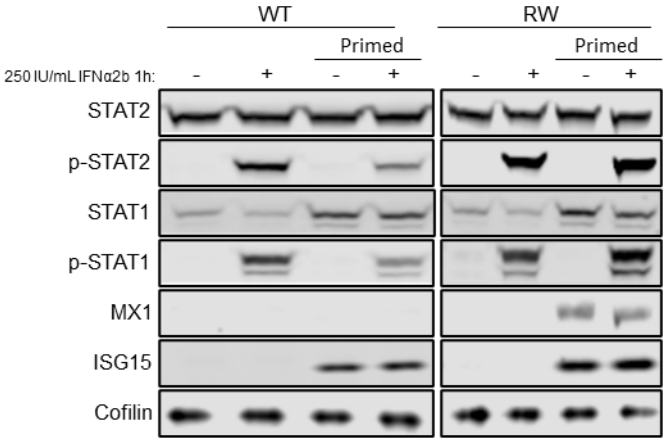

c

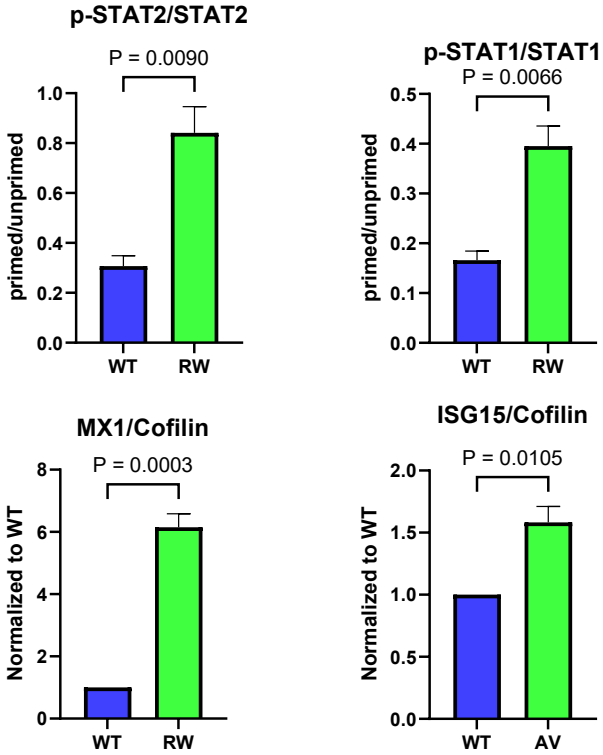

Fig. 10. Enhanced IFN signalling and ISG expression in cells transduced with STAT2 p.(R148W). a. qPCR analysis of ISG transcription in U6A cells stably transduced with either STAT2 WT or p.(R148W) ('RW') and stimulated for 16 h with 250 IU/mL IFNα2b. n = 3; two-way Anova with Sidak's multiple comparisons test. b. Immunoblotting analysis to assess the negative regulatory function of STAT2 p.(R148W) by stimulating cells with (''primed''), or without, a priming stimulus. (Blots for p.(R148W) were obtained in the same experiment alongside WT and p.(A219V). Blots for WT shown here are the same blots in Fig. 11b.) c. Densitometry quantification as in b. n=3; unpaired t test.

a

b

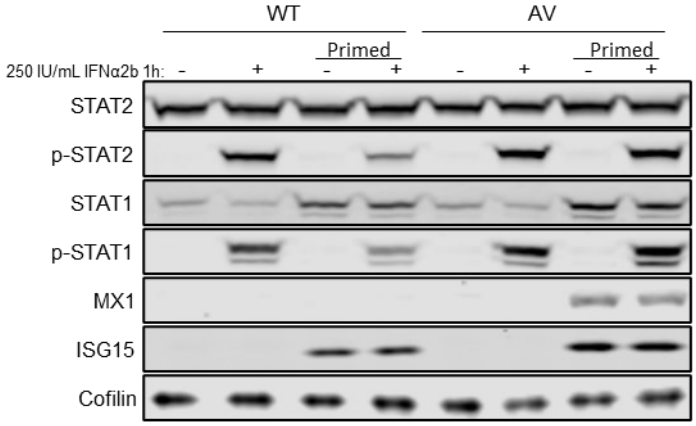

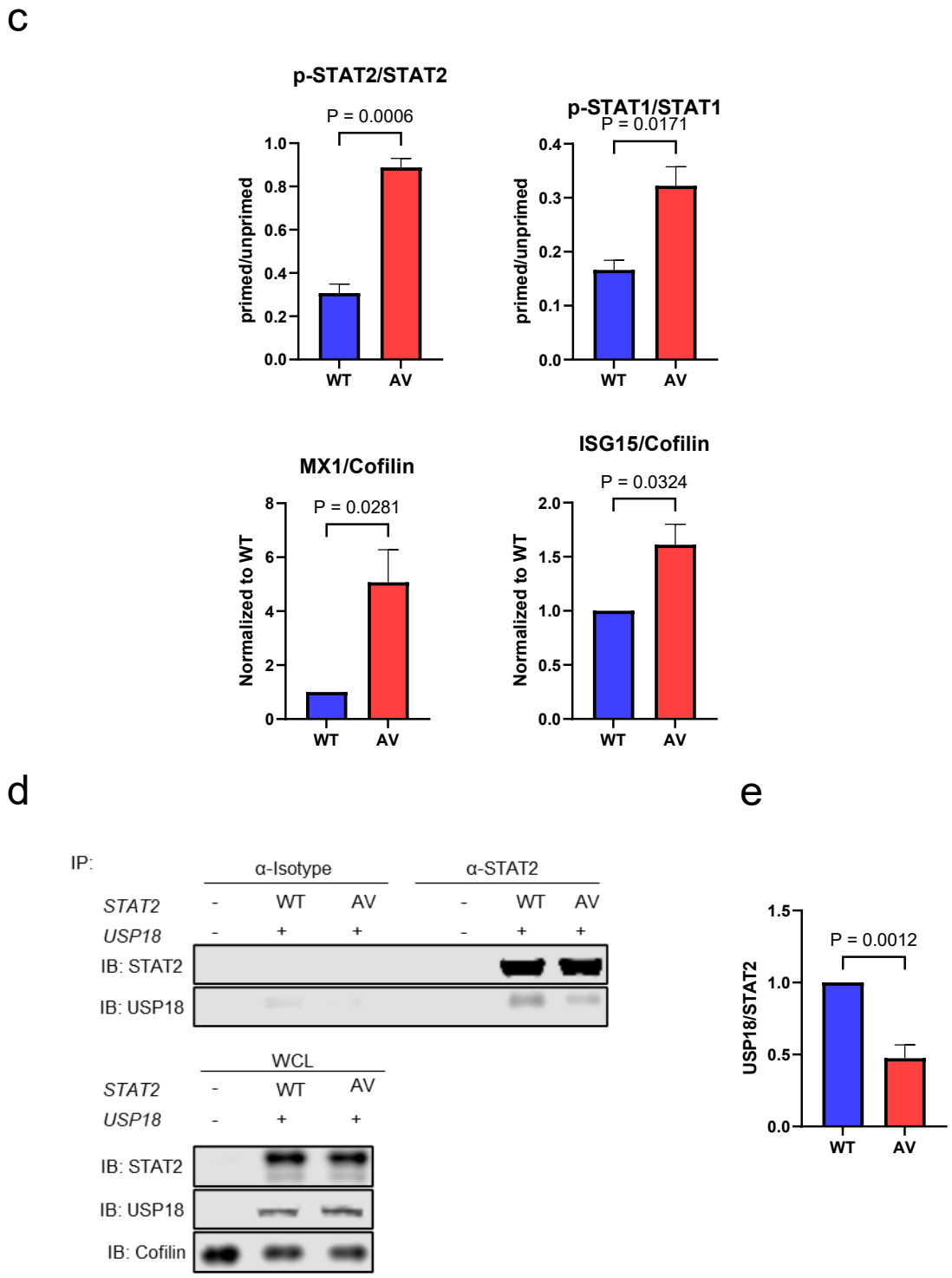

Fig. 11. Cells transduced with the p.(A219V) substitution lose the capacity to restrict IFN signalling upon a second stimulation due to defective binding with USP18. a. Experimental design. b. Immunoblotting analysis of negative regulation function of STAT2 p.(A219V) ("AV") by stimulating cells with (''primed''), or without, a priming stimulus. c. Densitometry quantification as in b. n = 3; unpaired t test. d. Co-immunoprecipitation of USP18 by STAT2 in HEK 293FT cells transiently transfected with STAT2 WT or p.(A219V), together with USP18. IB, immunoblot. WCL, whole-cell lysate. e. Densitometry quantification as in d. USP18/STAT2, ratio to WT; n = 4; unpaired t test.

Collectively, the above data suggest a model in which the homozygous STAT2 p.(A219V) mutation disrupts the interaction of STAT2 with USP18, leading to a failure of negative feedback regulation of IFN-I signalling and prolonged IFNAR activation and enhanced ISG expression (Fig. 12). In silico deep mutagenesis of the predicted STAT2-USP18 interface highlighted a further 3 amino acid residues (E144, D151, and R223) as critical to mediating this interaction (Fig. 13), all clustering in the STAT2 CCD domain in close proximity to the described mutant A219 and R148 residues.

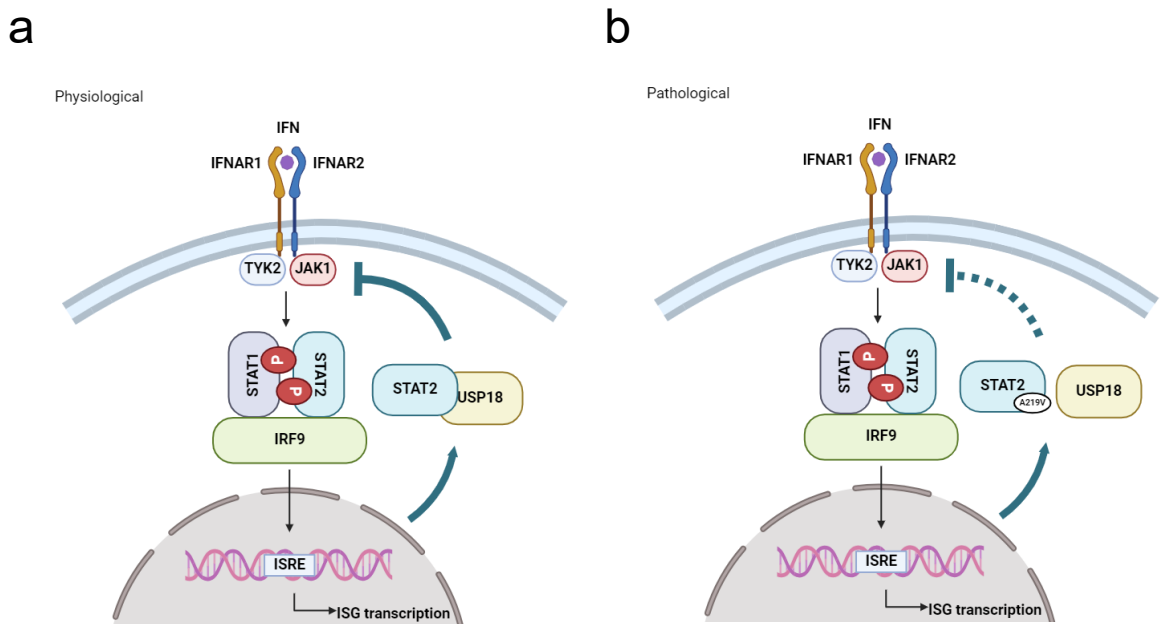

Fig. 12. Model of type I interferon (IFN) signalling pathway and regulation. a. Upon IFN binding, IFNAR1 and IFNAR2 activate TYK2 and JAK1, respectively, via phosphorylation, which in turn phosphorylate STAT1 and STAT2. Phosphorylated STAT1 and STAT2, together with IRF9, form the ISGF3 complex that enters the nucleus to bind genes with an ISRE element, thereby initiating an ISG transcriptional cascade. Under physiological conditions, in the later stages of the IFN response, USP18, can bind STAT2 and together, they displace JAK1 from IFNAR2, thus restricting IFN signalling. b. When STAT2 loses the ability to bind USP18, e.g., due to STAT2 p.(R148W) or p.(A219V), the negative regulation of IFN signalling is impaired, leading to an enhanced and prolonged IFN response. Graphs were created on BioRender.

a

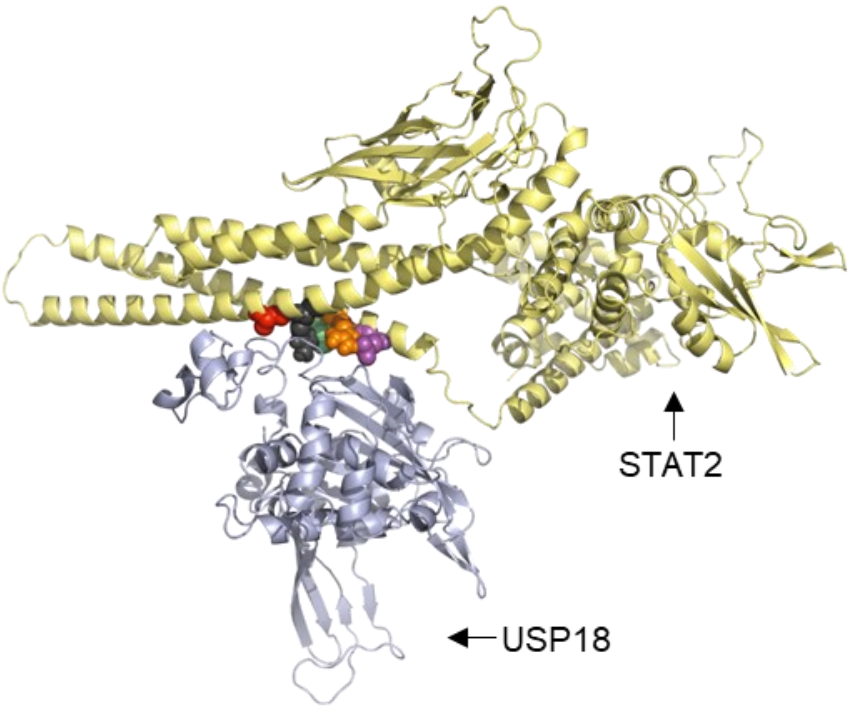

Fig. 13. STAT2-USP18 structural model. a. STAT2 is depicted in yellow and USP18 in pale blue. The reported amino acid residue arginine 148 (orange) and the alanine 219 (red) in this study are highlighted, along with glutamic acid 144 (purple), aspartic acid 151 (green) and arginine 223 (black), in whom mutations are predicted to disrupt the STAT2-USP18 interaction similar to A219 and R148.

2.3 Summary and discussion

In this study, we report a newly identified homozygous STAT2 mutation in a patient with features of a T1I. As an essential protein with dual functions in both transducing and restricting IFN-I signalling, deleterious STAT2 mutations are expected to be rare. Complete STAT2 deficiency can result in a primary immune deficiency and life-threatening viral disease.[244] In contrast, biallelic mutations affecting the negative regulatory function of STAT2 cause a T1I state, where patients demonstrate auto-inflammation.[239,240] To our knowledge, only three patients from two families with homozygous STAT2 mutations have been reported on PubMed to date,[239,240] in both cases involving the R148 residue. Of note, the three patients described in these previous reports all died in infancy. In contrast, the patient in the current study has survived into his third decade. While this observation might relate to a difference in the severity

of the mutations involved, our analysis does not support that possibility (see Figs. 8 and 10). Alternatively, there may be related to other genetic variants (susceptibility/protective alleles), and/or environmental exposures. We note that since only four cases (including ours) have been described to date, it is too early to draw conclusions as to the breadth of phenotype associated with such mutations in STAT2.

The data in this study indicate that mutant STAT2 p.(A219V) retains the ability to transduce IFN-I signalling, yet its negative regulatory function is impaired due to defective USP18 binding, much like the reported p.(R148W) mutation.[239] In contrast, the other reported mutation, p.(R148Q), was described to retain USP18-binding capacity, but the STAT2 p.(R148Q)-USP18 heterodimer could not traffic appropriately to IFNAR2 to displace JAK1.[240] Despite the described difference in USP18-binding capacity, in both cases, IFN-I signalling was prolonged due to loss of negative IFN-I regulation by STAT2-USP18. R148 and A219 are located within the CCD domain of STAT2, critical to the interaction of STAT2 with USP18 and thus inhibition of IFN-I signalling,[143] with in silico mutagenesis of the predicted STAT2-USP18 interface highlighting a further 3 amino acid residues (E144, D151, and R223) as potentially critical to this interaction, and in which mutations might be expected to result in prolonged IFN-I signalling due to loss of negative regulation by STAT2-USP18. Of note, defective negative feedback regulation of IFN-I signalling has also been reported in the case of a USP18 mutation, USP18-I60N, resulting in a T1I phenotype due to an impaired interaction of USP18-I60N and STAT2.[219]

In their report, Gruber et al. indicated the p.(R148Q) mutation to confer a ‘‘gain-of-function’’.[240] In our opinion, while an up-regulation of IFN-I signalling is observed, from a molecular perspective, the consequence of the substitution is a loss of a negative regulatory function of STAT2 on IFN-I signalling. Here, we focus on molecular pathology, so that in agreement with the definition set out by Backwell and Marsh,[245] and with the International Union of Immunological Societies 2022 update of the phenotypical classification of human inborn errors of immunity,[246,247] we refer to the mutations at R148 and A219 as ‘‘loss-of-function’’.

Another class of mutations observed in STAT2 results in loss of protein expression, with STAT2 deficiency causing a primary immunodeficiency and susceptibility to severe viral diseases.[244,248,249] Notably, in a recent report, Gothe et al. described a complete deficiency of STAT2 in patient cells to suppress,[186] but not completely abrogate, IFN-I signalling after IFNα2b stimulation. In this scenario, downstream IFN-I signalling was abnormally prolonged, as evidenced by JAK1 and STAT1 phosphorylation kinetics, in line with a failure of STAT2-USP18-mediated negative regulation. Induction of classical ISGs such as MX1, RSAD2, and IFI44L by IFN-I was suppressed. However, genes with a gamma-activated sequence (GAS) displayed elevated expression, mimicking the IFN-γ effect, which utilised p-STAT1 dimer as a transcriptional activator. These findings were suggested to explain the "paradoxical" observation of autoinflammation in such cases. All of these reports highlight the importance, and complexity, of the regulation of IFN-I signalling by STAT2.[250]

The patients carrying loss-of-inhibitory-function mutations in STAT2 (p.(A219V) and p.(R148Q/W)) display clinical features reminiscent of AGS, a paradigm T1I. More specifically, these patients demonstrated intracranial calcification, systemic autoinflammation, and multi-organ dysfunction. Similarly, USP18 deficiency underlies a particularly severe form of T1I associated with unrestrained systemic autoinflammation. To date, ten patients have been reported to display USP18 deficiency, with eight of them dying perinatally.[144,219-221] Of note, ISG15 has been shown to stabilise USP18 protein structure,[145,146] thus contributing to the USP18-mediated negative regulation of IFN-I signalling. Therefore, ISG15 deficiency has been described to cause T1I as well as a specific type of immune deficiency. Patients can display intracranial calcification (in line with T1I) and Mendelian susceptibility to mycobacterial disease (MSMD).[183,251] A subset of patients also demonstrate recurrent skin lesions associated with hyperinflammation in keratinocytes, endothelial and myeloid cells (interestingly, these skin lesions are quite distinct from the classical chilblain like vasculitic skin involvement seen in AGS, SAVI and other T1Is).[252] The broad spectrum of clinical phenotype in ISG15 deficiency highlights the protein's multifaceted functions. In addition to being able to stabilise intracellular

USP18 protein, ISG15 is secreted extracellularly by granulocytes and functions as a cytokine to activate lymphocytes for IFNγ production, which is critical to the anti-mycobacterial response.[253] ISG15 deficiency deceases IFNγ secretion and confers a MSMD state.[251] A comparison of disease phenotypes and molecular mechanisms in STAT2 loss-of-inhibitory-function, USP18 deficiency, and ISG15 deficiency can be found in Table 1.

2.4 Materials and methods

WGS

WGS was performed by the Commissariat à l'énergie atomique et aux énergies alternatives (CEA), as part of a collaboration between CEA-IBFJ/CNRGH, Institut Imagine, INSERM and Université Paris Descartes. One microgram of genomic DNA was used to prepare a library for WGS using the Illumina TruSeq DNA PCR-free library preparation kit, according to the manufacturer's instructions. After normalisation and quality control, qualified libraries were sequenced on a HiSeq X Five platform (Illumina), as paired-end 150 base pair reads. One lane of the HiSeq X Five flow cell was used for each sample to reach an average sequencing depth of 30 ×. The sequence quality parameters were assessed throughout the sequencing run, and standard bioinformatics analysis of sequencing data was based on the Illumina pipeline to generate FASTQ files for each sample. Variants were filtered according to a frequency on gnomAD of < 0.0001 and < 10 occurrences in our in-house variant database.

Cells and cytokine measurements

STAT2-deficient human fibrosarcoma cell line U6A and human embryonic kidney (HEK) 293FT cells were both cultured in Dulbecco's modified Eagle's medium (DMEM) supplemented by 10% fetal calf serum (FCS) and 1% penicillin/streptomycin (p/s). Unless otherwise specified, human recombinant IFNα2b (11105–1, PBL Assay Science) was used at 250 IU/mL.

Interferon signature testing

The analysis of 24 genes and 3 housekeeping genes was conducted using the NanoString customer designed CodeSets according to the manufacturer's recommendations (NanoString Technologies, Seattle, WA). One hundred nanograms of total RNA was loaded for each sample. Agilent Tapestation was used to assess the quality of the RNA. Data were processed with nSolver software (NanoString Technologies Seattle, WA). The data were normalised relative to the internal positive and negative calibrators, the three reference probes, and healthy control samples. The median of the 24 probes for each of 29 healthy control samples was calculated. The mean NanoString score of 29 healthy controls + 2 SD of the mean was calculated. Scores above this value (2.75) were designated as positive. Probes were *IFI27*, *IFI44L*, *IFIT1*, *ISG15*, *RSAD2*, *SIGLEC1*, *CMPK2*, *DDX60*, *EPSTI1*, *FBXO39*, *HERC5*, *HES4*, *IFI44*, *IFI6*, *IFIH1*, *IRF7*, *LAMP3*, *LY6E*, *MX1*, *NRIR*, *OAS1*, *OASL*, *OTOF*, and *SPATS2L*. Reference probes were *HPRT1*, *NRDC*, and *OTUD5*. Generation of an interferon signature by qPCR of a 6-gene panel is as described in Rice et al. (and see the "RNA isolation and qPCR" section below for further details of the probes used).[241]

Lentiviral constructs, site-directed mutagenesis, and lentiviral transduction

The bicistronic lentivirus vector (pHR-SIN-CSGW) containing the full length of WT human STAT2 or p.(R148W), as well as pLenti6/V5 vector containing the full length of WT human USP18, was a kind gift from Dr. Christopher Duncan (Newcastle University, UK). Site-directed mutagenesis on pHR-SIN-CSGW-STAT2 WT to generate p.(A219V) mutant was carried out with Q5 site-directed mutagenesis kit (E0552S, New England BioLabs) according to the manufacturer's instructions and verified by Sanger sequencing. Primer sequences for mutagenesis were GCCTCCAAAGTACTGCTAGGC (forward) and ATCCAGCACCTCCTTTCTC (reverse).

Lentiviruses were produced by co-transfection of pCMV-VSV-G (Addgene plasmid no. 8454), psPAX2 (Addgene plasmid no. 12260), and lentiviral transfer plasmid (pHR-SIN-CSGW-STAT2 WT, pHR-SIN-CSGW-STAT2 p.(A219V), or pHR-SIN-CSGW-STAT2 p.(R148W)) in HEK 293FT cells using Lipofectamine 2000 Transfection Reagent (11668019, Invitrogen). 24

hours post-transfection, cells were refreshed with DMEM supplemented with 10% FCS and 1% p/s. 48 hours post-transfection, virus-containing supernatant was collected and filtered through 0.45-µm sterile filter. U6A cells were then incubated with virus-containing supernatant supplemented with 8 µg/mL polybrene (TR-1003-G, Merk Millipore) for 24 h, and cells were then refreshed with DMEM supplemented with 10% FCS and 1% p/s. 48 hours post-transduction, cells were subjected to selection with puromycin (2.0 µg/mL) (A11138-03, Gibco).

RNA isolation and qPCR

U6A cells were lysed in TRIzol reagent (15596026, Thermo Fisher Scientific), and RNA was subsequently extracted with Direct-zol RNA MiniPrep kit (R2050, Zymo Research) following the manufacturer's instructions. RNA from whole-blood samples collected in PAXgene tubes (672165, PreAnalyticX) was extracted using PAXgene blood RNA kit (762174, PreAnalyticX). RNA was reverse-transcribed using high-capacity cDNA reverse transcription kit (4368814, Thermo Fisher Scientific). The expression of ISGs (*MX1*, *ISG15*, *USP18*, *IFI27*, *IFIT1*, *IFI44L*, *SIGLEC*, and *RSAD2*), relative to the *ACTB* and *GAPDH* housekeeping genes, was analysed by TaqMan quantitative real-time PCR (TaqMan Fast Universal PCR Master Mix (2 ×) No AmpErase UNG, 4352042, Thermo Fisher Scientific) on a 7900HT Sequence Detection System (Applied Biosystems). The TaqMan probes were Hs00895608_m1 (*MX1*), Hs00192713_m1 (*ISG15*), Hs00276441_m1 (*USP18*), Hs01086370_m1 (*IFI27*), Hs00356631_g1 (*IFIT1*), Hs00199115_m1 (*IFI44L*), Hs00988061_g1 (*SIGLEC1*), Hs01057264_m1 (*RSAD2*), Hs01060665_g1 (*ACTB*), and Hs02786624_g1 (*GAPDH*). The relative levels of ISG transcription were calculated by the ΔΔCt method, relative to the mean values for the mock-treated controls or healthy donors.

Immunoblotting

Whole-cell lysates for immunoblotting were prepared by incubating cells for 1 h at 4 °C with rotation in lysis buffer (25 mM Tris–HCl, pH 8.0, 1% NP-40, 150 mM NaCl, 1.5 mM MgCl2, 0.05% SDS, 0.5% sodium deoxycholate, supplemented with protease inhibitor cocktail

(04693159001, Roche)). Samples were then centrifuged at 12,000 rpm at 4 °C for 10 min. Supernatant containing soluble protein fraction was collected, and protein concentration was measured with Pierce BCA protein assay kit (23227, Thermo Fisher Scientific).

Thirty micrograms of protein from each sample with Pierce Lane marker reducing sample buffer (39000, Thermo Fisher Scientific) was denatured at 95 °C for 10 min and resolved on NuPage 4–12% Bis–Tris Gels (NP0336BOX, Invitrogen) in NuPage MOPS SDS running buffer (NP0001, Invitrogen). Proteins were then transferred onto the nitrocellulose membrane of an iBlot 2 NC Regular Stack (IB23001, Invitrogen) for 15 min at 15 V using the iBlot 2 Dry Blotting System (IB21001, Invitrogen). Membranes were blocked in intercept (TBS) blocking buffer (927–60001, LI-COR) for 30 min at room temperature and incubated overnight at 4 °C with primary antibodies of interest in blocking solution supplemented with 0.1% Tween 20 (EC-607, National Diagnostics). Primary antibodies used were STAT2 (sc-1668, Santa Cruz Biotechnology), p-STAT2 (07–224, Merk/Millipore), STAT1 (9176, Cell Signaling Technology), p-STAT1 (7649, Cell Signaling Technology), MX1 (ab95926, abcam), ISG15 (NBP1-04310, Novus Biologicals), USP18 (4813 s, Cell Signaling Technology), Cofilin (5175 s, Cell Signaling Technology), and Vinculin (13901, Cell Signaling Technology). IRdye-conjugated anti-mouse (926–68070, LI-COR) or anti-rabbit (925–32211, LI-COR) secondary antibodies diluted in intercept (TBS) blocking buffer plus TBS supplemented with 0.1% Tween 20 (TBS-T) (intercept (TBS) blocking buffer: TBS-T = 1:2 v/v) were used to detect targeted proteins. Membranes were scanned using the Odyssey CLx System (LI-COR). Densitometry quantification and analyses were performed using the Image Studio Lite software v.5.2 (LI-COR).

Co-immunoprecipitation (co-IP)

HEK 293FT cells were transiently transfected with pLenti6/V5-USP18 together with either pHR-SIN-CSGW-STAT2 WT or pHR-SIN-CSGW-STAT2 p.(A219V) using Lipofectamine 2000 Transfection Reagent and Opti-MEM Reduced Serum Medium, GlutaMAX Supplement (51985034, Gibco). 6 hours post-transfection, cells were refreshed with DMEM supplemented

with 10% FCS and 1% p/s. 24 hours post-transfection, cells were lysed in IP buffer (50 mM Tris–HCl, pH 7.5, 0.5% NP-40, 200 mM NaCl, 10% glycerol, 1 mM EDTA) supplemented with protease inhibitor cocktail (04693159001, Roche). Lysates were collected by centrifugation at 12,000 rpm at 4 °C for 10 min, and soluble fractions are collected to measure protein concentration with Pierce BCA protein assay kit. Lysates with the same amount of protein for each sample were then incubated with anti-STAT2 (A-7) antibody (sc-1668, Santa Cruz Biotechnology) overnight at 4 °C with rotation. Lysates were then incubated with Dynabeads Protein G (10003D, Invitrogen) for 2 h at 4 °C with rotation. Immunoprecipitates were eluted with Pierce Lane marker reducing sample buffer before being subjected to immunoblotting as previously described.

Immunofluorescence

Stably transduced U6A cells (with either pHR-SIN-CSGW-STAT2 WT or pHR-SIN-CSGW-STAT2 p.(A219V)) grown on coverslips were fixed with 4% paraformaldehyde in PBS for 15 min at room temperature, before being permeabilized with 0.1% Triton X-100 (T9284, Sigma-Aldrich) in PBS and then blocked in 1% normal goat serum in PBS. Cells were incubated for 1 h at room temperature with anti-STAT2 (A-7) primary antibody (1:100 v/v in PBS; sc-1668, Santa Cruz Biotechnology) and then washed 3 times with PBS. Secondary antibody incubation was performed with goat anti-mouse Alexa Fluor 594 (4 μg/mL; A11032, Thermo Fisher Scientific) for 1 h at room temperature in the dark followed by 3 times of PBS wash. Nuclear staining was then performed with 4′,6-diamidino-2-phenylindole (DAPI; 1 μg/mL; Thermo Fisher Scientific) for 5 min at room temperature in the dark followed by 3 times of PBS wash. Coverslips were mounted on glass slides with ProLong Gold anti-fade reagent (P36934, Invitrogen). Cells were imaged with a Stellaris confocal microscope with a 63 × oil immersion objective (Leica). STAT2-deficient cells were used to demonstrate the specificity and lack of non-specific background for this staining method. Image analysis was performed with ImageJ.

Structural modelling of the STAT2-USP18 interaction

Deletion mutagenesis in combination with coimmunoprecipitation assays has previously identified the amino acid region 138–572 of STAT2 and 51–112 of USP18 to be important for their interaction.[143] More recently, arginine 148 in STAT2 has been suggested to be directly involved in USP18 binding.[239] Based upon these criteria, molecular docking was performed to obtain a potential model of the interaction. The structure of STAT2 was obtained from the AlphaFold database removing residues 709–851 of the highly disordered C terminus. Then, a homology model of USP18 was generated with Phyre2,[254] using the available experimental structures in the Protein Data Bank.[255] ClusPro was adopted to dock the two proteins by deriving loose restraints in the following manner:[256] leucine 103 was deemed to be the residue closest to the centroid of the region 51–112 in the structure of USP18. A 20 Å restraint between arginine 148 (STAT2) and leucine 103 (USP18) was set to allow a large rotational space to be explored by decoys during docking covering the entire 51–112 region of USP18. The final model was taken as the top-ranking model of the hydrophobic-favoured scoring scheme.[256]

In silico mutagenesis of the predicted STAT2-USP18 interface

To prioritize substitutions in STAT2 that are likely to disrupt the interaction with USP18, we first determined the interface residues based upon the difference in the solvent accessible surface of STAT2 as a monomer and in complex with USP18 using FreeSASA 2.0.3.[257] Then, the structural effect of each of 19 substitutions of interface residues was calculated, measured as the predicted Gibbs free energy change (ΔΔG) by FoldX 5.0.[258] The “RepairPDB” command was run first to minimize the structures, and the ΔΔG values in the monomer (ΔΔGmonomer) and in the complex (ΔΔGfull) were calculated with the “BuildModel” command as the average of ten replicates. A rule-based method was applied to rank the substitutions. First, variants observed in gnomAD were excluded.[259] Second, only mutations with ΔΔGmonomer values between − 0.5 and + 0.5 were considered, which would more likely allow folding of the protein (mean ΔΔGmonomer of 14 gnomAD variants at the interface is 0.309). Third, mutations with ΔΔGfull > 2, were prioritized, i.e., those that are likely to have a disrupting effect at the interface

(only 3 out of 14 gnomAD variants are above this value with the maximum of 3.23). Lastly, the subset of mutations to residues that are no more than 5 Å distance away from the nearest atoms of residues R148 and A219 were further restricted to maximize the chance of the residue being biologically and thus pathologically important. Through this procedure, 10 substitutions from the possible 456 substitutions of 24 interface residues are shortlisted, with the 3 affected residues involved in these 10 substitutions highlighted in Fig. 13.

Statistical analysis

The number of experiments and the statistical tests performed are indicated in the figure legends. Statistical testing was undertaken in GraphPad Prism 9. Error bars represent standard error of the mean (SEM).

Chapter 3: Haploinsufficiency of PTP1B underlies a novel type I interferonopathy

3.1 Introduction

3.1.1 Discovery of PTP1B

Protein tyrosine phosphatase 1B (PTP1B), encoded by protein tyrosine non-receptor type 1 (*PTPN1*), is a ubiquitously expressed, ER-anchored non-receptor type PTP. It was first identified by Tonks and colleagues in 1988 as part of an effort to purify and characterise PTPs in human placenta,[260,261] which was the chosen tissue of interest due to the high abundance of PTPs and its relative availability. After purification, several phosphatases identified in this study were observed to display distinct molecular weights on SDS-PAGE (sodium dodecyl sulphate–polyacrylamide gel) electrophoresis. Further analysis revealed that all of the newly discovered phosphatases demonstrated absolute specificity towards phosphotyrosyl proteins, with no detectable activity on phosphoseryl or phosphothreonyl substrates. In particular, PTP1B exhibited high affinity and specificity in vitro on several synthetic substrates containing phospho-tyrosine residues, as well as in vivo on the insulin receptor. Further, at least one cysteine residue was suggested as critical in mediating the catalytic activity, as evidenced by the observation of a reversable inhibition of function by alkylating agents. By 1994, the crystal structure of PTP1B was already available to a high degree of resolution,[262] demonstrating the presence of a cysteine, as well as an arginine, residue, as catalytically essential.

3.1.2 Catalytic mechanism of PTP1B

Detailed molecular, biochemical, structural, and kinetic studies have shed light on the catalytic mechanism of action of PTP1B.[262-267] In brief, the removal of phosphate moieties from substrates occurs through a two-step process, in which a conserved Cys215 residue plays a fundamental role. First, the sulphur atom of Cys215 of PTP1B attacks the phosphate group of the substrate, while the tyrosyl-leaving group becomes protonated by the Asp181 residue of

PTP1B serving as a proton-donor, which forms a catalytic intermediate ‘‘cysteinyl-phosphate’’, thus completing the ‘‘dephosphorylation of substrate’’ step. Then, the hydrolysis of the catalytic intermediate is achieved via Gln262 coordinating with a donor H_2O molecule, and Asp181 acting as a general base to receive the lost proton in the first step. In this manner, the phosphate moiety is removed from the substrate, while the active PTP1B enzyme is regenerated (Fig. 14, created by Nicholas K. Tonks, *FEBS Letter*, 2003).[263,268]

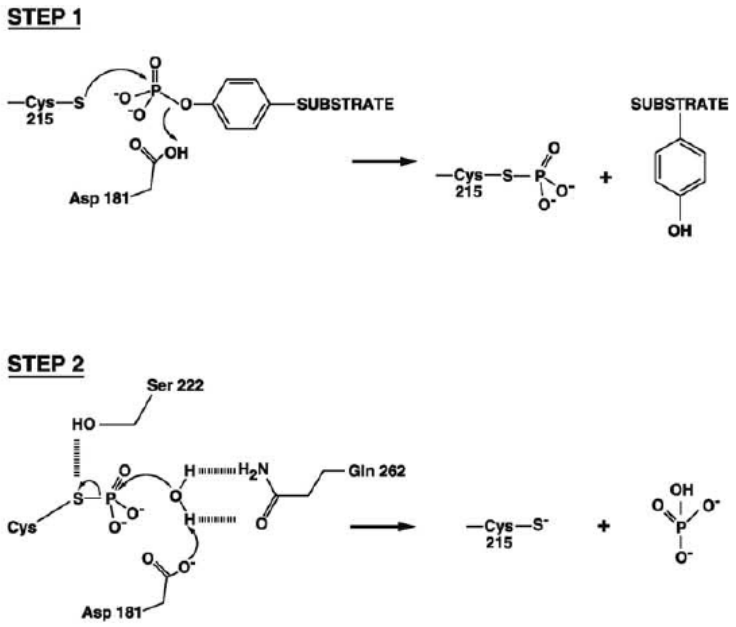

Fig. 14. Catalytic mechanism of PTP1B. The removal of phosphate from substrates occurs via a two-step process. First, the sulphur atom in Cys215 attacks the phosphate group of the substrate, and the Asp181 donates a proton to the tyrosyl-leaving group, forming a catalytic intermediate, and completing the ‘‘dephosphorylation’’ step. Then, the catalytic intermediate is hydrolysed with the help of the hydrogen bonds between Gln262, Asp181 and a water molecule. Asp181 serves as a general base to receive a proton from H_2O. This way, the active enzyme regenerated.

From a structural biology point of view, PTP1B consists of 435 amino acids which constitute four distinct domains, N terminal domain, catalytic domain, proline-rich domain, and C terminal ER-targeting domain.[269] Nestled inside the catalytic domain, a flexible loop consisting of residues 177-185, termed the WPD loop,[270] is essential to the catalytic activity of PTP1B. Prior to ligand-binding, the WPD loop displays an ‘‘open’’ conformation and is ready for substrate docking; upon ligand-binding, the loop closes and brings the aforementioned Asp181 close to the substrate for protonation and the Cys215 for nucleophilic attack.[263,268,271,272] The proline-

rich domain is inherently disordered, and is suggested to mediate interactions with substrates containing a src-homology 3 (SH3) domain such as Src and breast cancer anti-oestrogen resistance protein 1 (BCAR1).[273-275] Finally, the C terminal ER-targeting domain anchors PTP1B onto the ER where it is usually located and exerts its functions.[276] Of note, different studies suggest that PTP1B truncated for the ER-targeting domain becomes soluble in the cytosol with increased phosphatase activity, indicating an intrinsic regulatory mechanism of the protein.[277-279]

3.1.3 Regulation of PTP1B activity

Like many other enzymes, the regulation of PTP1B phosphatase activity can be achieved through various post-translational modifications (PTMs).[280] The protein per se is vulnerable to oxidation and nitrosylation due to the presence of the Cys215 residue.[281,282] Increased levels of reactive oxygen species (ROS) such as H_2O_2, and reactive nitrogen species (RNS), generated through several signalling events, can impair PTP1B activity due to significant conformational changes.[281-283] On a similar note, the endogenous PTP1B inhibitor LMO4 (LIM domain only 4) acts by promoting PTP1B oxidation to attenuate PTP1B activity.[284] Oxidised PTP1B loses its capacity to bind substrate due to conformational changes,[283] which can be reversed by certain antioxidants such as glutathione.[285] Additionally, PTP1B can be sumoylated on Lys335 and Lys347 shortly following insulin stimulation, which momentarily suppresses PTP1B activity and is thought to inhibit PTP1B's negative regulatory function on insulin signalling.[286] Further, PTP1B itself can be a substrate of certain kinases, with phosphorylation of serine or tyrosine residues exerting positive or negative effects on PTP1B enzymatic activity.[287-291] For example, insulin stimulation can lead to the tyrosine-phosphorylation of PTP1B on Tyr66, Tyr152 and Tyr153, which increases phosphatase activity and the dephosphorylation of insulin receptor;[287] while insulin-dependent phosphorylation at Ser50 by AKT decreases phosphatase activity and is regarded as a positive feedback mechanism on insulin signalling.[292] Moreover, PTP1B can subject to proteolytic cleavage.[279,293] In human aggregated platelets following stimulation, calpain cleaves

PTP1B proceeding position Ala77, which is a site upstream of the C-terminal ER-targeting region in PTP1B, and renders the re-localisation of the protein from ER to the cytosol as a soluble protein with enhanced phosphatase activity.[293] This phenomenon coincides with the irreversible aggregation of platelets in plasma.[279] Interestingly, oxidised PTP1B displays higher affinity to calpain and is more susceptible to calpain-dependent cleavage, with both aspects relying on Cys215, highlighting the importance of this residue in the regulation of PTP1B activity.[293]

3.1.4 Functions of PTP1B

Since its discovery, PTP1B has been appreciated as a master regulator of several signalling pathways including, but not limited to, insulin,[294,295] leptin,[296,297] brain-derived neurotrophic factor (BDNF),[298] and, particularly relevant to this study, STING and IFN-I signalling pathways,[299,300] via the dephosphorylation of a number of substrates. Initially, it was deemed essential for a consensus amino acid sequence (E/D)-pY-pY-(R/K) in the substrate to exist for PTP1B to exercise optimal recognition efficacy.[300] However, several studies have identified proteins that do not possess this consensus sequence to be dephosphorylated by PTP1B.[299,301,302] A summary of representative signalling pathways regulated by PTP1B, including the ones most relevant to this study (cGAS-STING and IFN-I signalling pathways), is given below.

Insulin signalling

Insulin, a small peptide hormone composed of 51 amino acids,[303] was first discovered in 1921, in an attempt to utilise pancreatic extracts for the treatment of diabetes mellitus (DM), during which patients experienced marked improvement regarding blood sugar levels, glycosuria and general health status.[304] For almost three decades, the mechanism of action of insulin was unclear, until Rachmiel Levine and colleagues suggested that insulin could facilitate glucose uptake into the cell by increasing cell membrane permeability to glucose.[305] It was a further 20 years before the first evidence was brought forward suggesting the existence of a membrane

receptor to insulin.[306] Thanks to the efforts of multiple research groups over many years, the series of signalling events driven by insulin binding to the insulin receptor (IR) are now well understood.[307-310] In brief, following insulin binding, the IR (a receptor tyrosine kinase) becomes activated through autophosphorylation and conformational changes, and further phosphorylates IR substrates (IRS), which allows the binding of a lipid kinase PI3K. PI3K synthesises a second messenger PIP3 (phosphatidylinositol-3,4,5-trisphosphate) that recruits PDK-1 (3-phosphoinositide dependent protein kinase 1). In turn, PDK-1 phosphorylates AKT at Thr308, followed by the Ser473 phosphorylation of AKT by mTORC2 (mammalian target of rapamycin complex 2), thus completing the activation of AKT. Active AKT is responsible for most of the downstream effects including glucose metabolism, protein, glycogen and lipid synthesis through the serine/threonine phosphorylation of substrates in various signalling pathways.[110,311]

The signalling pathway described above can be summarised as a series of phosphorylation evens initiated by the tyrosine phosphorylation of IR. Regulatory mechanisms maintaining homeostatic insulin signalling exist, involving kinases and phosphatases. One such regulator, PTP1B, came to light when in vitro studies using cell lines, and in vivo studies using mouse models, successfully established IR and IRS as direct substrates of PTP1B.[294,312,313] Cells overexpressing PTP1B WT decreased the autophosphorylation of the IR compared to parental cells; while cells overexpressing a catalytically inactive mutant PTP1B p.(C215S), demonstrating defective phosphatase activity, showed increased IR tyrosine phosphorylation.[294] Mice globally deleted of PTP1B were protected from high-fat-diet induced obesity and showed elevated baseline metabolic rate, total energy expenditure, and leanness attributed to the decreased fat cell mass.[295] These mice also exhibited heightened sensitivity to insulin in skeletal muscle leading to increased glucose uptake.[295] All these observations lead to the conclusion that PTP1B is a negative regulator of insulin signalling by directly dephosphorylating the IR and IRS (Fig. 15, taken from Abdelsalam et. al., *Biomolecules*, 2019.).[295,314]

Leptin signalling

Another important metabolic signalling pathway regulated by PTP1B is leptin signalling. Leptin was first discovered in 1994 by Zhang and colleagues as a 16 kD small peptide hormone encoded by the *LEP* gene (also called *OB* (*obese*) gene) through studies of obese mice,[315,316] and leptin receptor (LEPR) was described in 1996 by two other groups.[317,318] After leptin binds to its cognate receptor, the receptor-associated kinase JAK2 becomes activated through tyrosine-autophosphorylation and then phosphorylates LEPR on three residues Tyr985, Tyr1077 and Tyr1138, with each tyrosine phosphorylation representing a different downstream signalling event.[319,320] pTyr985 recruits SHP2 to facilitate ERK (extracellular signal-regulated kinase) signalling;[319,320] pTyr1077 mediates JAK2-STAT3 activation;[319,320] and pTyr1138 promotes JAK2-STAT5 activity.[319,320] Different branches of the leptin signalling pathway mediate different biological functions of leptin, such as the regulation of energy balance, appetite control, body weight and glucose homeostasis.[319,321,322]

Several phosphatases have been implicated in the regulation of leptin signalling, with PTP1B possibly the most studied negative regulator.[319,323] PTP1B dephosphorylates JAK2, thus restricting both JAK2-STAT3 and JAK2-STAT5 pathways, and thereby playing a role in the regulation of energy homeostasis and body weight.[319,320,323] The role of PTP1B in downregulating leptin signalling is presented in Fig. 15.[314]

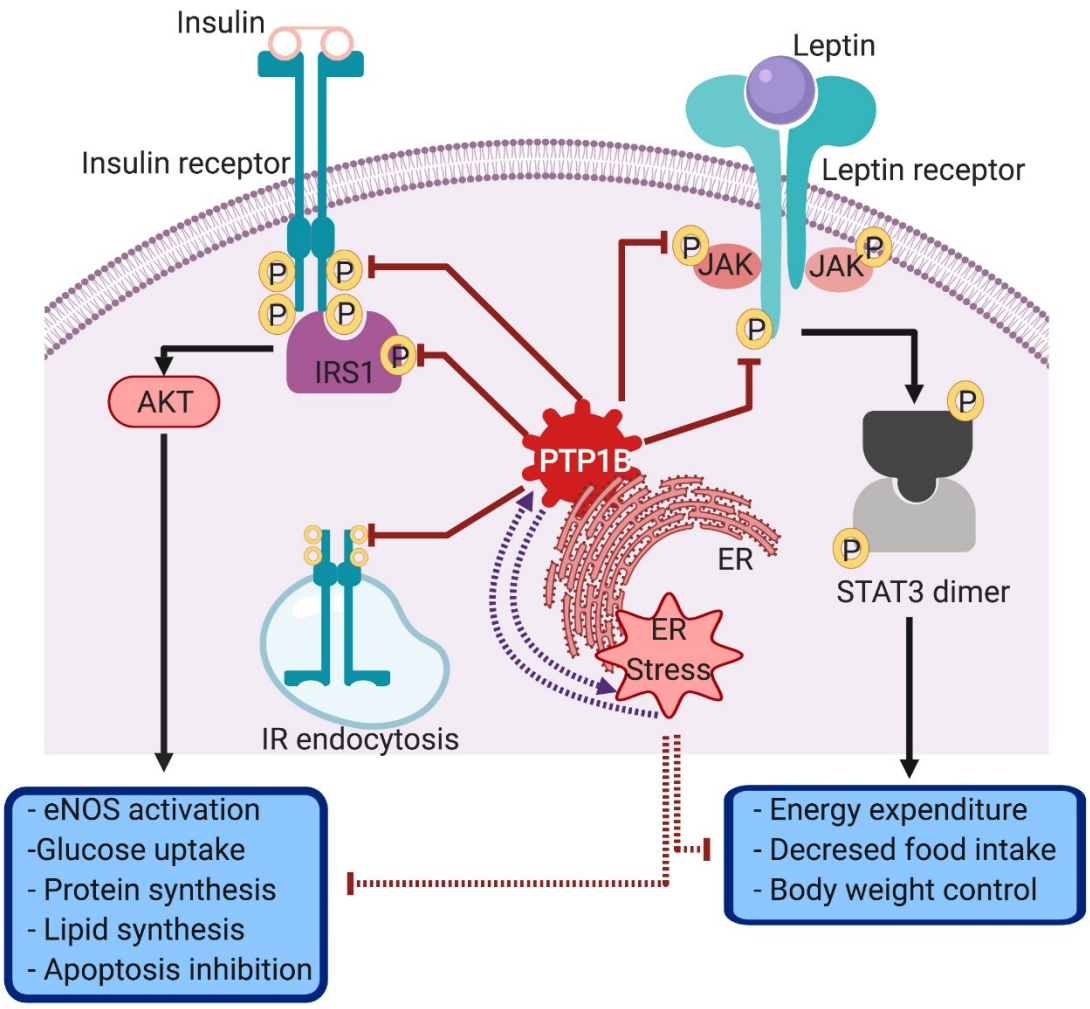

Fig. 15. Insulin and leptin signalling pathways are regulated by PTP1B. (Left) After insulin binds to insulin receptor (IR), IR undergoes autophosphorylation and conformational changes, leading to the phosphorylation of insulin receptor substrate (IRS). IRS further recruits lipid kinase PI3K (phosphoinositide 3 kinase, not shown) to synthesise second messenger PIP3 (phosphatidylinositol-3,4,5-trisphosphate, not shown), which recruits PDK-1 (3-phosphoinositide dependent protein kinase 1, not shown). PDK-1 phosphorylates ATK to drive the major transcriptional network downstream of insulin signalling. PTP1B is known to dephosphorylate both IR and IRS, negatively regulating insulin signalling magnitude. (Right) Leptin is also an extracellular small peptide hormone that binds to its cognate receptor, triggering the phosphorylation of receptor-associated JAK2, which in turn recruits and activates STAT3. Homodimerised STAT3 translocates into the nucleus to initiation the transcription of genes responsible for the physiological functions of leptin. ERK and JAK2-STAT5 pathways are also triggered by JAK2 phosphorylation (not shown). PTP1B dephosphorylates JAK2 to restrict leptin signalling. ER, endoplasmic reticulum.

BDNF-TrkB signalling

BDNF represents the most abundant neurotrophin in the CNS with major functions in modulating synaptic plasticity via the regulation of neuronal cell growth and survival.[283,324,325] BDNF signals through TrkB (tropomyosin receptor kinase B, a receptor tyrosine kinase), and the binding between the ligand and the receptor leads to receptor phosphorylation at Tyr515

and dimerisation, which further activates different downstream adaptor proteins.[326] There are three major signalling pathways post TrkB activation: the Ras (rat sarcoma)–MAPK pathway, the PLCγ (phospholipase Cγ1)–PKC (protein kinase C) pathway, and the PI3K–AKT pathway.[326,327] Ras-MAPK signalling promotes neuronal survival, plasticity and neurite growth; the PLCγ-PKC pathway is thought to enhance synaptic plasticity; and PI3K-AKT pathway promote neuron growth and survival.[277,324,326,327] A critical study established TrkB as a direct substrate of PTP1B,[298] indicating a negative role of this phosphatase in regulating BDNF signalling. Overexpression of PTP1B decreases TrkB phosphorylation and dampens signalling strength, with a subsequent impairment of cognitive abilities;[298,328] while inhibition of PTP1B activity was shown to improve memory in mice.[298]

cGAS-STING signalling

As a major cellular signalling pathway that responds to intracellular dsDNA species,[329] the cGAS-STING pathway has attracted much attention due to its implication in cancer, infectious disease, metabolic disorder, neurodegeneration, inflammation and autoimmunity.[6,19,330-332]

Upon DNA binding, cGAS undergoes conformational changes to a dimeric/oligomeric active form. The binding process does not require a specific DNA sequence, but, rather, is length-dependent. The dimerisation process leads to the activation of the cGAS catalytic site,[19,333] which in turn initiates the synthesis of cGAMP. Second messenger cGAMP is then recognised by and activates STING.[334] STING also undergoes conformational changes and PTMs,[19,335] as well as relocalising from the ER to the Golgi apparatus via COPII vesicles, where it recruits and interacts with TBK1.[18,19] TBK1 becomes activated through autophosphorylation, and, in turn, phosphorylates IRF3.[13,19,329,336] Phosphorylated IRF3 dimerises and enters the nucleus to initiate the transcription of IFN-I genes.[13] Activated TBK1 can also promote NF-κB signalling, which serves as a transcription factor for pro-inflammatory cytokines such as IL-1β and TNFα (tumour necrosis factor α).[13]

The human cell must deploy accurate regulatory mechanisms to maintain balanced cGAS-STING signalling, with inappropriate activation of the pathway predisposing to severe autoinflammatory disease,[18,331] and insufficient activation resulting in uncontrolled viral infection.[337,338] Among the many modulators of cGAS-STING pathway identified to date, PTP1B has been suggested as a negative regulator, with the dephosphorylation of STING at Tyr245 following viral infection serving to promote ubiquitin-independent 20S proteasomal degradation of STING, and thus restrict excessive signalling and production of IFN-I.[299] Deficiency of *PTPN1* in cell lines enhanced the downstream expression of antiviral genes and potentiated the antiviral response to DNA virus.[299] A summary of cGAS-STING signalling regulated by PTP1B is displayed in Fig. 16, created in Biorender.

IFN-I signalling

IFN-Is are a group of cytokines with inherent antiviral abilities.[163] Almost all nucleated cells in the human body can express some amount of IFN-I under certain stimuli, with pDCs seen as the major producer upon infection.[234,339] IFN-I signals through the universally expressed IFN receptor composed of IFNAR1 and IFNAR2 subunits.[340] Upon ligand binding, IFNARs bring the receptor-associated JAK1 and TYK2 into close proximity.[116,340] JAK1 and TYK2 become activated via tyrosine phosphorylation and then phosphorylate STAT1 and STAT2, which together form a heterodimeric complex and translocate into the nucleus to interact with IRF9.[116,340] The tripartite complex consisting of STAT proteins and IRF9 is termed ISGF3 and serves as a transcription activator by binding to genes with an ISRE sequence, thus initiating the transcription of a large repertoire of ISGs.[116,340]

IFN-I signalling requires tight regulation given that unbalanced signalling can result in pathological consequences.[93] Related to this study, PTP1B is a well-known negative regulator of IFN-I signalling through the dephosphorylation of TYK2 (Fig. 16).[300] TYK2 contains a PTP1B-recognition sequence (E-pY-pY-K), and is a bona fine substrate of PTP1B.[300] Additionally, a substrate-trapping mutant PTP1B p.(D181A) was shown to form stable complexes with TYK2 and JAK2 following IFN-I and IFN-II stimulation, respectively, with both

WT and mutant PTP1B inhibiting IFN-dependent transcriptional responses.[300] On the other hand, the catalytically inactive mutant p.(C215S) abolishes phosphatase activity, leading to hyperphosphorylation of JAK-STAT pathway components in cells following stimulation with IFN-I, IFN-II, and IL-4.[269,341,342] More detailed biochemical and structural studies further demonstrated that, besides TYK2 and JAK2, the other two members of the JAK family, JAK1 and JAK3, can also be dephosphorylated by PTP1B in vitro, albeit to varying extents.[301] Dephosphorylated TYK2 and JAK1 are unable to transduce signalling from the cell surface IFNARs to intracellular STAT proteins following IFN-I stimulation (Fig. 16). Along the same lines, somatic LOF mutations of PTP1B have been described previously in Hodgkin lymphoma (HL) and primary mediastinal B cell lymphoma (PMBCL), and are associated with upregulated JAK-STAT activity in these pathological states.[269,341,342]

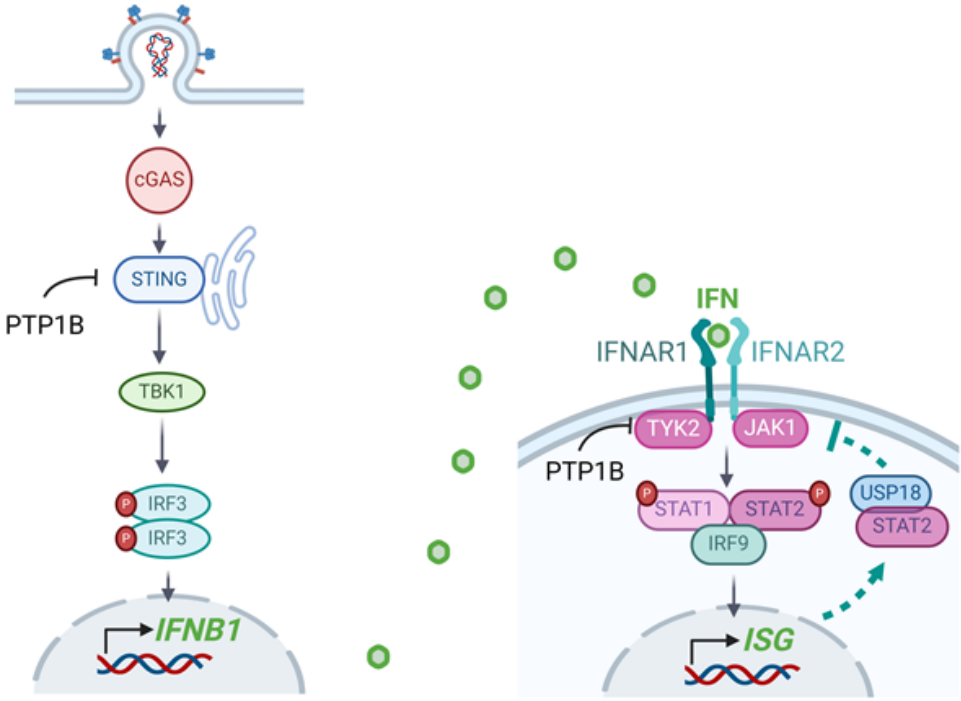

Fig. 16. PTP1B negatively regulates cGAS-STING and IFNAR signalling pathways. PTP1B has been shown to dephosphorylate STING at Y245, leading to its 20S proteasomal degradation. Further, PTP1B dephosphorylates TYK2 and JAK1 following IFN-I binding to IFNARs. Hence, dephosphorylated JAKs are unable to transduce signalling from the cell surface to intracellular STAT proteins.

3.1.5 Human diseases associated with altered PTP1B activity

Metabolic disorders

Diabetes mellitus (DM) is a disease typically characterised by hyperglycaemia, estimated to affect 529 million people worldwide in 2021.[343] DM is usually subcategorised into type 1 and 2 (T1DM and T2DM, respectively),[344] with T2DM being the more common type, constituting more than 90% of the total cases of diabetes.[345] T1DM is an autoimmune disease where the host immune system attacks the insulin-producing β-cells in the pancreas of the patient;[344] while T2DM is often associated with insulin resistance and/or defective insulin serecetion.[344] Therapeutic strategies vary depending on DM subtype. Specifically, life-long administration of insulin can be provided as a pharmacotherapy for T1DM, whereas hypoglycaemic drugs such as metformin represent the first line of treatment for T2DM, along with a balanced, active and healthy lifestyle.[346] However, life-long insulin administration poses a burden on patient physiological, psychological and economic wellbeing;[347-350] and around 50% of T2DM patients fail to adhere to metformin therapy due to adverse effects.[351] Hence, novel therapeutic approaches such as gene and stem cell therapy are being actively developed.[346]

The role of PTP1B in DM, especially T2DM, is well recognised, since PTP1B is a negative regulator of both the insulin and leptin signalling pathways by the dephosphorylation of the receptor and/or pathway kinase components,[284,352] which leads to pathway inactivation and insensitivity to insulin and leptin stimulation. Further, PTP1B overexpression can limit glucose uptake into the cell by decreasing the cell surface expression of glucose transporter GLUT4, thus creating a hyperglycaemic state.[353]

Similarly, leptin resistance caused by PTP1B overexpression underlies obesity.[296,354] Leptin signalling regulates body weight, glucose homeostasis and appetite control via JAK2-STAT3/5 signalling.[319,320,323] Dephosphorylation of leptin receptor-associated kinase JAK2 decreases its activity and results in leptin receptor desensitisation, with subsequent dysregulation of

downstream transcriptional regulation of glucose metabolism, energy expenditure and weight control.[319,320,323]

Cancers

PTP1B can act as both a tumour promoter and tumour suppressor, dependent on cancer type and cellular enviroment.[355,356] On one hand, overexpression of PTP1B has been suggested as a driver of progression and metastasis in several cancer types including ovarian carcinoma,[357] breast cancer,[358] colorectal cancer,[359] and malignant melanoma.[360] On the other, deficiency or inhibition of PTP1B has also been reported in certain forms of cancer. Thus, p53 and PTP1B double KO mice were more susceptible to B cell lymphoma, with a worse survival rate compared to p53 single KO mice.[361] An accumulation of B cells in the bone marrow and lymph nodes was noted in these double KO mice, suggesting that PTP1B plays a role in regulating B cell proliferation, differentiation and apoptosis.[361] LOF mutations in PTP1B, identified in tissue samples from human patients, have been implicated as driver mutations in HL and PMBCL,[341] due to the hyperactivation of JAK-STAT pathway components. Two further studies focusing on splicing mutations in *PTPN1* (∆2–4 and ∆6, respectively) validated the observation that a deficiency of PTP1B activity plays a role in HL oncogenesis,[269,342] while around 20% of human colon and thyroid cancer samples were found to harbour splicing mutations in *PTPN1*.[362]

Infectious diseases

PTP1B has been implicated to play a role in the innate antiviral response, at least in part through the regulation of IFN-I signalling.[352] It is established that PTP1B can dephosphorylate TYK2 kinase immediately downstream of IFNARs to restrict excessive signalling and ISG transcription.[300] For example, IAV triggers both RIG-I-MAVS and TLR3 signalling, inducing the host cell to express lncRNA-155, which antagonises the expression of PTP1B, thus enhancing the host IFN-I response towards clearance of virus.[363] Along the same lines, it has been shown that PTP1B mediates HSV-1 cell-to-cell transmission; and while pharmacological inhibition or

genetic ablation of PTP1B did not influence virus replication, it significantly reduced viral extracellular spread.[364]

The negative regulatory role of PTP1B in bacterial infection has been studied in the context of *Pseudomonas aeruginosa*.[365-367] Mice deficient in PTP1B showed enhanced clearance of *P. aeruginosa* and a less severe disease phenotype. Mechanistically, PTP1B deficiency enhanced IRF7 induced cytokine (IFNβ) and chemokine CXCL10 (C-X-C motif chemokine ligand 10) expression, facilitating more efficient bacterial killing.[365] On a cellular level, neutrophils absent for PTP1B exhibited heightened STAT1 activation dependent on TLR4 signalling and nitric oxide (NO) production, and were more competent at bacterial phagocytosis.[366] In a related study, it was observed that macrophages from *PTPN1* KO mice displayed enhanced phagocytosis towards the bacteria, with overexpression of cytokine and chemokine dependent on TRIF-IFN signalling.[367] Of note, STAT1, in this context, was dispensable to host defence against *P. aeruginosa*, as evidenced by the comparable pulmonary bacterial load in mice of PTP1B single KO genotype and PTP1B/STAT1 double KO genotype, following bacterial infection.[367]

3.1.6 Summary

PTP1B is an ER-resident protein tyrosine phosphatase with functions in a number of cellular signalling pathways participating in the regulation of cell growth, proliferation, energy balance, glucose metabolism, antiviral responses and possibly others. Thus, the balanced expression and activity of PTP1B is essential to physiological homeostasis. Overexpression or deficiency of PTP1B has been associated with diabetes, obesity, cancer and infectious disease. The diversity of (potential) substrates of PTP1B makes it a desirable, yet somewhat ‘‘problematic’’, target in pharmaceutical advances. Additionally, the intracellular ER-localisation and the positively-charged catalytic site of PTP1B add more layers of complexity to issues of cell permeability and efficient drug delivery.[281] PTP1B, and its paralogue TCPTP (T cell protein tyrosine phosphatase, also known as PTPN2, encoded by *PTPN2*), share a high degree of sequence similarity, especially in their respective catalytic domains (over 80%).[368-370]

Biochemical studies have illustrated that both PTP1B and TCPTP can catalyse the dephosphorylation of a common group of substrates, exemplified by tyrosine kinases such as EGFR, IR, and JAKs.[369,371] How to effectively modify PTP1B expression/activity in a certain cell type/tissue/organ or even a particular signalling pathway to maximise the desired outcome, while limiting unwarranted side effects, has long been a scientific struggle in PTP1B biological and pharmaceutical research. PTP1B was previously deemed ‘‘undruggable’’ by some researchers,[372] and promising pre-clinical PTP1B inhibitors have either failed or were discontinued in human clinical trials at various stages, due variably to low bioavailability, low specificity, toxicity or undisclosed reasons.[281,352,373] Nevertheless, innovative synthetic and naturally-sourced compounds are constantly being tested in preclinical models, with the hope to reach clinical trials, ever since the recognition of the role of PTP1B in the pathogenesis of multiple human diseases.[374,375]

To the author’s knowledge, somatic mutations in PTP1B, acting as drivers in certain types of cancer, represent the only described defined genetic cause of human PTP1B-related disease. Thus, the current study represents the first of its kind in describing germline heterozygous LOF mutations in PTP1B in the context of a Mendelian autoinflammatory disorder. Specifically, our laboratory ascertained a novel cohort of patients demonstrating highly stereotyped clinical features. All 12 patients underwent completely normal birth and early development, until the onset of subacute neuro-regression, manifesting as unspecific white matter disease, motor function deterioration, and decline in expressive speech. The 12 patients further demonstrated stabilisation of disease, with clear neurological improvement observed following immune suppression in six of eight treated patients. CSF neopterin levels, a marker of CNS inflammation, were raised in all ten cases where tested. IFN signalling testing with whole-blood RNA showed each patient to display an upregulation of ISG expression on at least one occasion, with serial testing revealing a trend to decrease, possibly correlating with clinical stabilisation. Through WGS and targeted Sanger sequencing, every patient was revealed to carry a novel or very rare variant in *PTPN1* in the heterozygous state. Eight of ten variants are

predicted to result in a loss of mRNA/protein expression, with the other two missense substitutions involving amino acid residues previously deemed essential to the allosteric regulation of PTP1B function.[376,377] Three variants appeared to arise de novo, while eight further probands inherited the variant from their clinically unaffected mutation-positive parent. Of note, one variant was recorded as de novo in one patient, and, in an unrelated family, this same variant was inherited from an asymptomatic mother. Further, *PTPN1* is a highly constrained gene with a pLI of 1, indicating strong negative selection against LOF mutations. Through molecular and cellular functional assays, the possible underlying mechanisms linking LOF mutations in PTP1B and an upregulation of IFN-I signalling were explored, suggesting an enhancement of both STING and IFNAR pathways resulting from a loss of IFN negative regulation by PTP1B. The clinical and experimental data are presented in the Results section below.

3.2 Results

Identification of a novel cohort of patients with highly stereotyped clinical features

The clinical phenotype of the symptomatic patients in this cohort is remarkable for a high degree of stereotypy. All patients experienced subacute neuro-regression after normal development (age range 15 months to 8 years), with weakness and spasticity, initially manifesting as a hemiparesis in seven patients and then becoming bilateral, dystonia and bulbar involvement (12/12 patients) in the absence of seizures (0/12 patients). Cerebral atrophy (10/12 patients), initially unilateral in four cases, was the major neuro-radiological feature, with non-specific white matter changes in eight individuals, and intracranial calcification reported in a single patient. Interestingly, all patients experienced subsequent clinical stabilisation, with all 12 ascertained patients alive at last contact (age range 3 – 20 years).

All patients displayed an elevation of ISG expression in whole-blood either via qPCR or NanoString analysis (Fig. 17a, b, upper panels) on at least one occasion, indicating a systemic inflammatory phenotype at the time of testing. Serial testing suggested a fall of IFN scores, consistent with stabilisation of clinical phenotype (Fig. 17a, b, lower panels). CSF levels of neopterin, a marker of CNS inflammation,[378] were elevated in all ten patients where tested (range 2 – 45 multiples of laboratory-specific upper limits of normal). Additionally, we recorded increased IFNα protein in CSF and serum in one patient, and increased CSF IFNα activity in two further patients. The nine asymptomatic carriers had no significant past medical history, and IFN signalling testing was completely normal in the three such individuals where assessed, and minimally elevated in a fourth (data not shown). Detailed clinical histories of each patient are given below.

AGS492.1: Cousin to AGS492.2, related through unaffected fathers, brothers to one another. Symptom onset was at age 2.5 years. Rapid onset of left-sided hemiparesis, with bilateral high T2 white matter changes on cerebral MRI and calcification of the basal ganglia calcification mainly on the right. His clinical phenotype evolved to a spastic-dystonic tetraparesis over several months, becoming unable to sit without support, with poor head control, and no language although his social interaction was relatively maintained. He was alive at last contact aged 11 years.

His father was clinically asymptomatic into adulthood (no other details available).

At 32 months of age CSF neopterin was recorded at 90 nmol/L (normal range 9 – 5 nmol/L), and IFNα activity in the CSF and serum was elevated at 6 IU/mL and 9 IU/mL (normal < 3 IU/mL), respectively. ISGs tested on two occasions were also elevated, with IFN scores of 8.131 and 8.009 at ages 3.62 and 4.1 years respectively.

Exome sequencing identified a paternally inherited heterozygous c.590A>G (p.K197R) variant in *PTPN1*, which was not present on gnomAD v4.1.0.

AGS492.4: Cousin to AGS492.1, related through unaffected fathers, brothers to one another. Aged 3.5 years, he experienced the rapid onset of initially right-sided weakness and spasticity, dysphasia and dribbling. His condition worsened over several weeks so that lost the ability to walk. Brain biopsy showed non-specific perivascular inflammatory changes in the cortical white matter and meninges. He was treated with methylprednisolone, which was associated with a partial response so that he began to regain some degree of independent ambulation. He remains aphasic, albeit with good understanding, and with bilateral spasticity and dystonia. There have been no further episodes of decompensation up to the age of 12 years.

His father was clinically asymptomatic at the age of 45 years.

ISGs were tested on two occasions, with a positive IFN score of 7.899 (by qPCR) at age 6.79 years and a negative IFN score of 2.48 (by NanoString) at age 12.76 years.

Exome sequencing identified a paternally inherited heterozygous c.590A>G (p.K197R) variant in *PTPN1*, which was not present on gnomAD v4.1.0.

AGS761: He was born with normal weight (> 7 lb) to non-consanguineous parents of white European ancestry after an unremarkable pregnancy and neonatal period. Having followed a completely normal developmental trajectory, a week following scheduled 15-month vaccinations, he presented with fever and irritability, accompanied by a rapid loss of motor skills, language, the ability to self-feed and to swallow (requiring the placement of a gastrostomy tube), with elevated liver enzymes and raised CSF neopterin. Cerebral imaging revealed patchy high T2 signal white matter abnormalities and cerebral atrophy. He was treated with IVIG without obvious benefit. Characterised by truncal hypotonia and spastic-dystonic quadriparesis, by age 2 years his condition appeared to have stabilised, and there had been no further episodes of decompensation up to the age of 11 years.

CSF neopterin was 300 nmol/L at age 16 months, and 239 nmol/L at age 21 months (normal range 7 – 65 nmol/L). IFNα activity in the CSF was elevated at 18 IU/mL and 9 IU/mL (normal

< 3 IU/mL) at 18 and 20 months of age respectively. ISGs tested on two occasions were also elevated, with IFN scores of 7.8 and 4.683 at ages 1.51 at 1.69 years respectively.

Exome sequencing identified a de novo heterozygous c.63+1G>C variant in *PTPN1*, which was not present on gnomAD v4.1.0.

AGS1036 (Case 2 in Sa et al.[379]): A previously well 5-year-old girl with a normal antenatal and developmental profile, presented with a subacute onset over three months of left sided weakness, frequent falls and difficulties climbing stairs. She was also unable to raise her left arm and had problems dressing and undressing. Her right side was also affected and her handwriting deteriorated. Her speech deteriorated and she developed swallowing difficulties with excessive drooling. There was no cognitive regression, sleep disturbance or history of seizures. On examination, her speech was dysarthric. She had a mixture of spasticity and dystonia with lower limbs more affected than upper limbs and left side more than right. Her tone was increased bilaterally with sustained clonus on the left and upgoing plantars bilaterally. Head circumference was normal. Brain MRI demonstrated generalized volume loss more marked in the right cerebral hemisphere (Fig. 17c). Liver transminases were elevated (ALT maximum of 393 U/L). At 12 months from onset the patient was treated with four cycles of pulse intravenous methyl prednisone (IVMP) (30 mg/kg/d for 5 days) and IVIG (2 g/kg) three to four months apart. This resulted in significant improvement in her movement disorder and in all domains of function (gross motor, fine motor and speech). Repeated imaging 23 months after treatment showed normalisation of MRI appearances (Fig. 17d).

His mother is clinically asymptomatic at the age of 37 years.

CSF neopterin was elevated (200 nmol/L, normal range 7 – 65 nmol/L) at the age of 5 years, and had fallen to within the normal range 24 months thereafter (29 nmol/L). ISGs were initially elevated on four occasions (interferon scores of 8.042, 8.447, 9.751 and 8.297 at ages 5.24, 5.32, 5.39 and 5.75 years respectively), falling to normal thereafter (interferon scores of 1.953,

1.348 and 0.663 at ages 6.05, 6.11 and 6.82 respectively). Maternal and paternal ISGs were not tested.

Exome sequencing identified a maternally inherited heterozygous c.466C>T (p.(Arg156*)) (R156*) variant in PTPN1 not present on gnomAD v4.1.0 (previously reported in primary mediastinal B cell lymphoma by Gunawardana et al. 2014.[341]). This variant was also observed to have arisen de novo in AGS2942. A younger brother (mentioned in Sa et al.[379]) did not carry this variation.

AGS1312 (Case 3 in Sa et al.[379]): A previously well 4-year-old girl with mild gross motor developmental delay (walking independently at age 21 months), presented with a progressive one-year history of frequent trips and falls, difficulty climbing stairs, and progressive walking difficulty needing the aid of a wheelchair for outdoors. There was also five-month history of speech regression; initially slurred incomprehensible words, followed by complete loss of expressive language. She had dysphagia with choking on solids and liquids and drooling. Behavioural difficulties were also reported with frequent angry outbursts and peer-relationship problems. There was no history of seizures. On examination, her tone was increased in the lower limbs with mixed spasticity and dystonia (right worse than left), and bilateral upgoing plantars. She walked with a wide gait with both her knees hyperextended. There was drooling but no cranial nerve abnormalities. Head circumference was below the 0.4th centile (no previous measurements available for comparison). There was no hepatosplenomegaly. MRI brain showed mild global cerebral volume loss mimicking atrophy (Fig. 17e). Liver transminases were minimally elevated (ALT maximum of 37 U/L). At 15 months from onset she had one course of three days IVMP (30 mg/kg/d), followed by IVIG (2 g/kg) cycles, five courses over 20 months. Marked improvement in her lower limb tone, with gain in both motor and expressive language skills, was observed. A repeat MRI at 13 months after treatment initiation showed reversal of previous changes (Fig. 17f). Currently, she is able to climb stairs unaided, her speech is clear, and she can produce three to four-word sentences.

His father is clinically asymptomatic at the age of 48 years.

CSF neopterin was elevated (151 nmol/L, and 93 nmol/L, normal range 7 – 65 nmol/L) at the age of 5 years and 12 months thereafter. ISGs tested on four occasions were elevated, with interferon scores of 4.913, 4.45, 5.312 and 3.905 at ages 4.6, 4.97, 5.29 and 5.56 years respectively. Maternal and paternal ISGs were normal on both occasions tested.

Exome sequencing identified a paternally inherited heterozygous c.1000delG (p.(Val334*)) (V334*) variant in PTPN1 not present on gnomAD v4.1.0.

AGS1421 (Case 1 in Sa et al.[379]). This previously developmentally normal male presented at age 22 months with a progressive left-sided hemiparesis. Five months later, he experienced fever, and the evolution of additional right sided weakness, together with speech regression and swallowing difficulties. Neurological examination revealed a spastic-dystonia more marked in the lower limbs. Head circumference was normal. Serial cerebral MRI demonstrated progressive, initially right hemispheric atrophy, subsequently evolving to global symmetric cerebral volume loss (Fig. 17g). Liver transminases were elevated (ALT maximum of 90 U/L). Brain biopsy revealed patchy gliosis with good neuronal preservation and no significant inflammation. 18 months after the initial presentation he was started on six weekly pulses of IVMP (30 mg/kg/d), followed by six weekly IVIG (2 g/kg). Treatment was associated with an improvement in fine motor and non-verbal communication skills, and less so in gross motor skills and speech. Aged 10 years his condition is stable, being able to sit unsupported, with the continued acquisition of communication skills. Brain MRI showed complete reversal of previous changes two years after treatment initiation (Fig. 17h). There have been no further episodes of decompensation up to the age of 11 years.

His father is clinically asymptomatic at the age of 49 years.

CSF neopterin was elevated (355 nmol/L, normal range 7 – 65 nmol/L) at age 22 months. ISGs tested at age 3.26 years were significantly elevated (interferon score of 16.135), but had normalised when reassessed at age 4.66 years.

Exome sequencing identified a paternally inherited heterozygous c.370_386del (p.(Tyr124Argfs*7)) (Y124Rfs*7) variant in PTPN1 not present on gnomAD v4.1.0.

AGS2942: This female child, born at term with a normal birth weight and head circumference to non-consanguineous parents of white European ancestry, demonstrated completely normal psychomotor development until 8 years of age. Then, over a period of approximately 1 year, she developed a left sided limp when running associated with a degree of lower limb spasticity, and began to demonstrate clear cognitive decline with reduced school performance, slowed dressing, asthenia, speech difficulties, a deterioration in her writing, disturbed sleep and recurrent fevers progressing over a period of one year. Definite cerebral atrophy was seen on MRI, with an absence of calcification on cerebral CT. An EEG was normal. Now aged 11 years, her condition has stabilised and she has regained skills, so that she no longer has features of lower limb spasticity, being able to walk and run without problem. She has continued slight difficulties with articulation. Vision and hearing are normal. She has experienced no further fevers. She has started puberty. Her most recent cerebral MRI showed a resolution of the features of cerebral atrophy seen previously, and a reduction of the T2 high signal white matter changes.

CSF neopterin (1100 nmol/L, normal range 10 – 24 nmol/L), as well as IFNα protein in the CSF (5706 fg/mL, normal <10 fg/mL) and serum (1448 and 1302 fg/mL, normal <10 fg/mL) were grossly elevated at age 10 years. ISGs tested on two occasions revealed IFN scores of 4.535 and 2.985 at 10.11 and 10.48 years of age respectively. A third ISGs assessment was performed at age 10.95 years with a negative IFN score of 1.935.

Exome sequencing identified a de novo heterozygous c.466C>T (p.R156*) variant in *PTPN1* not present on gnomAD v4.1.0.

AGS3148: This male child exhibited completely normal development during infancy, walking independently at the age of 10 months, and speaking his first words at 12 months of age. Aged 15 months he experienced a febrile seizure, and one month later he was noted to be losing

skills, so that by age 19 months his speech was completely absent, he was unable to walk, and he demonstrated upper and lower limb spasticity. Cranial MRI was said to show white matter changes consistent with a leukodystrophy. Now, aged 17 years, he demonstrates profound developmental delay with severe spasticity of upper and lower limbs.

ISGs tested on one occasion revealed an IFN score of 5.2 at age 17.79 years.

Exome sequencing identified an apparently de novo heterozygous c.154+1del variant in *PTPN1* not present on gnomAD v4.1.0.

AGS3165: This male demonstrated normal development until age 4.5 years, at which time he experienced a febrile episode associated with irritability and the onset of spasticity, dysarthria and swallowing difficulties progressing rapidly over 2 months, losing the ability to feed and dress himself, and to climb stairs. There was progression of his disease over a few months so that by age 5 years he was unable to walk, his language had become incomprehensible, and his swallowing of liquids unsafe. He was treated with 3 doses of corticosteroid without obvious benefit. By age 6 years he was regaining developmental skills, albeit in the context of a significant spastic paraparesis, becoming able to feed himself again, and demonstrating language skills appropriate for his age. Initial cerebral imaging (MRI and CT) was normal, but subsequent neuroimaging demonstrated T2 high signal consistent with a leukodystrophy, which became more diffuse over time. Cerebral CT did not reveal any calcifications.

His mother is clinically asymptomatic at the age of 34 years.

CSF neopterin was elevated at 323 nmol/L and 162 nmol/L (range 7 – 55 nmol/L) aged 5 and 6 years respectively. ISGs tested on two occasions revealed IFN scores of 7.29 and 5.925 at ages 4.85 and 5.46 years respectively. ISGs tested in the clinically asymptomatic mother were normal (IFN score of 1.29) at age 33 years.

Exome sequencing identified a maternally inherited heterozygous c.784C>T (p.Q262*) variant in *PTPN1* not present on gnomAD v.4.1.0.

AGS3479: This female was born to non-consanguineous parents of Jewish ancestry, and demonstrated a normal developmental profile up to 1.5 years of age. At this time she developed a left-sided hemiparesis associated with marked contralateral hemispheric atrophy. Brain biopsy at the age of 2 years and 3 months showed areas of gliosis, focal perivascular lymphohistiocytic infiltrates and suspected partial myelin loss. Over a several-month period her disease evolved to four-limb spastic-dystonia with drooling, dysphagia and no speech. Exhaustive workup was notable only for raised CSF neopterin (330 nmol/L with normal <30 nmol/L). A second MRI showed extension of the atrophy to the other hemisphere.

Her mother is clinically asymptomatic at the age of 43 years.

ISGs tested on two occasions revealed IFN scores of 8.01 and 8.67 at ages 2.46 and 2.66 years respectively. ISGs tested in the clinically asymptomatic mother were minimally elevated (interferon score of 2.91) at age 43 years.

Exome sequencing identified a maternally inherited heterozygous c.166C>T (p.R56W) variant in *PTPN1* present on 2 alleles on gnomAD v4.1.0 in the heterozygous state.

AGS3542: Following completely normal development, this female presented at age 23 months with progressive spastic tetraparesis more pronounced on the left side with initially normal cognition and speech. She then experienced a further period of regression at age 36 months, which also affected her speech and swallowing with limited articulation and drooling. Cerebral MRI demonstrated right-sided hemiatrophy which then extended bilaterally. There was improvement in brain volume following pulsed methylprednisolone and mycophenolate mofetil started at age 3 years. Now, aged 8 years, she has only very few words (< 20), but has relatively well-preserved communication via a computer-assisted language tool, and she can use an electric wheelchair unaided.

Her father is clinically asymptomatic at the age of 46 years.

CSF neopterin was elevated at 114 nmol/L and 352 nmol/L (range 5 – 53 nmol/L) at ages 2 and 3 years respectively, and normal when tested at 7 years of age. ISGs tested on one

occasion revealed an IFN score of 3.105 at age 8.22 years. ISGs tested in the clinically asymptomatic father were normal (interferon score of -1.28) at age 46 years.

Exome sequencing identified a paternally inherited heterozygous c.505C>T (p.R169*) variant in *PTPN1* present at 1 allele on gnomAD v4.1.0.

AGS3561: This female is the youngest of 8 children born to a non-consanguineous couple of Jewish ancestry. After normal development, shortly following infection with SARS-CoV-2, at age 7 years she experienced neurological regression with a progressive gait abnormality, speech disturbance and mild cognitive decline. She began to walk slowly, with unstable gait and recurrent falls, demonstrating cerebellar, extrapyramidal and pyramidal signs, weakness and dystonic posturing more so on the right side of the body. Her speech was dysarthric, so that she could only manage simple and short conversations, and her eating was slow and disorganized, albeit without aspiration. CSF neopterin was measured at 139 nmol/L at the age of 8 years (normal range < 20 nmol/L). There has been a subsequent re-attainment of some skills, so that she now speaks in relatively simple sentences with reduced comprehension. She can walk independently but only over a short distance. Cerebral MRI showed diffuse, patchy high T2 white matter signal abnormalities with cerebral atrophy.

Her father is clinically asymptomatic at the age of 52 years.

ISGs tested on one occasion revealed an IFN score of 7.27 at age 8.28 years.

Exome sequencing identified a paternally inherited heterozygous c.619G>T (p.E207*) variant in *PTPN1* not present on gnomAD v4.1.0.

Of the ten (Table 2, Fig. 18) putative mutations (the identical R156* being seen in two families, and the K197R in two affected first cousins from one family), six were predicted to introduce a premature stop codon, and two involved canonical splice site nucleotides likely to disrupt mRNA splicing and severely affect protein sequence. Further, while the two missense substitutions are predicted to have relatively mild effects on protein stability, they occur at evolutionarily conserved residues that have been described as playing important roles in the

allosteric regulation of PTP1B function.[376,377] *PTPN1* is a highly constrained gene with a pLI of 1, indicating strong negative selection against LOF variants. Consistent with this, of the variants recorded in our cohort, only the R56W and the R169* were present in gnomAD v4.1.0 (seen in the heterozygous state twice and once, respectively, out of > 1,600,000 alleles). While in three patients the variant appeared to have occurred de novo, in nine cases the variants were inherited from an asymptomatic parent (with two asymptomatic fathers to the two affected first cousins in family AGS492). It is of note that the R156* mutation was seen to occur de novo in one family (AGS2942), and to have been inherited from an asymptomatic mother in another (AGS1036). Of further note, the R156* and R56W mutations were previously reported as somatic driver mutations in, respectively, PMBCL and HL.[341]

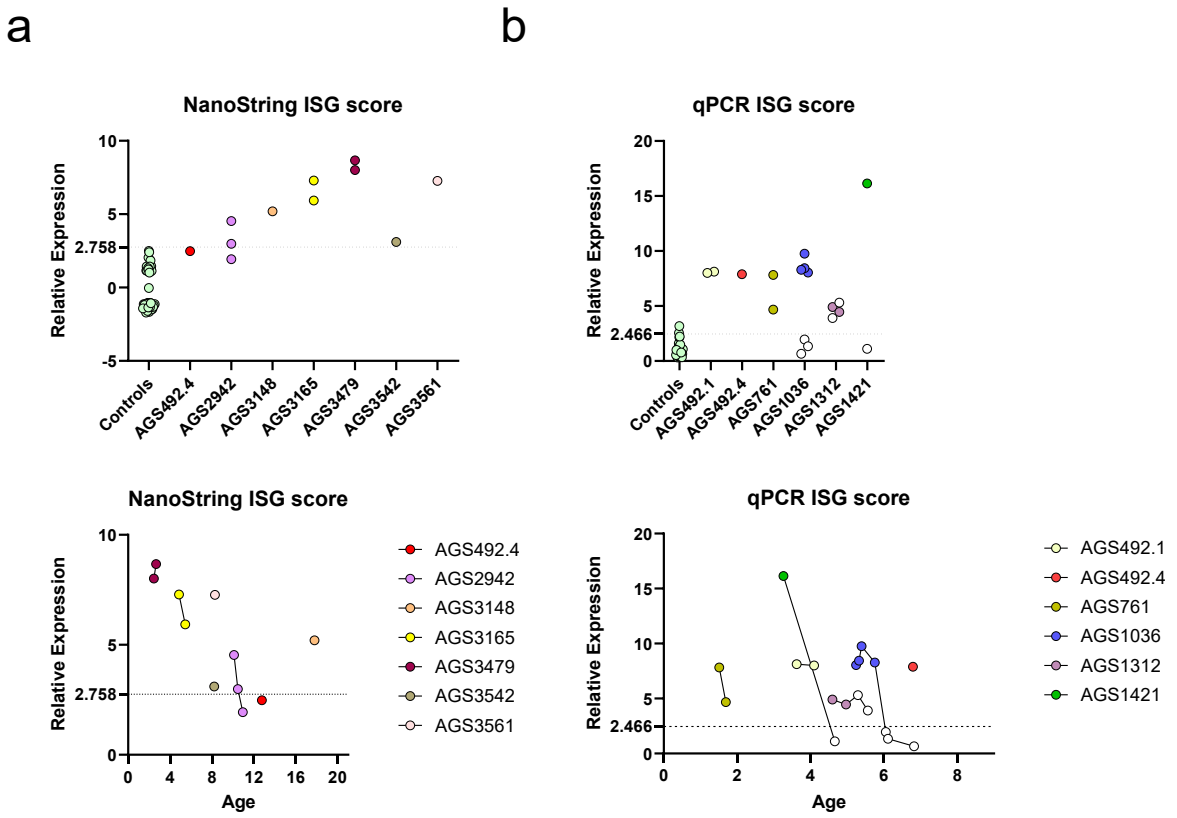
a
b
NanoString ISG score
Relative Expression
10
5
2.758
0
-5
Controls
AGS492.4
AGS2942
AGS3148
AGS3165
AGS3479
AGS3542
AGS3561
qPCR ISG score
20
15
10
5
2.466
0
Controls
AGS492.1
AGS492.4
AGS761
AGS1036
AGS1312
AGS1421
NanoString ISG score
Age
0
4
8
12
16
20
AGS492.4
AGS2942
AGS3148
AGS3165
AGS3479
AGS3542
AGS3561
qPCR ISG score
2
4
6
8
AGS492.1
AGS492.4
AGS761
AGS1036
AGS1312
AGS1421

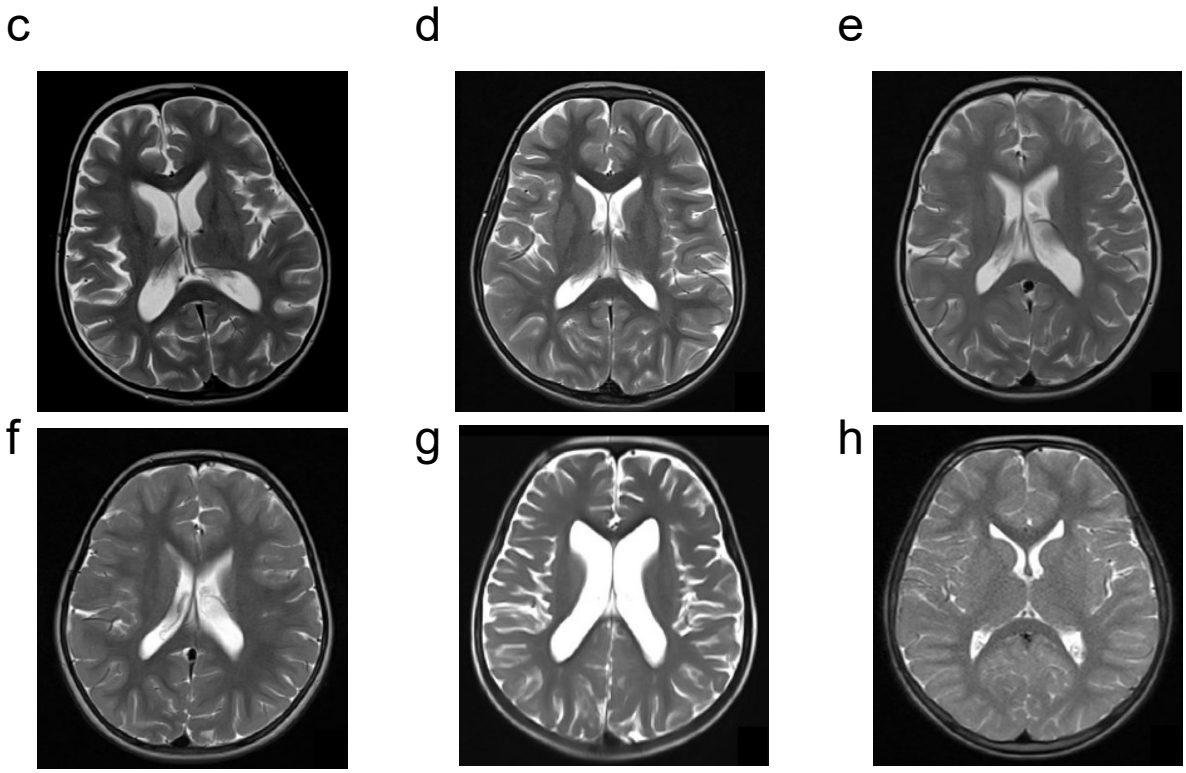
c
d
e
f
g
h

Fig. 17. Clinical features. a-b upper panels. Enhanced ISG expression in patient whole-blood evaluated by NanoString (a) or qPCR (b) compared to composite data from healthy controls. a-b lower panels. Same ISG scores plotted as the upper panel, with corresponding age for each testing. Horizontal dashed lines represent the thresholds for positive ISG scores (2.758 for NanoString and 2.466 for qPCR). Filled and empty circles denote the ISG scores tested before and after treatment, respectively. ISG score is calculated as the median of expression of 24 ISGs (NanoString) or 6 ISGs (qPCR). c-d (AGS1036), e-f (AGS1312) and g-h (AGS1421), Brain MRI axial T2 images. c. Generalised volume loss more prominent in the right cerebral hemisphere at age 5 years (5 months after initial described symptom onset). d. Significant reversal of previously noted appearances of ventricular and sulcal prominence 23 months after treatment with intravenous (IV) methylprednisolone (MP) and IV immunoglobulin (IG). e. Slight reduction in the cerebral and cerebellar white matter bulk at age 4 years (9 months after reported symptom onset). f. Improvement of white matter bulk 13 months after treatment with IVMG and IVIG. g. Bilateral ventricular and sulcal prominence demonstrating volume loss at age 32 months (12 months after reported symptom onset). h. Complete reversal of the previously noted changes 26 months after treatment with IVMP and IVIG. c-h taken from Sa et al.

Table 2. Novel or very rare heterozygous variants in *PTPN1* identified in patient cohort.

Patient	cDNA	Consequence	Inheritance	Allele count on gnomAD v4.1.0
AGS492.1	c.590A>G (exon 6)	p.(K197R)	Paternally inherited	0
AGS492.4	c.590A>G (exon 6)	p.(K197R)	Paternally inherited	0
AGS761	c.63+1G>C	Partial intron 1 retention and NMD	De novo	0
AGS1036	c.466C>T (exon 5)	p.(R156*)	Maternally inherited	0
AGS1312	c.1000delG (exon 8)	p.(V334*)	Paternally inherited	0
AGS1421	c.370_386del (exon 5)	p.(Y124Rfs*7)	Paternally inherited	0
AGS2942	c.466C>T (exon 5)	p.(R156*)	De novo	0
AGS3148	c.154+1del	Exon 2 skipping and premature stop codon	De novo	0
AGS3165	c.784C>T (exon 7)	p.(Q262*)	Maternally inherited	0
AGS3479	c.166C>T (exon 3)	p.(R56W)	Maternally inherited	2/1,612,624 alleles
AGS3542	c.505C>T (exon 6)	p.(R169*)	Paternally inherited	1/1,613,702 alleles
AGS3561	c.619G>T (exon 6)	p.(E207*)	Paternally inherited	0

Note: NMD = nonsense-mediated decay. p.(Arg56Trp) and p.(Arg156*) reported as somatic mutations in, respectively, Hodgkin lymphoma and primary mediastinal B cell lymphoma.[341]

a

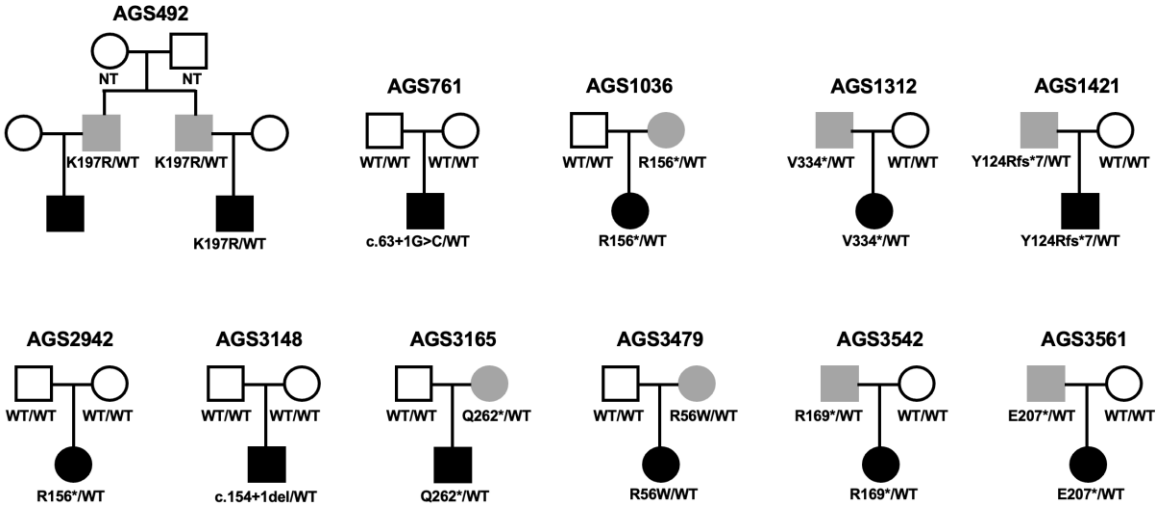

b

c

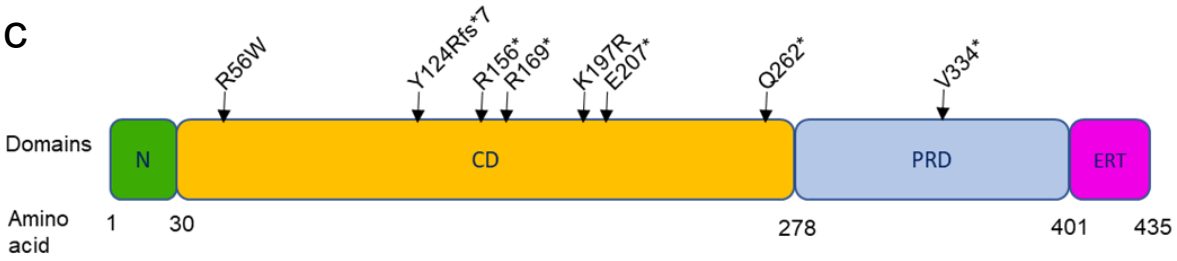

d

```
                    R56W                                K197R
Human       RNRYRDVSPFDHSRIKLHQEDNDYINASLI      VPESPASFLNFLFKVRESGSLS
Gorilla     RNRYRDVSPFDHSRIKLHQEDNDYINASLI      VPESPASFLNFLFKVRESGSLS
Chimpanzee  RNRYRDVSPFDHSRIKLHQEDNDYINASLI      VPESPASFLNFLFKVRESGSLS
Cow         RNRYRDVSPFDHSRIKLHQEDNDYINASLI      VPESPASFLNFLFKVRESGSLS
Cat         RNRYRDVSPFDHSRIKLHQEDNDYINASLI      VPESPASFLNFLFKVRESGSLS
Mouse       RNRYRDVSPFDHSRIKLHQEDNDYINASLI      VPESPASFLNFLFKVRESGSLS
Rat         RNRYRDVSPFDHSRIKLHQEDNDYINASLI      VPESPASFLNFLFKVRESGSLS
Chicken     RNRYRDVSPFDHSRIKLNQGDNDYINASLI      VPESPASFLNFLFKVRESGSLN
Zebrafish   RNRYRDVSPFDHSRICLQIGCNDYINASLI      VPESPASFLNFLFKVRESGCLS
Xenopus     RNRYRDVSPFDHSRIKLHREDNDYINASLI      VPESPASFLNFLFKVRESGSLN
            ************** *:   *********      ******************.*.
```

Fig. 18. Variants in *PTPN1* identified in patient cohort. a. Family pedigrees where an affected individual carries a novel or very rare heterozygous non-synonymous substitution in *PTPN1*. Circles and squares indicate female and males respectively. Dark and light colouring denote, respectively, affected and clinically asymptomatic mutation-positive individuals. NT = not tested; WT = wild-type. b. Cartoon of *PTPN1* locus with perpendicular black lines indicating exons numbered above. Numbers below (1, 22, 52, etc) indicate the first amino acid (AA) position in the respective exon. The two splicing variants are depicted on the top with red arrows showing the relative position next to the exon. c. Cartoon of the protein domains of PTP1B, with amino acid numbering below. STOP mutations and non-synonymous missense substitutions are indicated. N = N terminal domain; CD = catalytic domain; PRD = proline-rich domain; ERT = ER-targeting domain. d. Clustal Omega alignment of PTP1B, with the two non-synonymous missense substitutions identified in our cohort highlighted in yellow. Alignments are based on the human transcript of *PTPN1* / PTP1B: ENST00000371621.5; NM_002827.4.; NP_002818.1.

mRNA and protein expression of *PTPN1* variants in patient-derived material

Consistent with our genetic data, reduced expression of *PTPN1* mRNA (Fig. 19a), and of the encoded PTP1B protein (Fig. 19b), was observed in the three patient fibroblast cell lines available carrying a predicted nonsense mutation in *PTPN1*. Of note, Arg156* was previously shown to be unstable when expressed in HEK293 cells.[341] *PTPN1* mRNA expression was apparently preserved in the patient with the c.154+1del canonical donor splice site variant in intron 2 (Fig. 19a). Indeed, deep sequencing of captured *PTPN1* cDNA from primary fibroblasts of this patient revealed the skipping of exon 2 in 50% of transcripts (8036 reads versus 7931 reads for the canonically spliced transcript), suggesting preserved expression of the mutant allele and the absence of nonsense-mediated decay (NMD) (Fig. 19c). However, the skipping of exon 2 leads to a frameshift, and the introduction of a premature stop codon in exon 3 after 19 amino acids. The putative truncated protein translated would have a size of 40 amino acids and 4.6kDa (Fig. 19e). Deep sequencing also revealed the appearance of a splicing site inside exon 2, which would lead to a stop codon at the following codon and a 46 amino acid protein (Fig. 19e). Either truncation could not be detected by western blotting of primary fibroblasts lysates, a finding consistent with protein instability and the observed reduced protein expression (Fig.19b). In contrast, on sequencing of *PTPN1* cDNA captured from whole-blood in the context of the c.63+1G>C variant, we observed fewer reads (0-9723 to 0-5122 read range) and no major splicing defect, indicative of NMD of the mutated allele (Fig. 19d). We also observed the appearance of a novel minor splicing site in intron 1, which

could lead to retention of part of intron 1, a premature stop codon and the production of a 114 amino acid peptide (Fig. 19e).

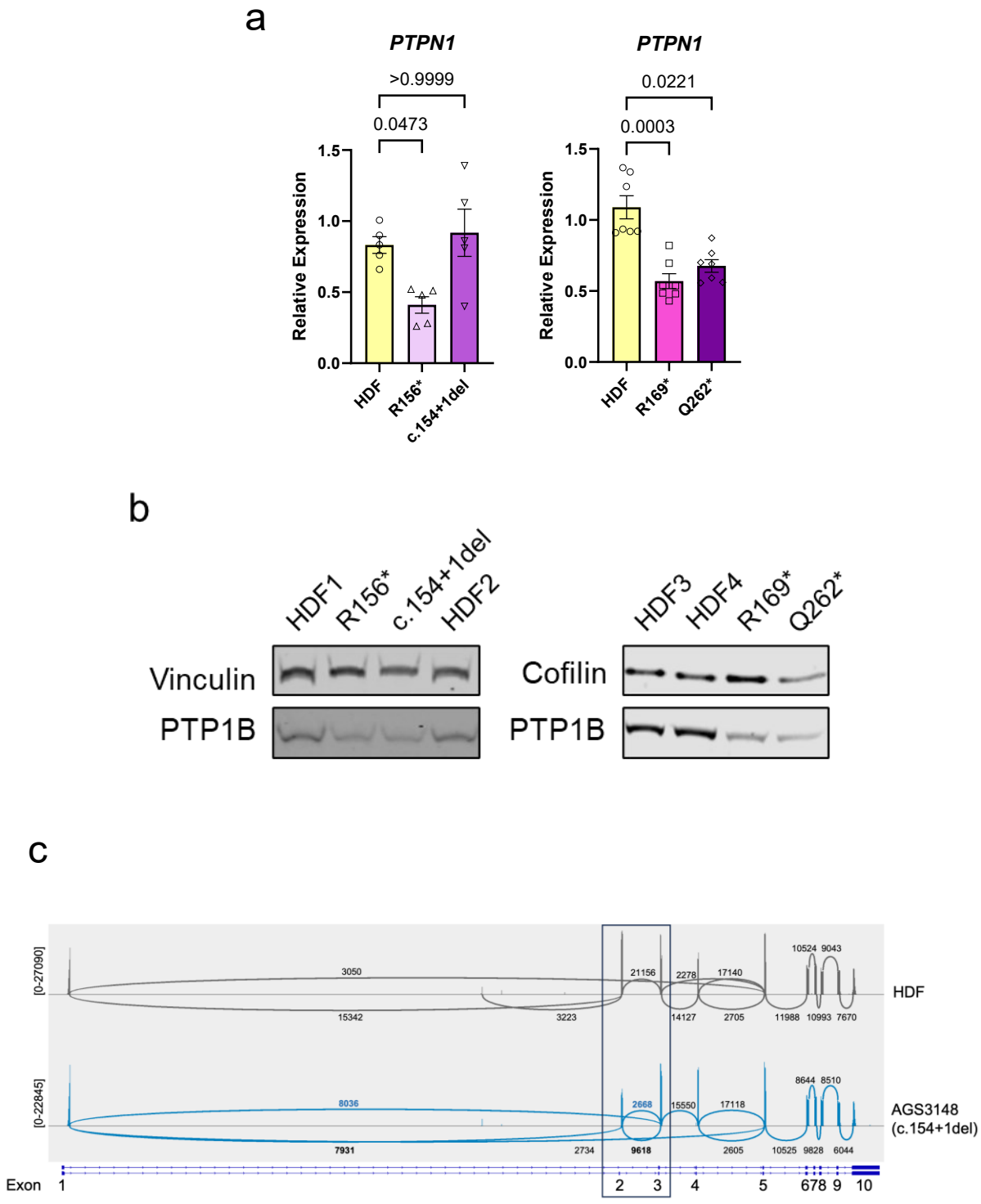

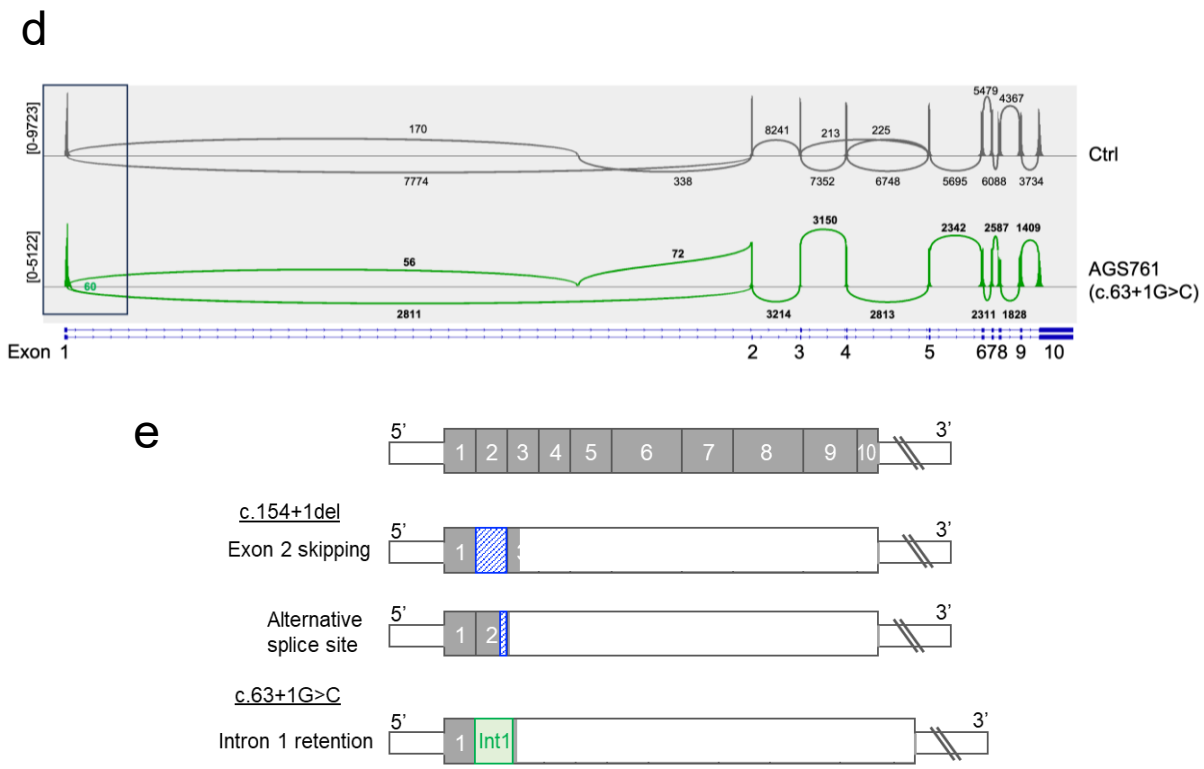

Fig. 19. Studies of mRNA and protein expression of *PTPN1* variants using patient-derived material. a-b. qPCR analysis (a) of *PTPN1* mRNA expression, and representative immunoblots (b) of PTP1B protein expression, in patient-derived primary dermal fibroblasts carrying the indicated heterozygous variants. HDF = control human dermal fibroblasts. For qPCR, n=5-7 experiments and Kruskal-Wallis test, with Dunn's post-hoc comparison, was used to compare the expression levels of *PTPN1* in healthy control cells and patient cells. c-d. Sashimi plots showing exon–exon junctions and splicing for *PTPN1* transcripts obtained by next generation sequencing of captured *PTPN1* cDNA from control (HDF) and patient AGS3148 primary fibroblast RNA, and from control (Ctrl) and AGS761 patient whole blood RNA. The *PTPN1* gene locus is shown along the horizontal axis. Histogram spikes represent the amount of reads sequenced for the relevant location, and total ranges of read number are indicted on the left. Numbers over the lines connecting exons represent the number of reads mapped to relevant exon–exon junctions: bold indicates a change in abundance, and blue or green colours indicate a novel junction. e. Schematic representation of full-length cDNA of WT and mutated *PTPN1*. The coding sequences of the exons are numbered and shown in grey, and the 5′- or 3′-UTR is shown in smaller open boxes. For the c.154+1del variant, capture RNA sequencing showed full and partial exon 2 skipping, represented by hashed blue boxes leading to stop codons, symbolised by an open box downstream. For the c.63+1G>C variant, we found a minor cDNA species with partial intron 1 retention, represented by the green box, leading to a stop codon in exon 3.

PTPN1-deficient immortalised fibroblasts and epithelial cells display an inflammatory phenotype

To study the link between disease-associated *PTPN1* variants (and, more generally, *PTPN1* deficiency) and IFN-I signalling, using CRISPR-Cas9 gene editing, I generated *PTPN1* WT and homozygous KO BJ-5ta fibroblast single-cell clones and stable *PTPN1* WT and KO RPE-

1 (retinal pigment epithelial) pools (two hTERT immortalised primary-like cell lines commonly used in innate sensing and IFN-I signalling studies). By western blot, KO BJ-5ta clones and RPE-1 pools demonstrated an apparently complete absence of PTP1B expression (Fig. 20a, b), indicating successful KO of both *PTPN1* alleles.

I first probed baseline ISG expression in these *PTPN1* WT and KO single-cell BJ-5ta clones using qPCR, with an ISG score calculated as the median of the expression of five ISGs. Compared to composite data derived from two to four WT control clones, clones deficient for *PTPN1* displayed significantly enhanced baseline ISG expression (Fig. 20c). The expression levels of other inflammatory genes such as those for pro-inflammatory cytokines *IL1B* and *TNF* were also elevated in *PTPN1* KO cells (Fig. 20c), implying an activation of NF-κB signalling in these cells. While an increase in IFNα protein levels in the CSF and serum was recorded in one patient, type I interferon mRNA expression was comparable between *PTPN1* WT and KO BJ-5ta cells (Fig. 20c, *IFNB1*). Similarly, *PTPN1*-deficient RPE-1 pool also demonstrated upregulation of ISG (with an ISG score calculated as the median of the expression of four ISGs), as well as pro-inflammatory cytokine *IL1B* and *IL6*, expression, compared to WT pool (Fig. 20d), but which was not the case for *IFNB1* expression (Fig. 20d, *IFNB1*).

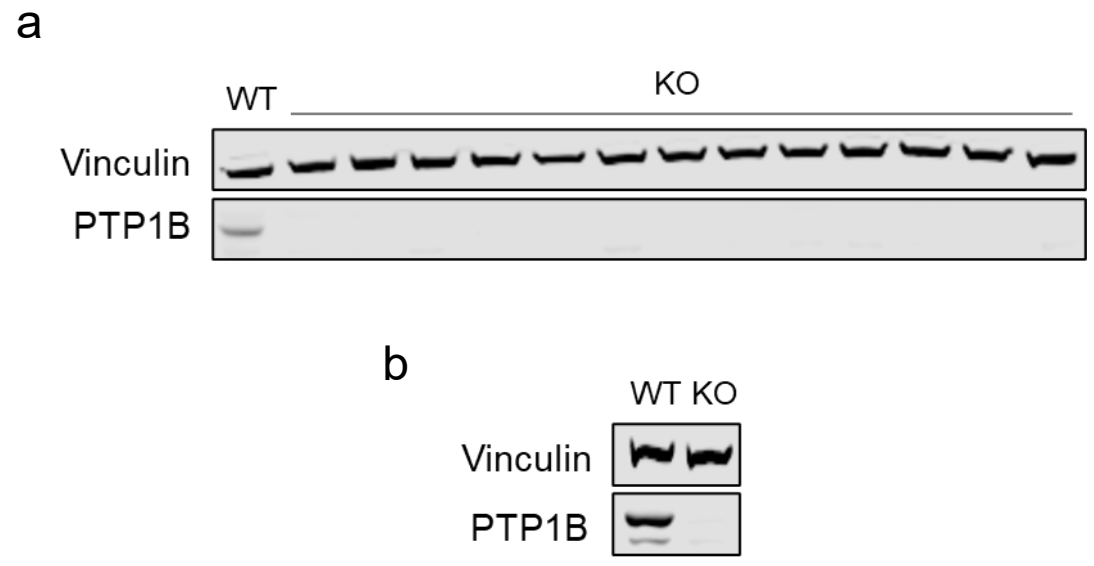

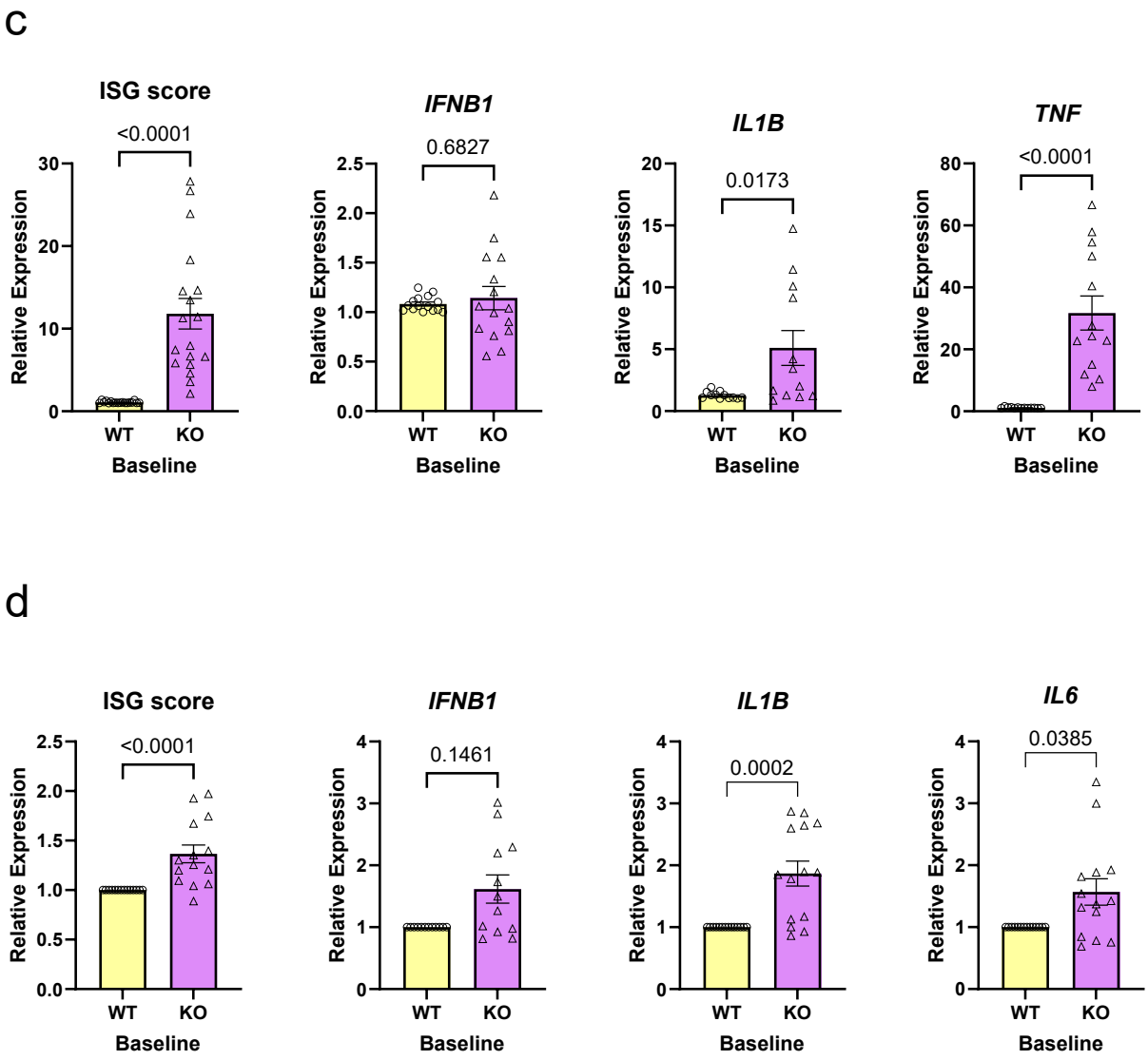

Fig. 20. *PTPN1*-deficient BJ-5ta and RPE-1 cells display an inflammatory phenotype. a-b. Representative immunoblots of BJ-5ta clones (a) and RPE-1 pools (b) either WT or KO for *PTPN1*. Vinculin is used as a loading control. c-d. qPCR analyses of baseline ISG, *IFNB1*, *IL1B*, *TNF* (for BJ-5ta), and *IL6* (for RPE-1), expression in *PTPN1* WT and KO BJ-5ta clones (c) and RPE-1 pools(d). c. Each circle or triangle represents the average ISG score or gene expression from two to four independent clones of the same genotype in one experiment. ISG score is calculated as the median of the expression of five ISGs, *IFI27*, *IFI44L*, *MX1*, *OAS1* and *RSAD2* for BJ-5ta; and of four ISGs, *IFI27*, *IFI16*, *IRF7*, and *MX1* for RPE-1. Mann-Whitney test was used to compared the difference of gene expression in WT and KO cells.

Since all the variants identified in the patients are heterozygous, complete *PTPN1* KO cells obtained using the above CRISPR-editing strategy do not precisely mimic patient genotypes. Thus, I next generated heterozygous WT/KO clones to investigate each of the presumed partial-loss-of-expression variants identified in our cohort. Additionally, I generated a WT/KI clone carrying a c.63+1G>C variant in the heterozygous state - seen in patient AGS761 - which is predicted to result in a splicing-defect and subsequent loss of mRNA expression. Assessing PTP1B expression in these clones, in contrast to homozygous KO cells, it was clear that all the heterozygous clones retained partial expression of PTP1B (Fig. 21a). Importantly, similar to complete *PTPN1* KO cells, heterozygous clones also exhibited raised baseline ISG expression compared to WT controls (Fig 21b). Again, as for homozygous KO clones (Fig. 21b), there was no significant difference in *IFNB1* expression between WT and heterozygous mutant cells (Fig. 21b, *IFNB1*).

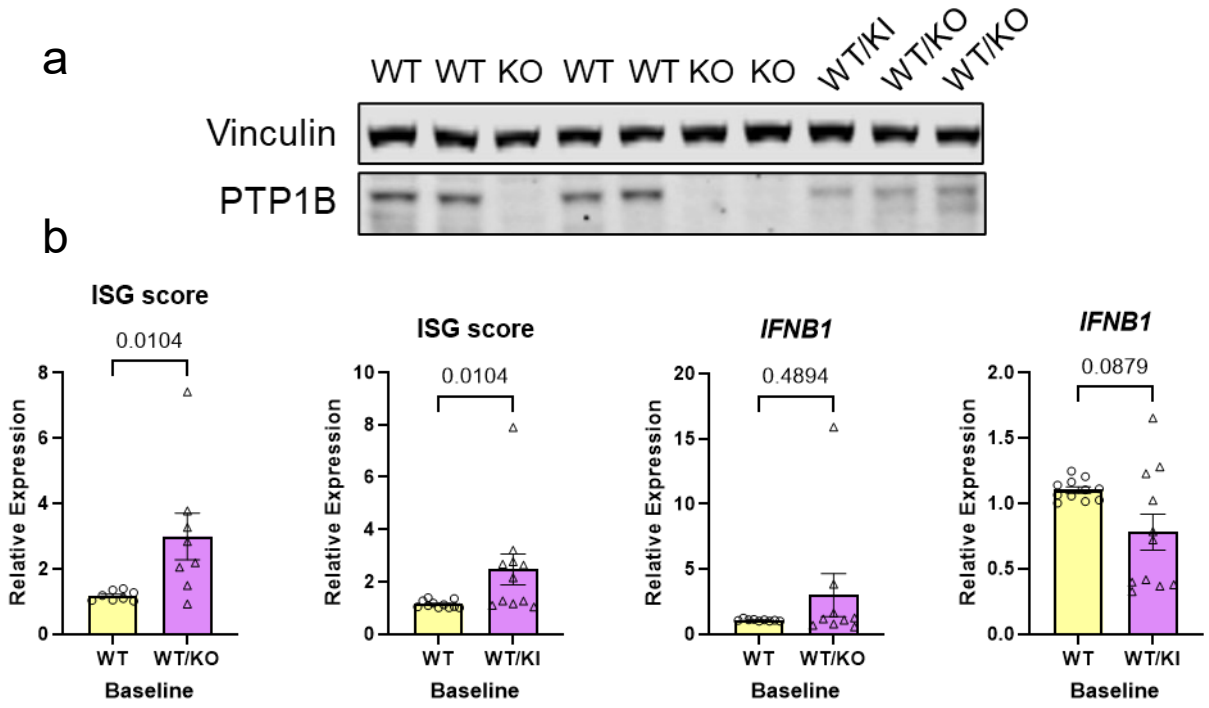

Fig. 21. Heterozygous *PTPN1*-deficienct BJ-5ta clones exhibit elevated baseline ISG expression, and equivalent levels of *IFNB1* expression, compared to WT controls. a. Representative immunoblot showing PTP1B expression in BJ-5ta single-cell clones. WT/KI represents WT/c.63+1G>C. Only three out of thirteen KO clones, and two out of four WT/KO clones, are shown here. Vinculin is used as a loading control. b. qPCR analyses of baseline expression of ISGs and *IFNB1*. Each circle or triangle represents the average ISG score or *IFNB1* expression from independent clones of the same genotype (WT, two to four clones; WT/KO, four clones; WT/KI, one clone) in one experiment. ISG score is calculated as the median of the expression of five ISGs, *IFI27*, *IFI44L*, *MX1*, *OAS1* and *RSAD2*. Mann-Whitney test was used to compared the difference of gene expression in WT and mutant cells.

PTPN1 deficiency renders cells hypersensitive to stimulations with IFNα2b and the STING agonist diABZI

PTP1B is a non-receptor tyrosine phosphatase, with defined functions in a number of signalling pathways through the removal of phosphate moieties from distinct substrates. One such pathway is the IFN-I signalling pathway. It has long been known that PTP1B acts as a negative regulator to restrict excessive IFN-I signalling,[300] preventing cellular and tissue damage resulted from sustained ISG expression. Through the dephosphorylation of TYK2 (and JAK1),[300,301] PTP1B effectively deactivates the signalling cascade. Another study also suggests that STING could be a substrate of PTP1B, leading to the ubiquitin-independent 20S proteasomal degradation of STING.[299] Given these past reports, I performed a time-course experiment following stimulations with IFNα2b (Fig. 22a) or the STING agonist diABZI (Fig. 22b) in *PTPN1* WT and KO BJ-5ta cells. By western blot, *PTPN1*-deficient cells demonstrated higher global phospho-tyrosine protein levels even at baseline (Fig. 22a-b, lanes labelled ‘‘UT’’; Fig. 22c). After stimulation for the indicated times, higher levels of global phospho-tyrosine protein expression were observed in KO cells compared to WT controls, especially at 1-hour following IFNα2b stimulation and 4-hour after stimulation with diABZI (Fig. 22a, b, d, e).

In light of the above observation, and to further investigate the activation status of STING and IFNAR pathways, I also examined the phosphorylation levels of key signalling molecules, namely phospho-STING (p-STING) and phospho-STAT1 (p-STAT1). As Fig. 23a shows, following 1000 IU/mL of IFNα2b stimulation for the indicated times, PTP1B KO cells exhibited higher amounts of p-STAT1 expression, especially at time point 1-hour (Fig. 23b). Similarly, at time point 4-hour following stimulation with 1 μM STING agonist diABZI, PTP1B KO cells expressed more p-STING, compared to WT controls (Fig. 23c, d). Additionally, in line with the reports by Xia, et al. that PTP1B dephosphorylates STING to promotes its 20S proteasomal degradation,[299] at baseline, PTP1B KO cells expressed higher amounts of STING protein (Fig. 23c, lanes labelled ‘‘UT’’; 23e). These data suggested that both STING and IFNAR pathways were hyperresponsive upon stimulation in PTP1B deficient cell.

a

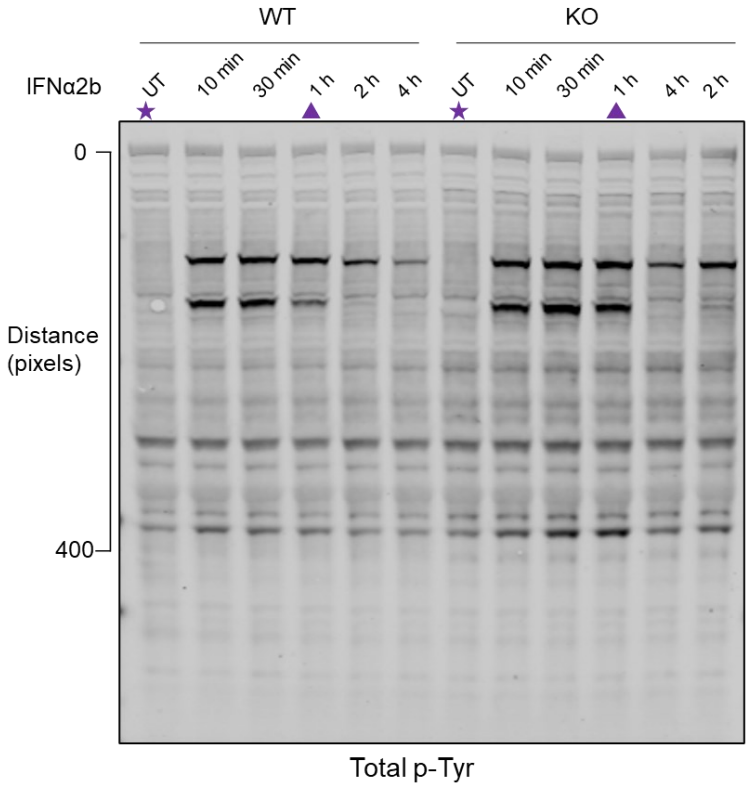
WT
KO
IFNα2b
UT
10 min
30 min
1 h
2 h
4 h
UT
10 min
30 min
1 h
4 h
2 h
0
Distance
(pixels)
400
Total p-Tyr

b

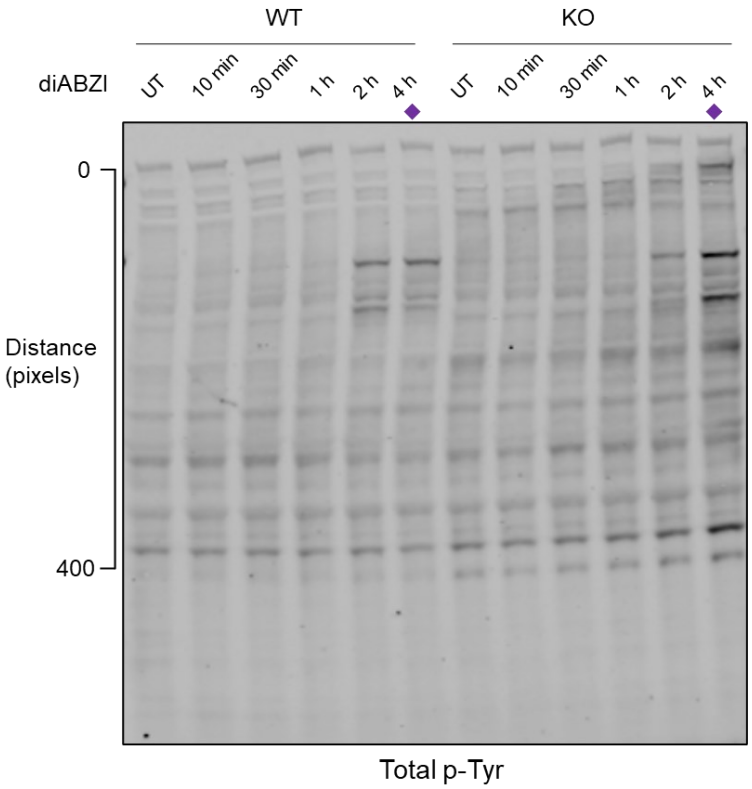
WT
KO
diABZI
UT
10 min
30 min
1 h
2 h
4 h
UT
10 min
30 min
1 h
2 h
4 h
0
Distance
(pixels)
400
Total p-Tyr

c

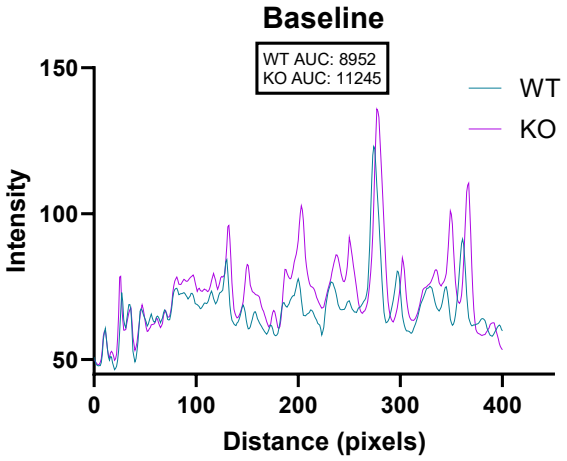

d

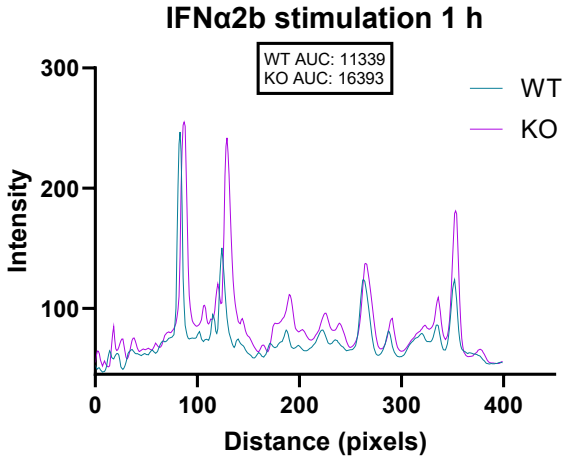

e

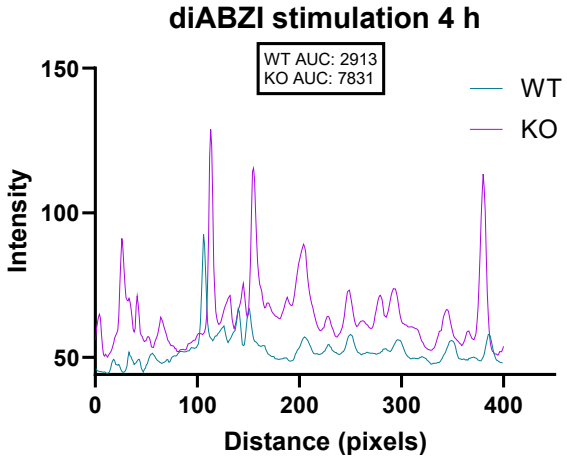

Fig. 22. PTP1B KO BJ-5ta cells display higher global tyrosine phosphorylatin at baseline and upon stimulation. a-b. Representative immunoblots for total phospho-tyrosine (p-Tyr) protein levels in a time-course experiment following stimulation with 1000 IU/mL IFNα2b (a) or 1 μM diABZI (b) for the indicated times. WT, one clone; KO, one clone. UT, untreated. Perpendicular scales (0 to 400) on the left indicate the direction and distance in the blots for densitometry quantification in c, d, and e. Purple stars, triangles, and diamonds indicate the lanes used for densitometry quantification in c, d, and e, respectively. Note the transposition of the 4h and 2h samples for the KO clone in (a). c-e. Densitometry quantification of lanes in a and b, as described above, for total phospho-tyrosine protein expression at baseline (c), and following stimulation with IFNα2b (d) for 1 hour, and with diABZI (e) for 4 hours. AUC, area under curve.

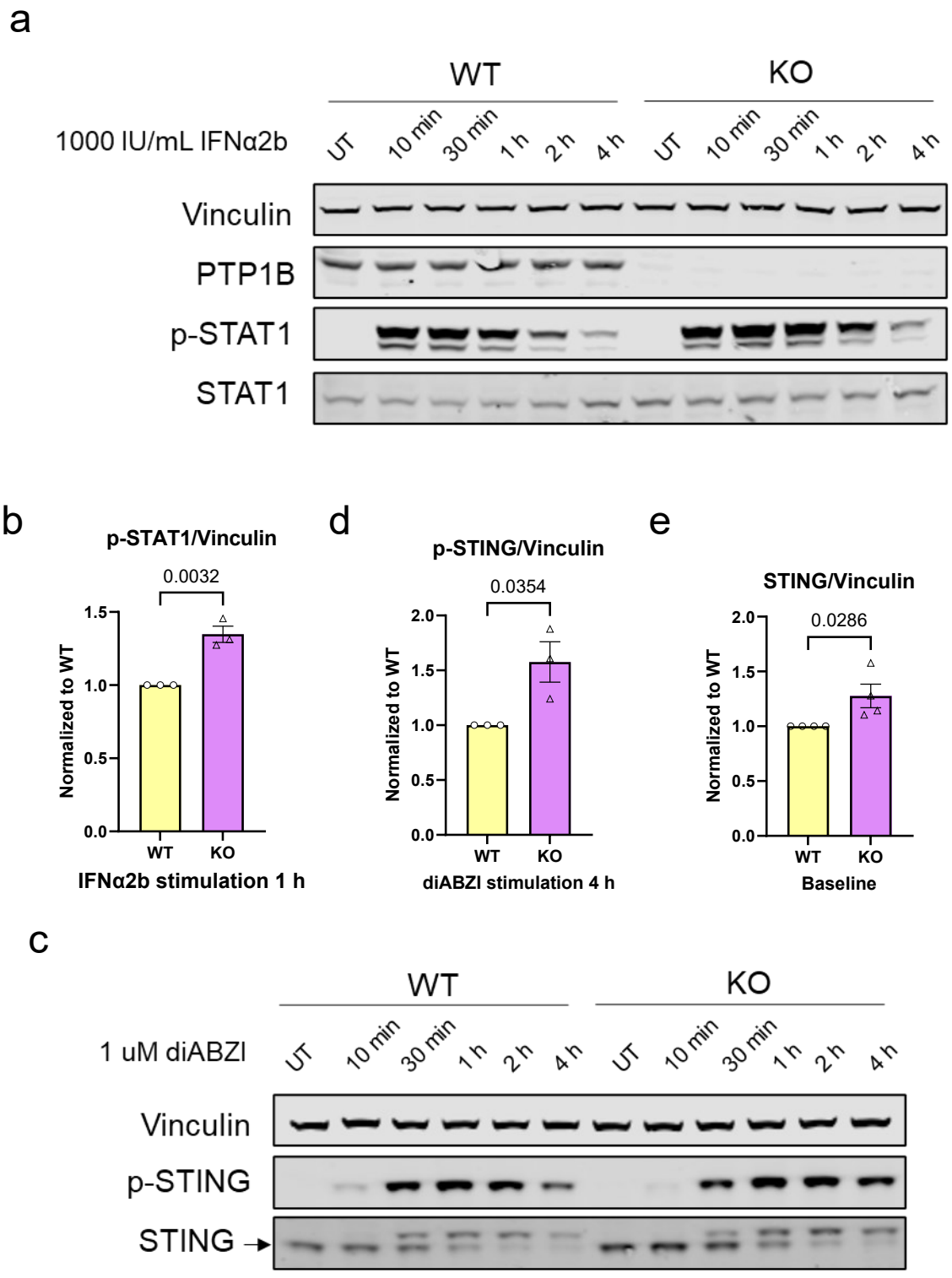

Fig. 23. Both IFNAR and STING pathways are hyperresponsive to stimulation in PTP1B KO BJ-5ta fibroblasts. a. Representative immunoblot of a time-course 1000 IU/mL IFNα2b stimulation for the indicated times. WT, one clone; KO, one clone. UT, untreated. b. Densitometry quantification of p-STAT1 at time point 1-hour. Unpaired t test was used to compare the difference of p-STAT1 expression in WT and KO cells. c. Representative immunoblot showing a time-course 1 μM diABZI stimulation for the indicated times. WT, one clone; KO, one clone. UT, untreated. Arrow indicates the band for STING. The band above it is p-STING. d-e. Densitometry quantifications of p-STING at diABZI stimulation time-point 4-hour (d) and total STING at baseline (e). Unpaired t test and Mann-Whitney test were used to compared the difference of p-STING (d) and total STING (e) in WT and KO cells.

Given evidence of higher levels of phospho-tyrosine protein expression after IFNα2b or diABZI stimulation in *PTPN1*-deficient cells, and higher phosphorylation levels of key effectors in IFNAR and STING pathways (p-STAT1 and p-STING, respectively), I went on to test the effects of IFNα2b or diABZI stimulation on ISG expression in these cells. Compared to WT clones, KO and WT/KI clones all displayed a significantly higher sensitivity to an IFN-I stimulus, as shown by the enhanced ISG expression assessed by qPCR analysis after a 6-hour 200 IU/mL IFNα2b stimulation (Fig. 24a). WT/KO cells also showed a similar trend of enhancement, albeit without a statistical significance (Fig. 24a). Similar to IFNα2b stimulation, *PTPN1*-deficient cells also displayed a higher response to diABZI stimulation. Thus, by qPCR analysis, *PTPN1* KO, WT/KO and WT/KI cells all demonstrated an increase in ISG expression compared to WT cells after a 0.01 μM diABZI stimulation for 6 hours (Fig. 24b). Besides the hyperactive IFN-I signalling pathway per se in *PTPN1*-deficient cells seen in Fig. 23a and Fig.24a, another possible explanation could be an overexpression of type I interferon *IFNB1* (Fig. 24c) in *PTPN1* mutant cells after diABZI stimulation.

Around the same lines, RPE-1 cells absent for PTP1B also displayed higher sensitivity to IFNα2b and diABZI stimulation. Phosphorylation levels of STAT1 were elevated in PTP1B KO RPE-1 cells compared to WT in time-course stimulation experiments with 500 IU/mL IFNα2b, at least at time points 10-min and 30-min (Fig. 25a, b). Consistently, overexpression of ISGs were observed in KO cells, following stimulation with 200 IU/mL IFNα2b for 6 hours (Fig. 25c). Moreover, higher amounts of ISGs, *IFNB1*, and pro-inflammatory cytokines *IL1B* and *IL6* were also expressed by KO RPE-1 cells after 0.1 μM diABZI stimulation for 6 hours (Fig. 25d). Finally, to further explore our hypothesis that a haploinsufficiency/deficiency of PTP1B activity leads to an inflammatory phenotype, I also treated WT parental hTERT RPE-1 cells with a selective, reversible, and non-competitive allosteric inhibitor of PTP1B, which binds to a novel site away from the catalytic pocket and inhibits phosphatase activity by preventing closure of the WPD loop.[380] qPCR analysis showed that cells treated with the PTP1B inhibitor

demonstrated higher levels of ISG expression compared to cells treated with DMSO control (Fig. 25e), implying that PTP1B activity is essential to homeostasis in IFN-I signalling.

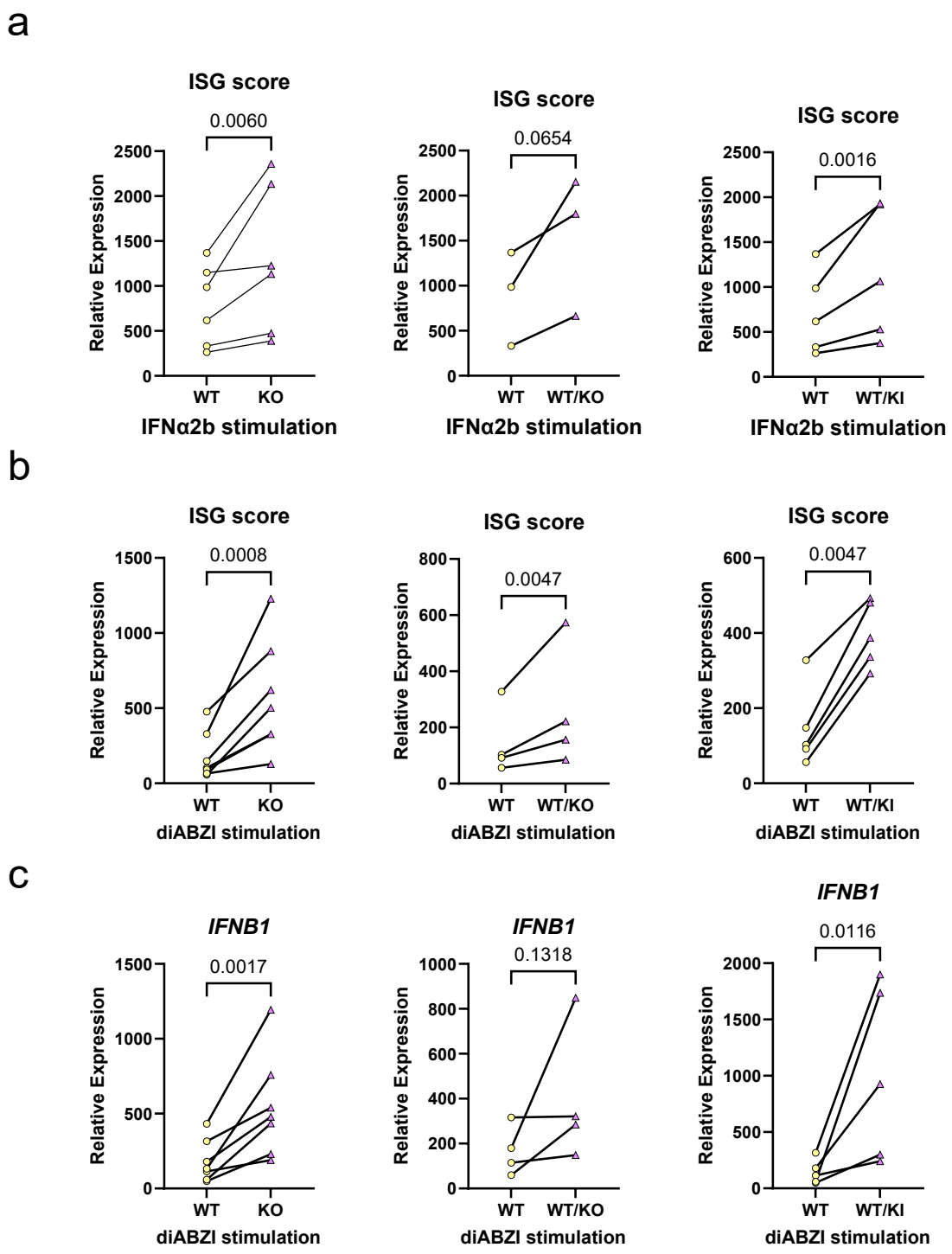

Fig. 24. qPCR analyses in *PTP1N* WT and mutant BJ-5ta cells. a-c. qPCR analyses of ISG (a-b) and *IFNB1* (c) expression after 200 IU/mL IFNα2b (a) or 0.01 μM diABZI (b-c) stimulation for 6 hours. Each circle or triangle represents the average ISG score or *IFNB1* expression from independent clones of the same genotype (WT, two to four clones; WT/KO, four clones; WT/KI, one clone) in one experiment. ISG score is calculated as the median of the expression of five ISGs, *IFI27*, *IFI44L*, *MX1*, *OAS1*, and *RSAD2*. Paired ratio t test was used to compared the difference of gene expression in WT and mutant cells.

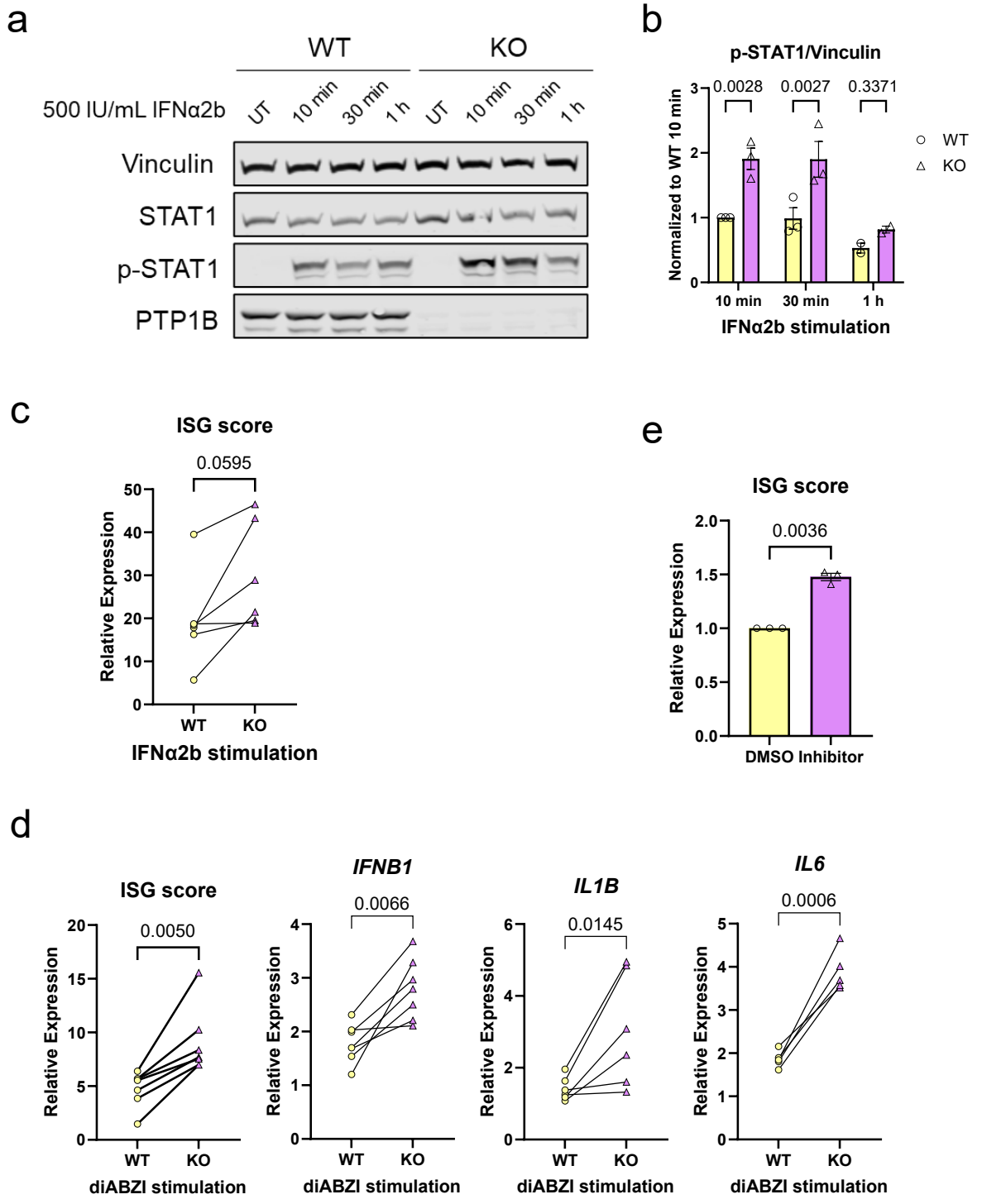

Fig. 25. *PTPN1*-deficient hTERT RPE-1 cells demonstrate higher sensitivity to IFNα2b and diABZI stimulation. a. Representative immunoblot showing a time-course following 500 IU/mL IFNα2b stimulation for the indicated times. UT, untreated. b. Densitometry quantification as in a. n = 3 for time points 10-min and 30-min. n = 2 for time point 1-h. Two-way ANOVA was used to compared the STAT1 phosphorylation levels between WT and KO cells in each time point. c-d. qPCR analyses of ISG expression in *PTPN1* WT and KO RPE-1 cells after stimulation with 200 IU/mL IFNα2b (c) or 0.1 μM diABZI (d) for 6 hours. e. qPCR analysis of WT parental RPE- cells treated with DMSO or PTP1B inhibitor. ISG score (c-e) is calculated as the median of the expression of four ISGs, *IFI27*, *IFI16*, *MX1*, and *IRF7*. Paired ratio t test was used to compare the difference of ISG scores between WT and KO cells (c-d) or between DMSO and inhibitor treated cells (e).

To gain a systematic overview of the transcriptomic changes associated with *PTPN1* deficiency at baseline and upon stimulation, I next conducted RNA sequencing experiments and analysis with *PTPN1* WT and KO BJ-5ta clones. Gene set enrichment analysis (GSEA) revealed that at baseline and after stimulation with diABZI, IFNα and IFNγ responses were the top two upregulated pathways in KO cells (Fig. 26a, c), consistent with the above data (Fig. 20c, Fig. 24b). As for IFNα2b stimulation, pathways related to protein translation, cell proliferation, DNA repair and replication checkpoint were the significantly upregulated signalling events in *PTPN1* KO cells (Fig. 26b). This might seem unexpected at first because IFNα responses were not ‘‘detected’’ after IFNα2b stimulation. However, from a physiology point of view, antiviral state after IFN induction and signalling encompasses a wide range of cellular activities, leading to anti-proliferative effects, global arrest of protein translation and DNA replication, and induction of apoptosis, through the actions of hundreds of ISGs.[92] Additioanlly, using the 255 ISGs defined by Rosenberg et al. in studies of IFNα2b-treated PBMCs (peripheral blood mononuclear cells) derived from patients with chronic HCV (hepatitis C virus) infection,[381] I calculated an ISG score as the median of the expression of these genes (Fig. 26d). Indeed, *PTPN1* KO cells expressed higher amounts of ISGs than WT controls upon IFNα2b stimulation, further supporting the findings obtained by targeted qPCR analyses with a panel of five ISGs (Fig. 24a). On the other hand, multiple pathways were also downregulated in cells deficient for *PTPN1*. For example, EMT (epithelial–mesenchymal transition) was one such pathway consistently downregulated in KO cells, in both baseline and the two stimulation conditions (Fig. 26a-c). EMT is a process frequently implicated in cancer metastasis and invastion.[382] The exact nature of EMT in relation to *PTPN1* deficiency is unclear, but speculations could be made based on a dysregulated JAK-STAT signalling, given the centrality of this pathway in tumourigenesis.[112,383,384]

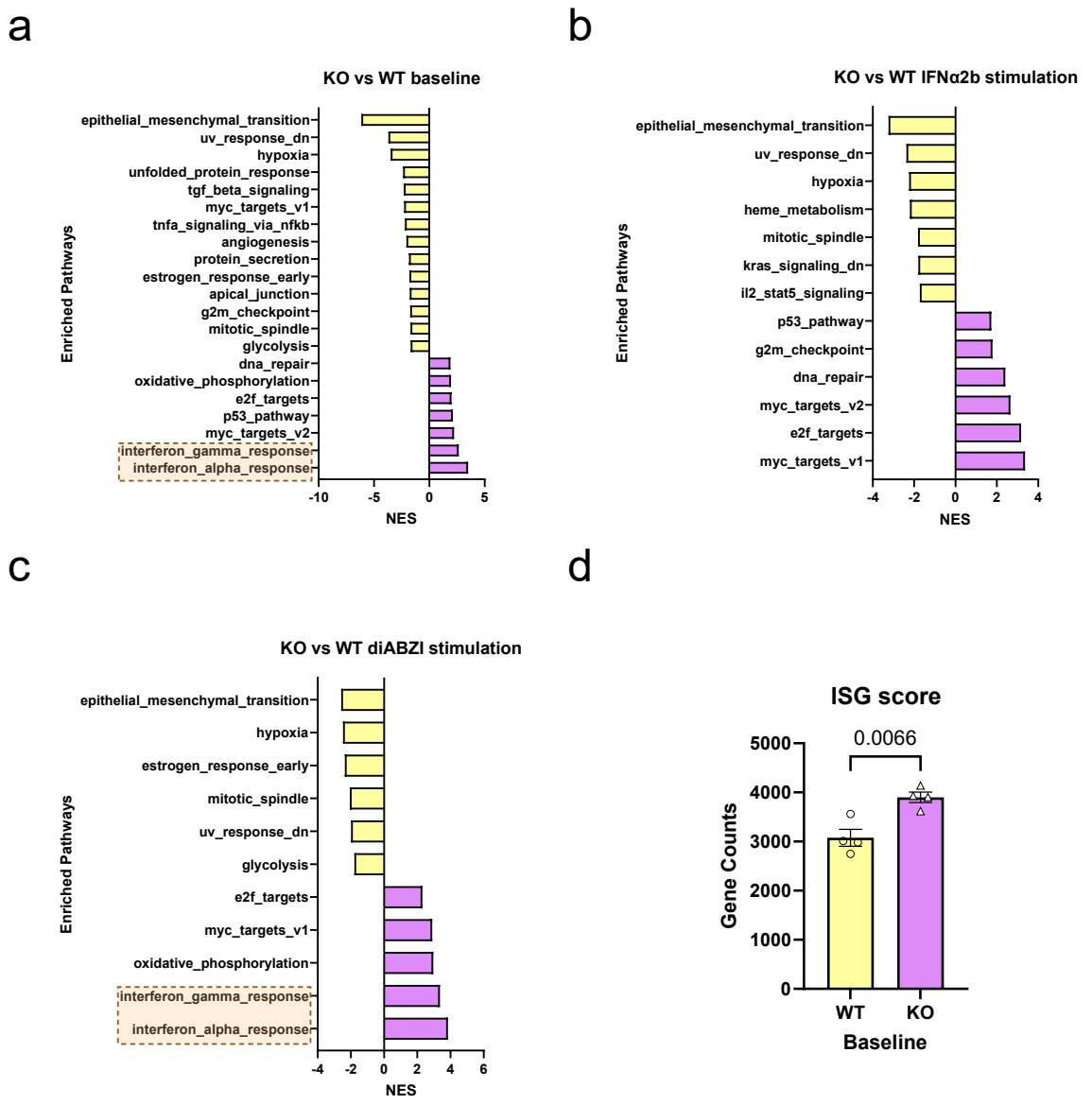

Fig. 26. RNA sequencing reveals distinct signalling pathways differentially regulated by PTP1B. a-c. GSEA (gene set enrichment analysis) bar plots displaying up- and down-regulated pathways in KO versus WT clones at baseline (a), IFNα2b (b), and diABZI (c) stimulation conditions. Differentially expressed genes with an adjusted p value < 0.1 are analysed. Enriched pathways with a nominal p value < 0.05 and FDR (false discovery rate) < 0.1 are shown. NES, normalised enrichment score. d. ISG scores calculated as the median of the expression of 255 ISGs from Rosenberg et al. Unpaired t test was used to compare the ISG score between WT and KO cells. WT, two clones; KO, two clones. Each condition was performed twice with two clones, so that two clones and two repeats for each condition were considered 4 biological replicates.

Combined *IFNAR1* and *STING1* KO, rather than either alone, rescues the enhanced baseline ISG expression in *PTPN1* KO hTERT RPE-1 cells

diABZI-activated STING signalling leads to the production of IFN-I (and pro-inflammatory cytokines), after which IFN-I molecules initiate IFNAR signalling and downstream transcriptional cascade leading to ISG production. One of the primary readouts for both IFNα2b and diABZI stimulation in this study is the expression of ISGs evaluated by qPCR. To better distinguish the effects of *PTPN1* deficiency on STING and IFNAR pathways, and having found out that BJ-5ta cells were intolerant to multiple rounds of CRISPR, I further generated *STING1* KO and *IFNAR1* KO pools in the previously described *PTPN1* WT and KO RPE-1 pools. Western blot demonstrated successful KO of either STING or IFNAR1 on the background of *PTPN1* WT and KO pools (Fig. 27a). Assessing the baseline ISG expression in these cell lines with distinct genotypes, it was revealed that neither *IFNAR1* nor *STING1* KO alone could rescue the enhanced baseline ISG expression in *PTPN1* KO cells (Fig. 27b). Further, I generated triple-knockout cell lines, i.e. combined KO of both *IFNAR1* and *STING1* on a *PTPN1* KO background. Baseline ISG expression in these genotypes indicated that when knocking out both *IFNAR1* and *STING1*, the elevated ISG expression in *PTPN1* KO cells was reversed to levels seen in *PTPN1* WT cells (Fig. 27c), indicating both STING and IFNAR pathways were affected in *PTPN1* deficiency.

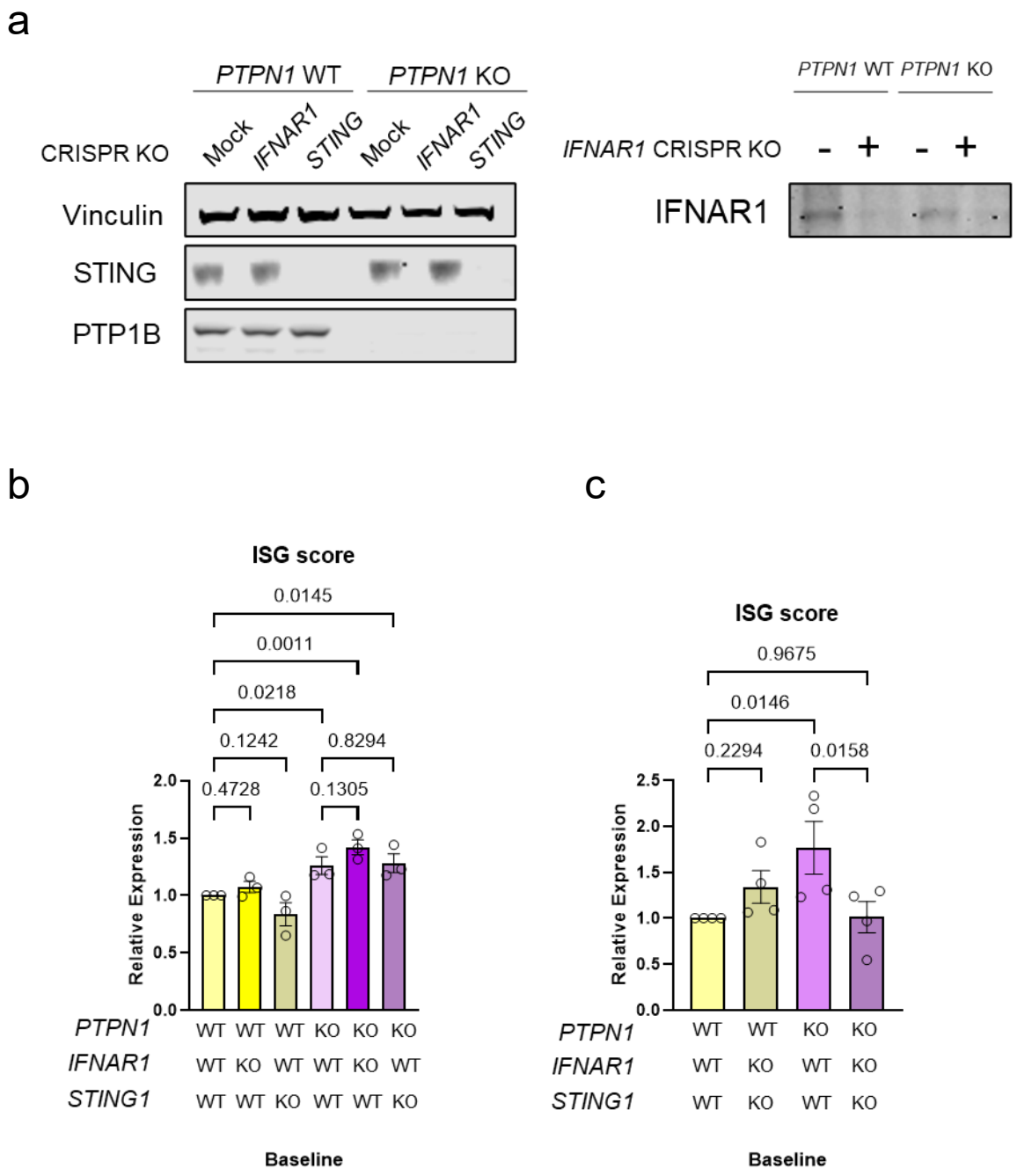

Fig. 27. Combined deletion of IFNAR1 and STING rescues enhanced baseline ISG expression in *PTPN1*-deficient RPE-1 cells. a. Representative immunoblot demonstrating successful KO of STING or IFNAR1 in *PTPN1* WT and KO cells. For IFNAR1 blot, samples were treated with PNGase F to remove glycosylation prior to gel electrophoresis. b-c. qPCR analyses of baseline ISG expression in the indicated genotypes. Ordinary one-way ANOVA was used to compare the baseline ISG expression among different genotypes. ISG score is calculated as the median of the expression of four ISGs, *IFI27*, *IFI16*, *MX1*, and *IRF7*.

3.3 Discussion

Comparison with PTPN2 haploinsufficiency

In July 2024, Jeanpierre et al. reported that haploinsufficiency of PTPN2 leads to early-onset systemic autoimmune disease in six unrelated patients diagnosed with paediatric SLE or Evans Syndrome.[385] Specifically, one patient developed SLE at the age of five years, presenting with skin rash, lupus nephritis, chronic hepatitis, cholangitis, hypergammaglobulinemia and a dysregulation of immune cell subtypes (moderately increased Tregs (regulatory T cells) and decreased B and natural killer cells). Five patients demonstrated autoimmune thrombocytopenia and haemolytic anaemia, features consistent with Evans Syndrome. Additionally, two patients experienced recurrent infections (otitis and pneumonitis), while two further patients demonstrated lymphoproliferation, evidenced by lymphoid hyperplasia and splenomegaly. Biochemical testing revealed five of six patients to harbour autoantibodies against platelets. Moreover, of these five patients, four displayed detectable antinuclear antibodies. Three patients required intermittent immunoglobulin infusions, and the other three received the immunosuppressant azathioprine to manage their inflammatory manifestations.

Through exome sequencing, each patient was identified to carry a different *PTPN2* variant in the heterozygous state. Three variants introduced a premature stop codon (one frameshift p.(F403Lfs*25) and two nonsense p.(W98*) and p.(W289*)), two led to non-synonymous missense substitutions (p.(Y126N) and p.(C216S)), and one involved a canonical splice acceptor site (c.70-2A>T) leading to the skipping of exon 2 and the introduction of a premature stop codon (p.(E24Mfs*20)). None of these newly discovered variants were present in gnomAD v4.1.0. Three variants (one frameshift p.(F403Lfs*25), one nonsense p.(W98*), and one missense substitution p.(C216S)) were inherited from a clinically asymptomatic father carrying the same variant in the heterozygous state, while the variant with the splicing defect appeared to arise de novo. Inheritance was undetermined due to unavailable genetic material

of the fathers of the other two patients carrying a nonsense (p.(W289*)) and a missense substitution (p.(Y126N)), respectively (with their mothers determined as WT for *PTPN2*). Five variants were located in the catalytic domain of PTPN2, with the sixth positioned in the C-terminus hydrophobic tail responsible for ER targeting.

PTPN2 is a ubiquitously expressed PTP, with highest expression levels in hematopoietic cells, consistent with its role in immune cell development, differentiation and function.[386] Two main isoforms of PTPN2 have been identified in humans. TC45 isoform is mostly found in the nucleus due to the exposed nuclear localisation signal (NLS) in exon 9A upon alternative splicing at the 3'-end of the gene.[387] Thus, TC45 contains exons 1 to 8, exon 9A, and exon 10. TC48 is the canonical sequence with an ER localisation motif. The TC48 isoform contains exons 1 to 8 and both parts of exon 9A and 9B, but not exon 10. The existence of a hydrophobic sequence in exon 9B inherently inhibits the nuclear relocalisation of TC48.[388] In primary immune cells, TC48 seems to be the predominant isoform, and its expression levels do not fluctuate following BCR (B cell receptor), TCR, or cytokine, stimulation.[385]

Prior to the paper discussed above,[385] human germline heterozygous or biallelic variants in *PTPN2*, leading to haploinsufficiency or LOF of the encoded protein, had been described in association with autoimmune enteropathy and immunodeficiency.[389-391] Furthermore, mice globally knocked out for *Ptpn2* die within 5 weeks of birth due to uncontrolled systemic autoinflammation driven by IFNγ, TNFα and IL-12.[392] Myeloid-specific deletion of *Ptpn2* was sufficient to promote intestinal inflammation with increased inflammasome activity and IL-1B production.[393] Another study suggested that haploinsufficiency of *Ptpn2* in mice leads to dysregulated Treg function owing to IL-6-driven pathogenic loss of FoxP3 in various mouse models of rheumatoid arthritis (RA).[394] GWAS (genome-wide association study) research has implicated PTPN2 as a susceptibility gene for autoimmune disorders including T1DM,[395] primary biliary cholangitis[396] and Crohn's disease.[397] All of these reports highlight the importance of PTPN2 in immune regulation, with LOF mutations in *PTPN2* potentially leading

to systemic autoinflammation possibly due to a loss of a negative brake involved in cytokine-induced JAK-STAT signalling pathways.[398]

Jeanpierre et al. observed that in in vitro activated T cells isolated from patients, the p.(W98*), p.(W289*), and p.(E24Mfs*20) variants were associated with loss of protein expression, indicating haploinsufficiency in the context of the disease studied; while the expression levels of p.(F403Lfs*25) and p.(Y126N) compared to WT were reduced by 15% and 35% respectively. No decrease in expression of the p.(C216S) variant was observed.[385] Assessing the intrinsic tyrosine phosphatase activity of ectopically expressed and immunoprecipitated mutant PTPN2 protein with normal or residual expression, and using p-STAT1 and p-STAT3 as substrates, it was revealed that the p.(C216S) completely abolished the phosphatase activity. In contrast, p.(Y126N) exhibited a 50% loss of phosphatase activity compared to WT, while p.(F403Lfs*25) retained comparable levels of phosphatase activity. Further, ISRE- and STAT3-luciferase assays with, respectively, IFNα and IL-6 stimulation indicated a reduction of activity for the p.(F403Lfs*25) variant.

Compared to healthy control cells, PBMCs isolated from patients with PTPN2 haploinsufficiency demonstrated higher sensitivity to stimulation with IL-2 and IFNγ, as evidenced by the hyperphosphorylation, respectively, of STAT5 and STAT1. In vitro preactivated T cells from patients also showed a delay in the dephosphorylation of STAT5 120 minutes following a 15-min pulse stimulation with IL-2. Along the same lines, patient T cells exhibited enhanced proliferation following IL-2, but not TCR, stimulation, suggesting PTPN2 regulates JAK-STAT, rather than TCR, signalling. Further, the authors showed that treatment with a JAK1/3 inhibitor, tofacitinib, reversed the overproliferation of patient T cells after IL-2 stimulation, to levels similar to WT controls. Measuring cytokine levels in serum from patients and healthy adult and paediatric controls, it was revealed that patients expressed higher amounts of IL-10, CXCL10 and IFNγ, reminiscent of STAT1 GOF and SOCS1 LOF patients. These data suggest an overlap in the pathogenesis of different mutant genotypes affecting JAK-STAT signalling.

Related to this thesis, PTP1B and PTPN2 are the two most studied members of the non-receptor PTP family, with over 80% of structural similarity in their catalytic domains.[368-370] Both are ubiquitously expressed proteins, with shared cellular substrates involved in various signalling pathways, particularly JAKs. Hence, PTP1B and PTPN2 have been implicated as master negative regulators of JAK-STAT signalling driven by a number of extracellular (cytokine) ligands. Notably however, our data, and that published relating to PTPN2 haploinsufficiency/LOF, indicate that mutations in PTP1B or PTPN2 result in distinct clinical phenotypes. Specifically, our patients manifest disease limited to the CNS. In contrast, patients with PTPN2 mutations display early-onset systemic autoimmunity and lymphoproliferation. The distinct phenotypes associated with PTP1B and PTPN2 mutations indicate that these two proteins play discrete roles in CNS and peripheral immune homeostasis, despite their similarities in structures and catalytic capacities. Differences in protein expression pattern may be relevant here. Thus, even though both proteins are universally expressed in most, if not all, tissues and cell types, their activity might be subject to differential regulation. It has been suggested that PTPN2 plays an especially important role in T cell development,[399-401] proliferation,[402,403] tolerance,[394,404,405] exhaustion,[406,407] TCR signalling,[403] and possibly other aspects of T cell function (hence another name for PTPN2 is TCPTP), with most of these studies performed in mice. As described previously, PTPN2 deletion in mice results in marked immune dysfunction. The patients with PTPN2 LOF mutations reported recently also display severe immunological abnormalities, further supporting the previously obtained data in mouse models.

On the other hand, evidence regarding the role of PTP1B in immune regulation is less concrete, and sometimes can seem contradictory. Firstly, global *Ptpn1* KO mice do not develop overt autoinflammation/autoimmunity.[295] Rather, these mice exhibit increased insulin sensitivity and energy expenditure, thus conferring resistance to obesity when fed a high fat diet. However, reports on the function of PTP1B in regulating the development and activity of several types of immune cells do exist, frequently related to JAK-STAT signalling. PTP1B has been shown

to participate in the maturation, migration, and T cell-activation function of DCs.[408] In contrast, the role of PTP1B in macrophage polarisation is elusive, resulting in both anti- and pro-inflammatory phenotypes, heavily dependent on the nature of the stimulant, the cellular/mouse model adopted, and whether KO of PTP1B involves the whole organism or only a certain type of cells.[409-411] Notably, the human patients haploinsufficient for PTP1B described in this study do not show obvious peripheral immune dysregulation. Phenotypic discrepancies between human patients and mouse models are well recognised in T1I research. For example, the neurological involvement characteristic of AGS is essentially absent in the equivalent mouse mutant genotypes. *Trex1* KO mice develop inflammatory myocarditis without CNS involvement,[412] and *Samhd1* KO mice only display a mild IFN signalling enhancement but no tissue damage.[413] An explanation for these differences could be a difference in the physiology of human and mouse, particularly the tissue and cell type expression profile of components of the IFN-I signalling and regulation pathways. Possibly more likely, the endogenous nucleic acid ligands triggering innate sensing and subsequent IFN-I signalling could be species/tissue/cell type specific.[188] Further, mice are usually kept in a specific-pathogen free (SPF) environment, and are often inbred to obtain a ‘‘pure’’ genetic background, which is never the case in the world inhabited by humans. In this regard, mouse models might not be the best system to study some types of T1Is, especially perhaps when it comes to CNS disease. In this study, I adopted two cellular systems, namely fibroblasts and epithelial cells, to study the effects of PTP1B deficiency, both of which appeared to demonstrate an upregulation of STING and IFNAR signalling pathways according to my preliminary data. However, these studies may not be particularly relevant to the patient clinical phenotype. Which is to acknowledge that, in order to better model the neurological involvement observed in patients, induced pluripotent stem cell (iPSC)-derived neural cells (neurons, microglia and astrocytes), as well as brain organoids, might represent more suitable models.

Incomplete penetrance

Another striking feature of our patient cohort is the high degree of nonpenetrance. Nonpenetrance relates to the fact that certain individuals carrying a known disease-causing variant do not manifest clinical features. In this study, we ascertained 21 PTP1B mutation-positive individuals, with 12 demonstrating overt clinical disease, resulting in an estimated nonpenetrance rate of 43%. Of note, Jeanpierre et al. identified six symptomatic patients, and a further three clinically unaffected individuals to carry a PTPN2 mutation, indicating a nonpentrance rate of 33%. Incomplete penetrance is increasingly recognised in inborn errors of immunity. For example, a high degree (around 25%) of nonpenetrance is observed in COPA syndrome.[206] A study of MDA5-associated disease reported a 13.5% rate of nonpenetrance where mutation-positive individuals displayed no clinical phenotype (although a cellular and/or molecular phenotype, i.e. an enhanced ISG signature in blood, was present in almost all such individuals).[231] Obviously, caution with these numbers is necessary given the small number of patients; although one might suspect the rate of nonpenetrance to be higher still - given a likely bias inherent in studies involving ascertainment through symptomatic individuals.[230] Both dominantly and recessively inherited T1Is have been documented to display incomplete penetrance.[18,231,232] In clinical genetics practice, the asymptomatic siblings of an affected proband are not always tested for the putative genetic variants (particularly so in the case of variants inherited as autosomal recessive traits). Hence, precise rates of penetrance/nonpenetrance are difficult to quantify. The term ‘‘variable expressivity’’ denotes a similar yet distinct concept from incomplete penetrance, referring to variability in the clinical features manifest by symptomatic individuals due a defined mutant genotype. For example, SAVI patients can demonstrate either lung or skin involvement, or both, with such variable expression of disease even seen within the same family (where the precise mutant genotype is identical).[331] Distinctions between incomplete penetrance and variable expressivity are illustrated in Fig. 28.[230]

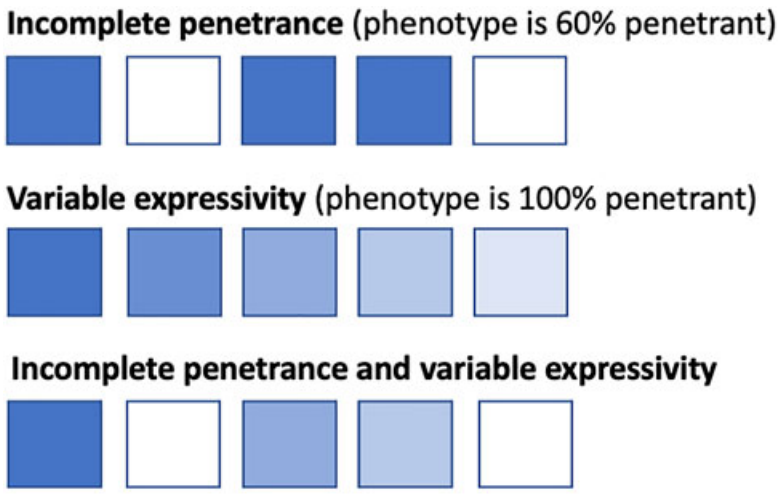

Fig. 28. Conceptual illustration of penetrance and expressivity often encountered in studies of inborn errors of immunity. Squares denote individuals with the same genotype, with different shades of blue representing individuals with the related phenotype, and empty squares indicating asymptomatic individuals. Top panel shows incomplete penetrance with 3 out 5 variant-carrying individuals displaying clinical features (a penetrance of 60%), with their phenotype being identical. Middle panel indicates a situation of complete penetrance where all patients demonstrate disease features (100% penetrance), but disease severity varies between individuals (variable expressivity). Bottom panel is a mixture of the above two situations, where both incomplete penetrance and variable expressivity exist in the patient cohort.

Various mechanisms could underly incomplete penetrance, with environmental triggers such as infections and vaccinations perhaps being the most obvious in the context of inborn errors of immunity. In this regard, individuals with mutations conferring a susceptibility to certain pathogens will likely not develop disease if they never encounter such pathogens, as is the case for BCG vaccination in patients with MSMD.[414] The frequency of infections and microbial load could also impact immune dysregulation or protective responses, leading to incomplete penetrance and variable expressivity.[415] As an example of the former, when individuals carrying mutations leading to familial HLH (haemophagocytic lymphohistiocytosis) are identified early in life, cellular dysfunction sometimes precedes clinical presentation, with upper respiratory and/or gastrointestinal infections frequently associated with disease onset. This temporal sequence indicates that an infectious agent might be necessary to trigger disease. As for the latter, patients who experience HSE in childhood usually do not develop HSE in adulthood, indicating that prior exposure may confer a protective immunisation against certain pathogens and regulate disease severity and penetrance. Along similar lines, the

presence and/or extent of infections (together with other enviromental factors such as the microbiome, diet and psychological stress), may underlie nonpenetrance in primary atopic disorders.[415] In the current study, one patient (AGS761), with a de novo PTP1B variant, developed a rapid loss of motor skills and speech one week after scheduled 15-month vaccination (DTaP-IPV/Hib); while another (AGS3561), with a variant inherited from an asymptomatic father, experienced neurological regression after SARS-CoV-2 infection at age 7 years. Potentially, both triggers might have contributed to disease onset. Of particular note, SARS-CoV-2 is known to invade the CNS leading to encephalitis, neuroinflammation, and tissue damage,[416,417] which could perhaps, at least in part, explain the nonpenetrance observed between AGS3561 and her clinically unaffected father (who did not contract SARS-Cov-2 in childhood). Other environmental triggers possibly relevant to nonpenentrance include the microbiome, diet, drug usage, radiation exposure and socio-economic status.[229,230] Associations between variant effects and certain environmental factors sometimes might seem apparent (such as traceable infection history), but in most cases are difficult to assess, as the complete and systemic cataloguing of one's environment is almost impossible. Relating to PTP1B haploinsufficiency, no obvious temporal relationship between vaccination/infection and disease onset was recorded in patients other than AGS761 and AGS3561.

Other (epi)genetic variations could also confer either deleterious or protective effects in the context of a mutant allele, leading to incomplete penetrance. In the case of common variable immunodeficiency (CVID), *TNFRSF13B* variants (which also exist in the general population at a frequency of 1-2%,) do not directly cause disease, but, rather, act as a risk factor in around 10% of patients with CVID.[418] As for epigenetic factors, through studies on monozygotic twins, certain hypermethylated B cell genes were revealed to predispose to severe and fully penetrant forms of CVID, while hypomethylated B cells genes were found in either healthy or incompletely penetrant patients.[419,420] In our study of PTP1B deficiency, WGS was performed in three cases, and no other suspicious genetic variants were identified, perhaps providing some (albeit weak) evidence that genetic modifiers might not play a role in nonpenetrance in

these patients. Methylation status was not assessed in any of the patients, leaving open the possibility of a role for epigenetic factors.

Somatic mosaicism, which arises during post zygotic division, might also explain nonpenetrance in some cases. Mosaicism leads to heterogeneous cell populations with different genotypes in an individual. In practice, especially in cancer research, genetic testing to look for potentially disease-associated variants is often performed in cells derived from more than one post embryonic development tissue, namely ectoderm (buccal swabs), mesoderm (PBMCs), and endoderm (epithelial lining of gastrointestinal tract).[228] In our study, DNA from whole-blood was sequenced in the search for potentially damaging genetic variants, and in some cases, direct Sanger sequencing of dermal fibroblast DNA was used to confirm the identified PTP1B variants. In these cases (both probands and mutation-carrying parents), no evidence of somatic mosaicism was observed.

Other factors may contribute to incomplete penetrance. For example, there exists an overlap of substrate spectrum between PTP1B and PTPN2, which could theoretically confer some degree of compensatory effect in the context of PTP1B deficiency. However, through western blot and qPCR analyses, at least in the four primary dermal fibroblast lines from patients tested, no obvious overexpression of PTPN2 was observed compared to controls (data not shown). Along the same lines, even though preferential allelic expression has been documented in dominantly inherited conditions where haploinsufficiency drives pathogenesis,[421,422] data in Fig. 19 suggest a complete loss of the mutant allele in the four primary fibroblast lines examined, with around 50% of protein expression remaining. That is, no overexpression of the WT allele was observed.

In short, clinical nonpenetrance is a well recognised phenomenon in T1I research, with an estimated rate of 43% in our cohort of PTP1B mutation carriers. Many factors could contribute to this phenomenon, including environmental triggers, genetic and epigenetic modifiers, somatic mosaicism, and possibly others. While these factors may be appreciated in general to drive nonpenetrance, with discrete examples supporting each notion, it is not easy to identify

the exact mechanism in a given genetic disorder. In the case of PTP1B deficiency, only hypotheses can be suggested at this point, warranting further experimental and clinical research in the future.

Concerns regarding the use of PTP1B inhibitors

PTP1B is an important dephosphorylation enzyme involved in a variety of signalling pathways, which, as discussed above, has been implicated in several human disease states including T2DM, obesity, neurodegeneration, and certain cancers.[283,284,321] With overexpression of PTP1B being the underlying disease-causing mechanism in several of these pathologies, the search for highly specific and effective PTP1B inhibitors has been a goal of many scientists and pharmaceutical companies. While PTP1B inhibitors have been tested in clinical trials for the treatment of T2DM and obesity, most of them have been discontinued due to low efficiency, lack of specificity, and overt side effects.[423,424] For example, MSI-1436 (also known as Trodusquemine) is a selective and reversible PTP1B inhibitor binding to its C terminal domain, with little impact on PTPN2 (with an IC_{50} of 1 μM for PTP1B and 224 μM for PTPN2).[425] Unfortunately, due to low activity and poor bioavailability, MSI-1436 was discontinued in phase I clinical trials. Similarly, JTT-551, developed by the Japan Tobacco Company, also displayed high specificity for PTP1B versus PTPN2. Mice chronically administered with this inhibitor showed an antiobesity effect possibly due to enhanced leptin signalling.[426] JTT-551 went into pre-clinical trials, but was then discontinued due to low efficacy and unwanted side effects.[281]

Novel synthetic and naturally sourced compounds are now being actively tested in the search for a ‘‘perfect’’ PTP1B inhibitor. Various strategies exist to inhibit PTP1B activity and/or expression, including targeting the PTP1B catalytic site, allosteric inhibition, and silencing of *PTPN1* mRNA using antisense oligonucleotides. As shown in Fig. 25e, the inhibition of PTP1B activity using a selective, reversible, and non-competitive allosteric inhibitor led to overexpression of ISGs, suggesting an inflammatory phenotype. The human patients ascertained in this study also highlight a potential role of PTP1B in regulating STING and IFNAR pathways in the CNS, with LOF mutations in PTP1B resulting in a T1I state. Together

with the contradictory data relating to the role of PTP1B in cancer biology,[355,356] further mechanistic studies of PTP1B function in the pathogenesis of human disease are warranted. Until then, our discovery indicates the need for caution in the use of PTP1B inhibition in the clinical trial setting.

3.4 Materials and methods

Samples obtained from patients

Samples were obtained from the probands and parents with written informed consent. The study was approved by the Comité de Protection des Personnes (ID-RCB/EUDRACT: 2014-A01017-40) and the Leeds (East) Research Ethics Committee (10/H1307/132).

Genetic studies

DNA was extracted from whole-blood using standard methods. Exome sequencing was performed on genomic DNA using a SureSelect Human All Exon kit (Agilent Technologies) for targeted enrichment, and Illumina HiSeq2000 for sequencing. Variants were assessed using the in silico programs SIFT (http://sift.jcvi.org) and Polyphen2 (http://genetics.bwh.harvard.edu/pph2/), and the splicing module of Alamut® Visual. Population allele frequencies were obtained from the gnomAD v4.1.0 database (http://gnomad.broadinstitute.org). Sanger sequencing was performed to confirm the identified *PTPN1* variants. The reference sequence used for primer design and nucleotide numbering was ENST00000371621.5 / NM_002827.4 / NP_002818.1.

Protein structural analysis

The highest resolution crystal structure of PTP1B of the apo form was used for visualisation and modelling.[427] The A chain was used for visualisation with ChimeraX .[428] The effects of missense variants on protein stability were modelled using FoldX ,[429] taking the average ΔΔG over three separate replicates of both chains present in the asymmetric unit.

IFN status

Whole-blood was collected into PAXgene tubes (Qiagen) and total RNA extracted using a PreAnalytix RNA isolation kit. IFN scores were generated in one of two ways as previously described.[18,241] Using TaqMan probes to measure the mRNA expression of six ISGs (*IFI27*, *IFI44L*, *IFIT1*, *ISG15*, *RSAD2*, and *SIGLEC1*) normalised to the expression levels of *HPRT1* and *18S rRNA*. The median fold change of the ISGs is compared with the median of 29 healthy controls to create an IFN score for each individual, with an abnormal score being defined as greater than 2.46. For NanoString ISG analysis, total RNA was similarly extracted from whole-blood with a PAXgene (PreAnalytix) RNA isolation kit. Analysis of 24 genes and 3 housekeeping genes (probes of interest [n = 24]: *IFI27*, *IFI44L*, *IFIT1*, *ISG15*, *RSAD2*, *SIGLEC1*, *CMPK2*, *DDX60*, *EPSTI1*, *FBXO39*, *HERC5*, *HES4*, *IFI44*, *IFI6*, *IFIH1*, *IRF7*, *LAMP3*, *LY6E*, *MX1*, *NRIR*, *OAS1*, *OASL*, *OTOF*, and *SPATS2L*; reference probes [n = 3]: *NRDC*, *OTUD5*, and *TUBB*) was conducted using the NanoString customer designed CodeSets according to the manufacturer's recommendations (NanoString Technologies). Agilent Tapestation was used to assess the quality of the RNA. 100 ng total RNA was loaded for each sample. Data were processed with nSolver software (NanoString Technologies). The data were normalised relative to the internal positive and negative calibrators, the three reference probes, and the control samples. The median of the 24 probes for each of 41 healthy control samples was calculated, and the mean NanoString score of the 41 healthy controls +2 SD of the mean was calculated. Scores above this value (2.75) were designated as positive.

Cell culture and reagents

Primary human dermal fibroblasts derived from healthy controls (HDF) and patients, and BJ-5ta hTERT immortalised fibroblasts (CRL-4001, ATCC) were cultured in Dulbecco's modified Eagle's medium (DMEM), high glucose, GlutaMAX supplement, pyruvate (31966047, Gibco) supplemented by 10% fetal calf serum (FCS) and 1% penicillin/streptomycin (p/s). hTERT RPE-1 cells were a generous gift from Prof. Andrew P. Jackson Laboratory, MRC HGU, The University of Edinburgh, and were originally purchased from ATCC (CRL-4000). hTERT RPE-

1 cells were cultured in Advanced DMEM/F-12 (12634010, Gibco) supplemented by 10% FCS, 1% p/s and 1X GlutaMAX (35050038, Gibco). BJ-5ta cells were maintained in a 37°C, 5% CO_2 and 3% O_2 hypoxic incubator while primary human dermal fibroblasts and hTERT RPE-1 cells were maintained in a 37°C, 5% CO_2 incubator. Cells were routinely checked for the absence of mycoplasma contamination with Mycoplasma PCR Detection Kit (ab289834, abcam). Dose and duration for stimulation of cells with IFNα2b (11105, PBL Assay Science) and diABZI (28054, Cayman Chemical) were specified for each experiment in the figure legends.

CRISPR-Cas9 gene editing

Direct delivery of ribonucleoprotein (RNP) complex consisting of Cas9 protein and single guide RNA (sgRNA) was achieved by electroporation. For gene knock-out (KO), CRISPR Gene Knockout Kit v2 from Lonza comprising three guides targeting one gene is used. sgRNA sequences for *PTPN1* KO were UAAGAUCUCUCGAGUUUCUU, AAGAAUGAGGCUGGUGAUUC and CCCGGAGCACGGGCCCGUUG; sgRNA sequences for *STING1* KO were CGGGAUGGAUGGAUGCAGGC, UUAACAGCAGUCCCAGCUGC and CCUGCCUGGUGACCCUUUGG; sgRNA sequences for *IFNAR1* KO were UUUACUUUAAAGAACUGGGA, GAGUGAAGAAAAGUUGCAUU and AAACACUUCUUCAUGGUAUG. sgRNA(s) and Alt-R S.p. Cas9 Nuclease 3NLS (1081059, IDT) were gently mixed and incubated in room temperature for 15 minutes for RNP complex formation, which later was introduced into the cells via P2 Primary Cell 4D-Nucleofector™ X Kit L (V4XP-2024, Lonza) for BJ-5ta or P3 Primary Cell 4D-Nucleofector® X Kit L (V4XP-3024, Lonza) for hTERT RPE-1. Electroporation was performed with 4D-Nucleofector® X Unit (AAF-1003X, Lonza). Programs for BJ-5ta and hTERT RPE-1 were CZ-167 and EA-104, respectively. For *PTPN1* knock-in (KI) of variant c.63+1G>C by homologous recombination, an sgRNA (sequence GCGCTCCCGCACCTGGTAAA) and a single-stranded oligodeoxynucleotide (ssODN, sequence GGCCGAGAAGGAGGCGCAGCAGCCGCCCTGGCCCGTCATGGAGATGGAAAAGGAGTT

CGAGCAGATCGACAAGTCCGGGAGCTGGGCGGCAATTTACCAGcTGCGGGAGCGCCC
CGGAGCGTGGCGGGCCCTTCGCTTAGGCCGCTTGAACATCCCCTCAGACCTCCAGGC
CCCAGACTCCCTCTGGGTCTTGCCCTCTG) serving as a repair template were used.

To generate BJ-5ta clones, two days post electroporation, electroporated pools were single-cell sorted into a 96-well plate via flow cytometry. After cells reached confluency, a PCR-based selection method was used to identify clones with the desired genotypes. Primer sequences for *PTPN1* were GAAGCAGCAGCGGCTAGG (forward) and CCTCAAGCAGTAGGAGCGAG (reverse). Successful gene-editing for either pools or single-cell clones was first assessed by the Synthego ICE CRISPR Analysis Tool, then followed by western blot confirmation.

RNA extraction, reverse transcription and qPCR for primary cells and cell lines

RNA from primary fibroblasts or cell lines was extracted using RNAqueous-Micro Kit (for primary fibroblasts, AM1931, Ambion) or RNeasy Micro Kit (for other cell lines, 74004, Qiagen) following the manufacturer's instructions. Reverse transcription of extracted RNA was performed using High-Capacity cDNA Reverse Transcription Kit (4368814, Thermo Fisher Scientific). The expression of genes of interest, relative to the geomean of the expression of housekeeping genes (*ACTB* and *HPRT1* for BJ-5ta and *ACTB*, *GAPDH* and *HPRT1* for hTERT RPE-1), was analysed by TaqMan quantitative real-time PCR (TaqMan Fast Universal PCR Master Mix (2 ×) No AmpErase UNG, 4352042, Thermo Fisher Scientific) on a QuantStudio 5 real-time PCR machine (A28140, Applied Biosystems). TaqMan probes used were *PTPN1* (Hs00942477_m1), *IFNB1* (Hs01077958_s1), *IFI16* (Hs00986757_m1), *IFI27* (Hs01086370_m1), *IFI44L* (Hs00199115_m1), *MX1* (Hs00895608_m1), *OAS1* (Hs00973637_m1), *RSAD2* (Hs01057264_m1), *IRF7* (Hs00185375_m1), *ACTB* (Hs01060665_g1), *GAPDH* (Hs02786624_g1) and *HPRT1* (Hs03929096_g1). The $\Delta\Delta$Ct method was adopted to calculate the relative levels of gene transcription, relative to the mean values of the healthy controls or wild-type controls. The calculation method for an ISG score is specified in the figure legends.

Western blotting

BJ-5ta and hTERT RPE-1 cells were incubated for 1 h at 4°C with rotation in lysis buffer (25 mM Tris–HCl, pH 8.0, 1% NP-40, 150 mM NaCl, 1.5 mM $MgCl_2$, 0.05% SDS, 0.5% sodium deoxycholate, supplemented with 750 U/mL benzonase nuclease (E1014-25KU, Scientific Laboratory Supplies), protease inhibitor cocktail (04693159001, Roche) and phosphatase inhibitor cocktail (04906837001, Roche)) to obtain whole-cell lysates (WCLs). WCLs were then subjected to centrifugation at 12,000 rpm at 4°C for 10 min to remove insoluble fraction. Supernatant containing soluble protein fraction was collected, and total protein concentration was measured using Pierce BCA protein assay kit (23227, Thermo Fisher Scientific). Same amount of protein from each sample with Pierce Lane Marker Reducing Sample Buffer (39000, Thermo Fisher Scientific) was denatured at 95°C for 10 min and resolved on NuPage 4–12% Bis–Tris Gels (NP0336BOX, Invitrogen) in 1X NuPage MOPS SDS running buffer (NP0001, Invitrogen). Proteins were then transferred from the gel onto the nitrocellulose membrane of an iBlot 2 NC Regular Stack (IB23001, Invitrogen) for 15 min at 15 V using the iBlot 2 Dry Blotting System (IB21001, Invitrogen). Proteins were extracted from primary fibroblasts using radioimmunoprecipitation assay lysis buffer (89900, Life Technologies) supplemented with 1 % protease inhibitor (Halt Protease Inhibitor Cocktail, Life Technologies) and 1 % phosphatase inhibitor (Phosphatase Inhibitor Cocktail 2, Sigma-Aldrich). Bolt LDS Sample Buffer (Novex, Life Technologies) and Bolt Sample Reducing agent (Novex, Life Technologies) were added to protein lysates, denatured at 70°C for 10 min. Protein extracts were then resolved on 4–12 % Bolt Bis-Tris Plus gels (Invitrogen) and transferred to nitrocellulose membranes (iBlot Invitrogen). Membranes were blocked in intercept (TBS) blocking buffer (927–60001, LI-COR) for 30 min at room temperature and incubated overnight at 4°C with rotation with primary antibodies of interest diluted in blocking solution supplemented with 0.1% Tween 20 (EC-607, National Diagnostics). Primary antibodies used in this study were Vinculin (13901S), Cofilin (5175S), phospho-tyrosine (8954S), p-STAT1 (7649S), STAT1 (9176S), p-STING (19781S), STING (13647S), all of which are from Cell Signalling Technology; PTP1B (MABS197, Sigma-

Aldrich), STING (66680-1-Ig, proteintech), and IFNAR1 (ab124764, abcam). After washing away unspecific binding of primary antibodies, IRdye-conjugated anti-mouse (926–68070, LI-COR) or anti-rabbit (925–32211, LI-COR) secondary antibodies diluted in intercept (TBS) blocking buffer were used to detect targeted proteins. Membranes were then scanned using the Odyssey CLx System (LI-COR). Densitometry quantification and analyses were performed using either the Image Studio Lite software v.5.2 (LI-COR) or ImageJ.

Samples to be blotted for IFNAR1 were treated with PNGase F (P0704S, NEB) to remove glycosylation prior to western blotting following manufacturer's instructions. Briefly, WCLs were obtained using the same lysis buffer as above for hTERT RPE-1 cells, but without 0.05% SDS and 0.5% sodium deoxycholate. Then, samples containing glycoprotein, together with 1X Glycoprotein Denaturing Buffer was denatured at 100°C for 10 min. After chilling on ice for 10 s, samples were mixed with 1X GlycoBuffer 2, 1% NP-40, 25 U/μL PNGase F and incubated at 37°C for 1 h.

Bulk RNA sequencing and analysis of BJ-5ta clones

Two independent clones per genotype (WT and KO) and two experimental repeats for each clone were used. Libraries were prepared using the NEBNEXT Ultra II Directional RNA Library Prep kit (7760, NEB), and the Poly-A mRNA magnetic isolation module (E7490, NEB) was used for mRNA enrichment per the manufacturer's protocol. After library preparation, Sequencing (2x60) was performed on the NextSeq 2000 platform (20038897, Illumina Inc) using NextSeq 2000 P3 Reagents (100 Cycles) (20040559, Illumina Inc). Coverage was relatively even, and the majority of libraries generated ≥45M reads (Min: 41.2M, Max: 57.1M, Mean: 49.7M). RNA sequencing was analysed via nf-core/rnaseq pipeline (v3.14.0) and the obtained length-scaled gene counts were subjected to DESeq2 analysis in R. For gene set enrichment analysis (GSEA),[430] differentially expressed genes (DEGs) were uploaded to GSEA software, and hallmark gene sets was chosen to identify the enriched pathways.[431]

PTPN1 capture RNA sequencing

Total RNA was extracted from primary fibroblasts (HDF and AGS3148) or from whole-blood sampled on a Paxgene RNA tube (Ctrl and AGS761) as described above. RNA was quantified using a Qubit Fluorometer and High Sensitivity RNA assay (Thermo Fisher Scientific). Quantities > 800 ng of RNA were used as starting material for the first strand synthesis using the VILO SuperScript III (Thermo Fischer Scientific). The second strand was synthesised using the Second Strand cDNA Synthesis Kit (Thermofischer Scientific). Then, 50 ng of cDNA for each sample was prepared with Twist's unique dual indexes (Twist Bioscience) by steps of fragmentation, end repair, and dA-tailing. Adapters were ligated and indexes were added to the amplified cDNA. Samples were pooled to a total mass of 1500 ng and the hybridisation reaction was performed for 16 h using home-made biotinylated single strand DNA probes designed to cover *PTPN1* gene region. During the capture process, barcoded libraries molecules bound to the biotinylated beads are retained by streptavidin coated magnetic beads on a magnet and amplified by 12 PCR cycles. The purified libraries were then controlled by fluorimetry Qubit Double Strand DNA (Thermo Fischer Scientific) and capillary electrophoresis double strand DNA on the Fragment Analyzer (Agilent Technologies). An equimolar pool of all the libraries was prepared according to these 2 measurements. The concentration of this pool was measured by qPCR (KAPA Library Quantification kit, Roche). The libraries were sequenced on the NovaSeq6000, Illumina (S1 FlowCells, PE100, ~30 millions of reads/clusters per library were targeted).

After demultipexing, the reads were aligned to the reference genome GRCh37/Hg19 using the STAR software (version 2.7.5). Following alignment, PCR duplicates were identified and removed using Picard Tools (https://broadinstitute.github.io/picard/). Splice junctions on regions of interest were then visualized using the Integrative Genomics Viewer (IGV V2.14.1).

Statistics

All statistical analyses were performed in GraphPad Prism 10. The testing method for each experiment is specified in the figure legends. p values are annotated in the graphs. Error bars represent standard error of the mean.

References

1. Ishikawa H, Barber GN. STING is an endoplasmic reticulum adaptor that facilitates innate immune signalling. *Nature* 2008; **455**(7213): 674-8.
2. Ishikawa H, Ma Z, Barber GN. STING regulates intracellular DNA-mediated, type I interferon-dependent innate immunity. *Nature* 2009; **461**(7265): 788-92.
3. Wu J, Sun L, Chen X, et al. Cyclic GMP-AMP is an endogenous second messenger in innate immune signaling by cytosolic DNA. *Science* 2013; **339**(6121): 826-30.
4. Sun L, Wu J, Du F, Chen X, Chen ZJ. Cyclic GMP-AMP synthase is a cytosolic DNA sensor that activates the type I interferon pathway. *Science* 2013; **339**(6121): 786-91.
5. Reinert LS, Lopusna K, Winther H, et al. Sensing of HSV-1 by the cGAS-STING pathway in microglia orchestrates antiviral defence in the CNS. *Nat Commun* 2016; **7**: 13348.
6. Gulen MF, Samson N, Keller A, et al. cGAS-STING drives ageing-related inflammation and neurodegeneration. *Nature* 2023; **620**(7973): 374-80.
7. Du M, Chen ZJ. DNA-induced liquid phase condensation of cGAS activates innate immune signaling. *Science* 2018; **361**(6403): 704-9.
8. Andreeva L, Hiller B, Kostrewa D, et al. cGAS senses long and HMGB/TFAM-bound U-turn DNA by forming protein-DNA ladders. *Nature* 2017; **549**(7672): 394-8.
9. Huang YH, Liu XY, Du XX, Jiang ZF, Su XD. The structural basis for the sensing and binding of cyclic di-GMP by STING. *Nat Struct Mol Biol* 2012; **19**(7): 728-30.
10. Shang G, Zhu D, Li N, et al. Crystal structures of STING protein reveal basis for recognition of cyclic di-GMP. *Nat Struct Mol Biol* 2012; **19**(7): 725-7.
11. Shu C, Yi G, Watts T, Kao CC, Li P. Structure of STING bound to cyclic di-GMP reveals the mechanism of cyclic dinucleotide recognition by the immune system. *Nat Struct Mol Biol* 2012; **19**(7): 722-4.
12. Ran Y, Xiong MG, Xu ZS, Luo WW, Wang SY, Wang YY. YIPF5 Is Essential for Innate Immunity to DNA Virus and Facilitates COPII-Dependent STING Trafficking. *J Immunol* 2019; **203**(6): 1560-70.
13. Yum S, Li M, Fang Y, Chen ZJ. TBK1 recruitment to STING activates both IRF3 and NF-kappaB that mediate immune defense against tumors and viral infections. *Proc Natl Acad Sci U S A* 2021; **118**(14).
14. Gui X, Yang H, Li T, et al. Autophagy induction via STING trafficking is a primordial function of the cGAS pathway. *Nature* 2019; **567**(7747): 262-6.
15. Liu D, Wu H, Wang C, et al. STING directly activates autophagy to tune the innate immune response. *Cell Death Differ* 2019; **26**(9): 1735-49.
16. Kuchitsu Y, Mukai K, Uematsu R, et al. STING signalling is terminated through ESCRT-dependent microautophagy of vesicles originating from recycling endosomes. *Nat Cell Biol* 2023; **25**(3): 453-66.
17. Jeltema D, Abbott K, Yan N. STING trafficking as a new dimension of immune signaling. *J Exp Med* 2023; **220**(3).
18. Lepelley A, Martin-Niclos MJ, Le Bihan M, et al. Mutations in COPA lead to abnormal trafficking of STING to the Golgi and interferon signaling. *J Exp Med* 2020; **217**(11).
19. Decout A, Katz JD, Venkatraman S, Ablasser A. The cGAS-STING pathway as a therapeutic target in inflammatory diseases. *Nat Rev Immunol* 2021; **21**(9): 548-69.
20. Volkman HE, Cambier S, Gray EE, Stetson DB. Tight nuclear tethering of cGAS is essential for preventing autoreactivity. *Elife* 2019; **8**.
21. Boyer JA, Spangler CJ, Strauss JD, et al. Structural basis of nucleosome-dependent cGAS inhibition. *Science* 2020; **370**(6515): 450-4.
22. Zhao B, Xu P, Rowlett CM, et al. The molecular basis of tight nuclear tethering and inactivation of cGAS. *Nature* 2020; **587**(7835): 673-7.
23. Pathare GR, Decout A, Gluck S, et al. Structural mechanism of cGAS inhibition by the nucleosome. *Nature* 2020; **587**(7835): 668-72.
24. Kujirai T, Zierhut C, Takizawa Y, et al. Structural basis for the inhibition of cGAS by nucleosomes. *Science* 2020; **370**(6515): 455-8.

25. Cao D, Han X, Fan X, Xu RM, Zhang X. Structural basis for nucleosome-mediated inhibition of cGAS activity. *Cell Res* 2020; **30**(12): 1088-97.
26. Michalski S, de Oliveira Mann CC, Stafford CA, et al. Structural basis for sequestration and autoinhibition of cGAS by chromatin. *Nature* 2020; **587**(7835): 678-82.
27. Uggenti C, Lepelley A, Depp M, et al. cGAS-mediated induction of type I interferon due to inborn errors of histone pre-mRNA processing. *Nat Genet* 2020; **52**(12): 1364-72.
28. Guey B, Wischnewski M, Decout A, et al. BAF restricts cGAS on nuclear DNA to prevent innate immune activation. *Science* 2020; **369**(6505): 823-8.
29. Xu P, Liu Y, Liu C, et al. The CRL5-SPSB3 ubiquitin ligase targets nuclear cGAS for degradation. *Nature* 2024; **627**(8005): 873-9.
30. Li T, Huang T, Du M, et al. Phosphorylation and chromatin tethering prevent cGAS activation during mitosis. *Science* 2021; **371**(6535).
31. Hemmi H, Takeuchi O, Kawai T, et al. A Toll-like receptor recognizes bacterial DNA. *Nature* 2000; **408**(6813): 740-5.
32. Lai JH, Wang MY, Huang CY, et al. Infection with the dengue RNA virus activates TLR9 signaling in human dendritic cells. *EMBO Rep* 2018; **19**(8).
33. De Dios R, Nguyen L, Ghosh S, McKenna S, Wright CJ. CpG-ODN-mediated TLR9 innate immune signalling and calcium dyshomeostasis converge on the NFkappaB inhibitory protein IkappaBbeta to drive IL1alpha and IL1beta expression. *Immunology* 2020; **160**(1): 64-77.
34. Lee BL, Moon JE, Shu JH, et al. UNC93B1 mediates differential trafficking of endosomal TLRs. *Elife* 2013; **2**: e00291.
35. Majer O, Liu B, Woo BJ, Kreuk LSM, Van Dis E, Barton GM. Release from UNC93B1 reinforces the compartmentalized activation of select TLRs. *Nature* 2019; **575**(7782): 371-4.
36. Dongye Z, Li J, Wu Y. Toll-like receptor 9 agonists and combination therapies: strategies to modulate the tumour immune microenvironment for systemic anti-tumour immunity. *Br J Cancer* 2022; **127**(9): 1584-94.
37. Zhang Z, Yuan B, Bao M, Lu N, Kim T, Liu YJ. The helicase DDX41 senses intracellular DNA mediated by the adaptor STING in dendritic cells. *Nat Immunol* 2011; **12**(10): 959-65.
38. Singh RS, Vidhyasagar V, Yang S, et al. DDX41 is required for cGAS-STING activation against DNA virus infection. *Cell Rep* 2022; **39**(8): 110856.
39. Unterholzner L, Keating SE, Baran M, et al. IFI16 is an innate immune sensor for intracellular DNA. *Nat Immunol* 2010; **11**(11): 997-1004.
40. Almine JF, O'Hare CA, Dunphy G, et al. IFI16 and cGAS cooperate in the activation of STING during DNA sensing in human keratinocytes. *Nat Commun* 2017; **8**: 14392.
41. Jonsson KL, Laustsen A, Krapp C, et al. IFI16 is required for DNA sensing in human macrophages by promoting production and function of cGAMP. *Nat Commun* 2017; **8**: 14391.
42. Kang DC, Gopalkrishnan RV, Lin L, et al. Expression analysis and genomic characterization of human melanoma differentiation associated gene-5, mda-5: a novel type I interferon-responsive apoptosis-inducing gene. *Oncogene* 2004; **23**(9): 1789-800.
43. Andrejeva J, Childs KS, Young DF, et al. The V proteins of paramyxoviruses bind the IFN-inducible RNA helicase, mda-5, and inhibit its activation of the IFN-beta promoter. *Proc Natl Acad Sci U S A* 2004; **101**(49): 17264-9.
44. Yoneyama M, Kikuchi M, Natsukawa T, et al. The RNA helicase RIG-I has an essential function in double-stranded RNA-induced innate antiviral responses. *Nat Immunol* 2004; **5**(7): 730-7.
45. Barral PM, Sarkar D, Su ZZ, et al. Functions of the cytoplasmic RNA sensors RIG-I and MDA-5: key regulators of innate immunity. *Pharmacol Ther* 2009; **124**(2): 219-34.
46. Bruns AM, Leser GP, Lamb RA, Horvath CM. The innate immune sensor LGP2 activates antiviral signaling by regulating MDA5-RNA interaction and filament assembly. *Mol Cell* 2014; **55**(5): 771-81.
47. Brisse M, Ly H. Comparative Structure and Function Analysis of the RIG-I-Like Receptors: RIG-I and MDA5. *Front Immunol* 2019; **10**: 1586.

48. Kato H, Takeuchi O, Mikamo-Satoh E, et al. Length-dependent recognition of double-stranded ribonucleic acids by retinoic acid-inducible gene-I and melanoma differentiation-associated gene 5. *J Exp Med* 2008; **205**(7): 1601-10.
49. Seth RB, Sun L, Ea CK, Chen ZJ. Identification and characterization of MAVS, a mitochondrial antiviral signaling protein that activates NF-kappaB and IRF 3. *Cell* 2005; **122**(5): 669-82.
50. Xu LG, Wang YY, Han KJ, Li LY, Zhai Z, Shu HB. VISA is an adapter protein required for virus-triggered IFN-beta signaling. *Mol Cell* 2005; **19**(6): 727-40.
51. Kawai T, Takahashi K, Sato S, et al. IPS-1, an adaptor triggering RIG-I- and Mda5-mediated type I interferon induction. *Nat Immunol* 2005; **6**(10): 981-8.
52. Meylan E, Curran J, Hofmann K, et al. Cardif is an adaptor protein in the RIG-I antiviral pathway and is targeted by hepatitis C virus. *Nature* 2005; **437**(7062): 1167-72.
53. Horner SM, Liu HM, Park HS, Briley J, Gale M, Jr. Mitochondrial-associated endoplasmic reticulum membranes (MAM) form innate immune synapses and are targeted by hepatitis C virus. *Proc Natl Acad Sci U S A* 2011; **108**(35): 14590-5.
54. Dixit E, Boulant S, Zhang Y, et al. Peroxisomes are signaling platforms for antiviral innate immunity. *Cell* 2010; **141**(4): 668-81.
55. Liu S, Chen J, Cai X, et al. MAVS recruits multiple ubiquitin E3 ligases to activate antiviral signaling cascades. *Elife* 2013; **2**: e00785.
56. Fang R, Jiang Q, Zhou X, et al. MAVS activates TBK1 and IKKepsilon through TRAFs in NEMO dependent and independent manner. *PLoS Pathog* 2017; **13**(11): e1006720.
57. Wu J, Chen ZJ. Innate immune sensing and signaling of cytosolic nucleic acids. *Annu Rev Immunol* 2014; **32**: 461-88.
58. Lee BL, Barton GM. Trafficking of endosomal Toll-like receptors. *Trends Cell Biol* 2014; **24**(6): 360-9.
59. Lim CS, Jang YH, Lee GY, et al. TLR3 forms a highly organized cluster when bound to a poly(I:C) RNA ligand. *Nat Commun* 2022; **13**(1): 6876.
60. Sun H, Li Y, Zhang P, et al. Targeting toll-like receptor 7/8 for immunotherapy: recent advances and prospectives. *Biomark Res* 2022; **10**(1): 89.
61. Brown GJ, Canete PF, Wang H, et al. TLR7 gain-of-function genetic variation causes human lupus. *Nature* 2022; **605**(7909): 349-56.
62. Stremenova Spegarova J, Sinnappurajar P, Al Julandani D, et al. A de novo TLR7 gain-of-function mutation causing severe monogenic lupus in an infant. *J Clin Invest* 2024; **134**(13).
63. David C, Badonyi M, Kechiche R, et al. Interface Gain-of-Function Mutations in TLR7 Cause Systemic and Neuro-inflammatory Disease. *J Clin Immunol* 2024; **44**(2): 60.
64. Chattopadhyay S, Sen GC. dsRNA-activation of TLR3 and RLR signaling: gene induction-dependent and independent effects. *J Interferon Cytokine Res* 2014; **34**(6): 427-36.
65. Yamamoto M, Sato S, Hemmi H, et al. Role of adaptor TRIF in the MyD88-independent toll-like receptor signaling pathway. *Science* 2003; **301**(5633): 640-3.
66. Patinote C, Karroum NB, Moarbess G, et al. Agonist and antagonist ligands of toll-like receptors 7 and 8: Ingenious tools for therapeutic purposes. *Eur J Med Chem* 2020; **193**: 112238.
67. Duan T, Du Y, Xing C, Wang HY, Wang RF. Toll-Like Receptor Signaling and Its Role in Cell-Mediated Immunity. *Front Immunol* 2022; **13**: 812774.
68. Barton GM, Kagan JC, Medzhitov R. Intracellular localization of Toll-like receptor 9 prevents recognition of self DNA but facilitates access to viral DNA. *Nat Immunol* 2006; **7**(1): 49-56.
69. Fukui R, Saitoh S, Kanno A, et al. Unc93B1 restricts systemic lethal inflammation by orchestrating Toll-like receptor 7 and 9 trafficking. *Immunity* 2011; **35**(1): 69-81.
70. Majer O, Liu B, Kreuk LSM, Krogan N, Barton GM. UNC93B1 recruits syntenin-1 to dampen TLR7 signalling and prevent autoimmunity. *Nature* 2019; **575**(7782): 366-70.
71. David C, Arango-Franco CA, Badonyi M, et al. Gain-of-function human UNC93B1 variants cause systemic lupus erythematosus and chilblain lupus. *J Exp Med* 2024; **221**(8).

72. Wolf C, Lim EL, Mokhtari M, et al. UNC93B1 variants underlie TLR7-dependent autoimmunity. *Sci Immunol* 2024; **9**(92): eadi9769.
73. Mishra H, Schlack-Leigers C, Lim EL, et al. Disrupted degradative sorting of TLR7 is associated with human lupus. *Sci Immunol* 2024; **9**(92): eadi9575.
74. Al-Azab M, Idiiatullina E, Liu Z, et al. Genetic variants in UNC93B1 predispose to childhood-onset systemic lupus erythematosus. *Nat Immunol* 2024; **25**(6): 969-80.
75. Drappier M, Michiels T. Inhibition of the OAS/RNase L pathway by viruses. *Curr Opin Virol* 2015; **15**: 19-26.
76. Dey M, Mann BR, Anshu A, Mannan MA. Activation of protein kinase PKR requires dimerization-induced cis-phosphorylation within the activation loop. *J Biol Chem* 2014; **289**(9): 5747-57.
77. Nair P, Sapre SU. Significance of RNA Sensors in Activating Immune System in Emerging Viral Diseases. *Dynamics of Immune Activation in Viral Diseases* 2020: 229-42.
78. Isaacs A, Lindenmann J. Virus interference. I. The interferon. *Proc R Soc Lond B Biol Sci* 1957; **147**(927): 258-67.
79. Isaacs A, Lindenmann J, Valentine RC. Virus interference. II. Some properties of interferon. *Proc R Soc Lond B Biol Sci* 1957; **147**(927): 268-73.
80. Lindenmann J, Burke DC, Isaacs A. Studies on the production, mode of action and properties of interferon. *Br J Exp Pathol* 1957; **38**(5): 551-62.
81. Gresser I, Bourali C, Levy JP, Fontaine-Brouty-Boye D, Thomas MT. Increased survival in mice inoculated with tumor cells and treated with interferon preparations. *Proc Natl Acad Sci U S A* 1969; **63**(1): 51-7.
82. Havell EA, Berman B, Ogburn CA, Berg K, Paucker K, Vilcek J. Two antigenically distinct species of human interferon. *Proc Natl Acad Sci U S A* 1975; **72**(6): 2185-7.
83. Maeda S, McCandliss R, Gross M, et al. Construction and identification of bacterial plasmids containing nucleotide sequence for human leukocyte interferon. *Proc Natl Acad Sci U S A* 1980; **77**(12): 7010-3.
84. Nagata S, Taira H, Hall A, et al. Synthesis in E. coli of a polypeptide with human leukocyte interferon activity. *Nature* 1980; **284**(5754): 316-20.
85. Zoon KC, Smith ME, Bridgen PJ, Anfinsen CB, Hunkapiller MW, Hood LE. Amino terminal sequence of the major component of human lymphoblastoid interferon. *Science* 1980; **207**(4430): 527-8.
86. Knight E, Jr., Hunkapiller MW, Korant BD, Hardy RW, Hood LE. Human fibroblast interferon: amino acid analysis and amino terminal amino acid sequence. *Science* 1980; **207**(4430): 525-6.
87. Sherwin SA, Knost JA, Fein S, et al. A multiple-dose phase I trial of recombinant leukocyte A interferon in cancer patients. *JAMA* 1982; **248**(19): 2461-6.
88. Merlin G, Chebath J, Benech P, Metz R, Revel M. Molecular cloning and sequence of partial cDNA for interferon-induced (2'-5')oligo(A) synthetase mRNA from human cells. *Proc Natl Acad Sci U S A* 1983; **80**(16): 4904-8.
89. Levy DE, Kessler DS, Pine R, Reich N, Darnell JE, Jr. Interferon-induced nuclear factors that bind a shared promoter element correlate with positive and negative transcriptional control. *Genes Dev* 1988; **2**(4): 383-93.
90. Der SD, Zhou A, Williams BR, Silverman RH. Identification of genes differentially regulated by interferon alpha, beta, or gamma using oligonucleotide arrays. *Proc Natl Acad Sci U S A* 1998; **95**(26): 15623-8.
91. Zhang Q, Kisand K, Feng Y, et al. In search of a function for human type III interferons: insights from inherited and acquired deficits. *Curr Opin Immunol* 2024; **87**: 102427.
92. Borden EC, Sen GC, Uze G, et al. Interferons at age 50: past, current and future impact on biomedicine. *Nat Rev Drug Discov* 2007; **6**(12): 975-90.
93. Crow YJ, Casanova JL. Human life within a narrow range: The lethal ups and downs of type I interferons. *Sci Immunol* 2024; **9**(97): eadm8185.
94. Hillyer P, Mane VP, Schramm LM, et al. Expression profiles of human interferon-alpha and interferon-lambda subtypes are ligand- and cell-dependent. *Immunol Cell Biol* 2012; **90**(8): 774-83.

95. Fitzgerald-Bocarsly P, Dai J, Singh S. Plasmacytoid dendritic cells and type I IFN: 50 years of convergent history. *Cytokine Growth Factor Rev* 2008; **19**(1): 3-19.
96. LaFleur DW, Nardelli B, Tsareva T, et al. Interferon-kappa, a novel type I interferon expressed in human keratinocytes. *J Biol Chem* 2001; **276**(43): 39765-71.
97. Fung KY, de Geus ED, Ying L, et al. Expression of Interferon Epsilon in Mucosal Epithelium is Regulated by Elf3. *Mol Cell Biol* 2024; **44**(8): 334-43.
98. Schneider WM, Chevillotte MD, Rice CM. Interferon-stimulated genes: a complex web of host defenses. *Annu Rev Immunol* 2014; **32**: 513-45.
99. Uze G, Lutfalla G, Gresser I. Genetic transfer of a functional human interferon alpha receptor into mouse cells: cloning and expression of its cDNA. *Cell* 1990; **60**(2): 225-34.
100. Fu XY, Kessler DS, Veals SA, Levy DE, Darnell JE, Jr. ISGF3, the transcriptional activator induced by interferon alpha, consists of multiple interacting polypeptide chains. *Proc Natl Acad Sci U S A* 1990; **87**(21): 8555-9.
101. Fu XY, Schindler C, Improta T, Aebersold R, Darnell JE, Jr. The proteins of ISGF-3, the interferon alpha-induced transcriptional activator, define a gene family involved in signal transduction. *Proc Natl Acad Sci U S A* 1992; **89**(16): 7840-3.
102. Wilks AF. Cloning members of protein-tyrosine kinase family using polymerase chain reaction. *Methods Enzymol* 1991; **200**: 533-46.
103. Harpur AG, Andres AC, Ziemiecki A, Aston RR, Wilks AF. JAK2, a third member of the JAK family of protein tyrosine kinases. *Oncogene* 1992; **7**(7): 1347-53.
104. Kraus MH, Aaronson SA. Detection and isolation of novel protein-tyrosine kinase genes employing reduced stringency hybridization. *Methods Enzymol* 1991; **200**: 546-56.
105. Velazquez L, Fellous M, Stark GR, Pellegrini S. A protein tyrosine kinase in the interferon alpha/beta signaling pathway. *Cell* 1992; **70**(2): 313-22.
106. Colamonici OR, D'Alessandro F, Diaz MO, Gregory SA, Neckers LM, Nordan R. Characterization of three monoclonal antibodies that recognize the interferon alpha 2 receptor. *Proc Natl Acad Sci U S A* 1990; **87**(18): 7230-4.
107. Colamonici OR, Pfeffer LM, D'Alessandro F, et al. Multichain structure of the IFN-alpha receptor on hematopoietic cells. *J Immunol* 1992; **148**(7): 2126-32.
108. Colamonici OR, Domanski P. Identification of a novel subunit of the type I interferon receptor localized to human chromosome 21. *J Biol Chem* 1993; **268**(15): 10895-9.
109. Novick D, Cohen B, Rubinstein M. The human interferon alpha/beta receptor: characterization and molecular cloning. *Cell* 1994; **77**(3): 391-400.
110. Boucher J, Kleinridders A, Kahn CR. Insulin receptor signaling in normal and insulin-resistant states. *Cold Spring Harb Perspect Biol* 2014; **6**(1).
111. Zanin N, Viaris de Lesegno C, Lamaze C, Blouin CM. Interferon Receptor Trafficking and Signaling: Journey to the Cross Roads. *Front Immunol* 2020; **11**: 615603.
112. Hu X, Li J, Fu M, Zhao X, Wang W. The JAK/STAT signaling pathway: from bench to clinic. *Signal Transduct Target Ther* 2021; **6**(1): 402.
113. Tolomeo M, Cavalli A, Cascio A. STAT1 and Its Crucial Role in the Control of Viral Infections. *Int J Mol Sci* 2022; **23**(8).
114. Steen HC, Gamero AM. STAT2 phosphorylation and signaling. *JAKSTAT* 2013; **2**(4): e25790.
115. Lukhele S, Boukhaled GM, Brooks DG. Type I interferon signaling, regulation and gene stimulation in chronic virus infection. *Semin Immunol* 2019; **43**: 101277.
116. Mazewski C, Perez RE, Fish EN, Platanias LC. Type I Interferon (IFN)-Regulated Activation of Canonical and Non-Canonical Signaling Pathways. *Front Immunol* 2020; **11**: 606456.
117. Arimoto KI, Miyauchi S, Stoner SA, Fan JB, Zhang DE. Negative regulation of type I IFN signaling. *J Leukoc Biol* 2018.
118. Ivashkiv LB, Donlin LT. Regulation of type I interferon responses. *Nat Rev Immunol* 2014; **14**(1): 36-49.
119. Perry ST, Buck MD, Lada SM, Schindler C, Shresta S. STAT2 mediates innate immunity to Dengue virus in the absence of STAT1 via the type I interferon receptor. *PLoS Pathog* 2011; **7**(2): e1001297.

120. van Boxel-Dezaire AH, Rani MR, Stark GR. Complex modulation of cell type-specific signaling in response to type I interferons. *Immunity* 2006; **25**(3): 361-72.
121. Hsu YA, Huang CC, Kung YJ, et al. The anti-proliferative effects of type I IFN involve STAT6-mediated regulation of SP1 and BCL6. *Cancer Lett* 2016; **375**(2): 303-12.
122. Gil MP, Ploquin MJ, Watford WT, et al. Regulating type 1 IFN effects in CD8 T cells during viral infections: changing STAT4 and STAT1 expression for function. *Blood* 2012; **120**(18): 3718-28.
123. Ho HH, Ivashkiv LB. Role of STAT3 in type I interferon responses. Negative regulation of STAT1-dependent inflammatory gene activation. *J Biol Chem* 2006; **281**(20): 14111-8.
124. Zhao LJ, Hua X, He SF, Ren H, Qi ZT. Interferon alpha regulates MAPK and STAT1 pathways in human hepatoma cells. *Virol J* 2011; **8**: 157.
125. Joshi S, Kaur S, Redig AJ, et al. Type I interferon (IFN)-dependent activation of Mnk1 and its role in the generation of growth inhibitory responses. *Proc Natl Acad Sci U S A* 2009; **106**(29): 12097-102.
126. Saleiro D, Platanias LC. Interferon signaling in cancer. Non-canonical pathways and control of intracellular immune checkpoints. *Semin Immunol* 2019; **43**: 101299.
127. Vigo T, La Rocca C, Faicchia D, et al. IFNbeta enhances mesenchymal stromal (Stem) cells immunomodulatory function through STAT1-3 activation and mTOR-associated promotion of glucose metabolism. *Cell Death Dis* 2019; **10**(2): 85.
128. Jefferies CA. Regulating IRFs in IFN Driven Disease. *Front Immunol* 2019; **10**: 325.
129. Honda K, Takaoka A, Taniguchi T. Type I interferon [corrected] gene induction by the interferon regulatory factor family of transcription factors. *Immunity* 2006; **25**(3): 349-60.
130. Sato M, Suemori H, Hata N, et al. Distinct and essential roles of transcription factors IRF-3 and IRF-7 in response to viruses for IFN-alpha/beta gene induction. *Immunity* 2000; **13**(4): 539-48.
131. Ning S, Pagano JS, Barber GN. IRF7: activation, regulation, modification and function. *Genes Immun* 2011; **12**(6): 399-414.
132. Colina R, Costa-Mattioli M, Dowling RJ, et al. Translational control of the innate immune response through IRF-7. *Nature* 2008; **452**(7185): 323-8.
133. Rengachari S, Groiss S, Devos JM, Caron E, Grandvaux N, Panne D. Structural basis of STAT2 recognition by IRF9 reveals molecular insights into ISGF3 function. *Proc Natl Acad Sci U S A* 2018; **115**(4): E601-E9.
134. Ashley CL, Abendroth A, McSharry BP, Slobedman B. Interferon-Independent Upregulation of Interferon-Stimulated Genes during Human Cytomegalovirus Infection is Dependent on IRF3 Expression. *Viruses* 2019; **11**(3).
135. Porritt RA, Hertzog PJ. Dynamic control of type I IFN signalling by an integrated network of negative regulators. *Trends Immunol* 2015; **36**(3): 150-60.
136. Meraz MA, White JM, Sheehan KC, et al. Targeted disruption of the Stat1 gene in mice reveals unexpected physiologic specificity in the JAK-STAT signaling pathway. *Cell* 1996; **84**(3): 431-42.
137. Sakata S, Tsumura M, Matsubayashi T, et al. Autosomal recessive complete STAT1 deficiency caused by compound heterozygous intronic mutations. *Int Immunol* 2020; **32**(10): 663-71.
138. Thoresen DT, Galls D, Gotte B, Wang W, Pyle AM. A rapid RIG-I signaling relay mediates efficient antiviral response. *Mol Cell* 2023; **83**(1): 90-104 e4.
139. Berghall H, Siren J, Sarkar D, et al. The interferon-inducible RNA helicase, mda-5, is involved in measles virus-induced expression of antiviral cytokines. *Microbes Infect* 2006; **8**(8): 2138-44.
140. Thompson MR, Sharma S, Atianand M, et al. Interferon gamma-inducible protein (IFI) 16 transcriptionally regulates type i interferons and other interferon-stimulated genes and controls the interferon response to both DNA and RNA viruses. *J Biol Chem* 2014; **289**(34): 23568-81.
141. Ji L, Li T, Chen H, et al. The crucial regulatory role of type I interferon in inflammatory diseases. *Cell Biosci* 2023; **13**(1): 230.

142. Sleijfer S, Bannink M, Van Gool AR, Kruit WH, Stoter G. Side effects of interferon-alpha therapy. *Pharm World Sci* 2005; **27**(6): 423-31.
143. Arimoto KI, Lochte S, Stoner SA, et al. STAT2 is an essential adaptor in USP18-mediated suppression of type I interferon signaling. *Nat Struct Mol Biol* 2017; **24**(3): 279-89.
144. Meuwissen ME, Schot R, Buta S, et al. Human USP18 deficiency underlies type 1 interferonopathy leading to severe pseudo-TORCH syndrome. *J Exp Med* 2016; **213**(7): 1163-74.
145. Hermann M, Bogunovic D. ISG15: In Sickness and in Health. *Trends Immunol* 2017; **38**(2): 79-93.
146. Vuillier F, Li Z, Commere PH, Dynesen LT, Pellegrini S. USP18 and ISG15 coordinately impact on SKP2 and cell cycle progression. *Sci Rep* 2019; **9**(1): 4066.
147. Pinto-Fernandez A, Salio M, Partridge T, et al. Deletion of the deISGylating enzyme USP18 enhances tumour cell antigenicity and radiosensitivity. *Br J Cancer* 2021; **124**(4): 817-30.
148. Duncan SA, Baganizi DR, Sahu R, Singh SR, Dennis VA. SOCS Proteins as Regulators of Inflammatory Responses Induced by Bacterial Infections: A Review. *Front Microbiol* 2017; **8**: 2431.
149. Perez-Quintero LA, Abidin BM, Tremblay ML. Immunotherapeutic implications of negative regulation by protein tyrosine phosphatases in T cells: the emerging cases of PTP1B and TCPTP. *Front Med (Lausanne)* 2024; **11**: 1364778.
150. David M, Chen HE, Goelz S, Larner AC, Neel BG. Differential regulation of the alpha/beta interferon-stimulated Jak/Stat pathway by the SH2 domain-containing tyrosine phosphatase SHPTP1. *Mol Cell Biol* 1995; **15**(12): 7050-8.
151. You M, Yu DH, Feng GS. Shp-2 tyrosine phosphatase functions as a negative regulator of the interferon-stimulated Jak/STAT pathway. *Mol Cell Biol* 1999; **19**(3): 2416-24.
152. Liu S, Jiang M, Wang W, et al. Nuclear RNF2 inhibits interferon function by promoting K33-linked STAT1 disassociation from DNA. *Nat Immunol* 2018; **19**(1): 41-52.
153. Honda K, Mizutani T, Taniguchi T. Negative regulation of IFN-alpha/beta signaling by IFN regulatory factor 2 for homeostatic development of dendritic cells. *Proc Natl Acad Sci U S A* 2004; **101**(8): 2416-21.
154. Rouyez MC, Lestingi M, Charon M, Fichelson S, Buzyn A, Dusanter-Fourt I. IFN regulatory factor-2 cooperates with STAT1 to regulate transporter associated with antigen processing-1 promoter activity. *J Immunol* 2005; **174**(7): 3948-58.
155. Chae M, Kim K, Park SM, et al. IRF-2 regulates NF-kappaB activity by modulating the subcellular localization of NF-kappaB. *Biochem Biophys Res Commun* 2008; **370**(3): 519-24.
156. Hida S, Ogasawara K, Sato K, et al. CD8(+) T cell-mediated skin disease in mice lacking IRF-2, the transcriptional attenuator of interferon-alpha/beta signaling. *Immunity* 2000; **13**(5): 643-55.
157. Negishi H, Ohba Y, Yanai H, et al. Negative regulation of Toll-like-receptor signaling by IRF-4. *Proc Natl Acad Sci U S A* 2005; **102**(44): 15989-94.
158. Xu D, Meyer F, Ehlers E, Blasnitz L, Zhang L. Interferon regulatory factor 4 (IRF-4) targets IRF-5 to regulate Epstein-Barr virus transformation. *J Biol Chem* 2011; **286**(20): 18261-7.
159. Li Y, Fan X, He X, et al. MicroRNA-466l inhibits antiviral innate immune response by targeting interferon-alpha. *Cell Mol Immunol* 2012; **9**(6): 497-502.
160. Witwer KW, Sisk JM, Gama L, Clements JE. MicroRNA regulation of IFN-beta protein expression: rapid and sensitive modulation of the innate immune response. *J Immunol* 2010; **184**(5): 2369-76.
161. Zhang C, Han L, Zhang A, et al. Global changes of mRNA expression reveals an increased activity of the interferon-induced signal transducer and activator of transcription (STAT) pathway by repression of miR-221/222 in glioblastoma U251 cells. *Int J Oncol* 2010; **36**(6): 1503-12.
162. Smith S, Fernando T, Wu PW, et al. MicroRNA-302d targets IRF9 to regulate the IFN-induced gene expression in SLE. *J Autoimmun* 2017; **79**: 105-11.

163. McNab F, Mayer-Barber K, Sher A, Wack A, O'Garra A. Type I interferons in infectious disease. *Nat Rev Immunol* 2015; **15**(2): 87-103.
164. Arico E, Castiello L, Capone I, Gabriele L, Belardelli F. Type I Interferons and Cancer: An Evolving Story Demanding Novel Clinical Applications. *Cancers (Basel)* 2019; **11**(12).
165. Crow MK, Olferiev M, Kirou KA. Type I Interferons in Autoimmune Disease. *Annu Rev Pathol* 2019; **14**: 369-93.
166. Cao W. In sickness and in health-Type I interferon and the brain. *Front Aging Neurosci* 2024; **16**: 1403142.
167. Lamborn IT, Jing H, Zhang Y, et al. Recurrent rhinovirus infections in a child with inherited MDA5 deficiency. *J Exp Med* 2017; **214**(7): 1949-72.
168. Asgari S, Schlapbach LJ, Anchisi S, et al. Severe viral respiratory infections in children with IFIH1 loss-of-function mutations. *Proc Natl Acad Sci U S A* 2017; **114**(31): 8342-7.
169. Chen J, Jing H, Martin-Nalda A, et al. Inborn errors of TLR3- or MDA5-dependent type I IFN immunity in children with enterovirus rhombencephalitis. *J Exp Med* 2021; **218**(12).
170. Zhang SY, Jouanguy E, Ugolini S, et al. TLR3 deficiency in patients with herpes simplex encephalitis. *Science* 2007; **317**(5844): 1522-7.
171. Lim HK, Huang SXL, Chen J, et al. Severe influenza pneumonitis in children with inherited TLR3 deficiency. *J Exp Med* 2019; **216**(9): 2038-56.
172. Zhang Q, Bastard P, Liu Z, et al. Inborn errors of type I IFN immunity in patients with life-threatening COVID-19. *Science* 2020; **370**(6515).
173. Garcia-Garcia A, Perez de Diego R, Flores C, et al. Humans with inherited MyD88 and IRAK-4 deficiencies are predisposed to hypoxemic COVID-19 pneumonia. *J Exp Med* 2023; **220**(5).
174. von Bernuth H, Picard C, Jin Z, et al. Pyogenic bacterial infections in humans with MyD88 deficiency. *Science* 2008; **321**(5889): 691-6.
175. Picard C, von Bernuth H, Ghandil P, et al. Clinical features and outcome of patients with IRAK-4 and MyD88 deficiency. *Medicine (Baltimore)* 2010; **89**(6): 403-25.
176. Bastard P, Hsiao KC, Zhang Q, et al. A loss-of-function IFNAR1 allele in Polynesia underlies severe viral diseases in homozygotes. *J Exp Med* 2022; **219**(6).
177. Duncan CJA, Skouboe MK, Howarth S, et al. Life-threatening viral disease in a novel form of autosomal recessive IFNAR2 deficiency in the Arctic. *J Exp Med* 2022; **219**(6).
178. Bastard P, Rosen LB, Zhang Q, et al. Autoantibodies against type I IFNs in patients with life-threatening COVID-19. *Science* 2020; **370**(6515).
179. Alotaibi F, Alharbi NK, Rosen LB, et al. Type I interferon autoantibodies in hospitalized patients with Middle East respiratory syndrome and association with outcomes and treatment effect of interferon beta-1b in MIRACLE clinical trial. *Influenza Other Respir Viruses* 2023; **17**(3): e13116.
180. Zhang Q, Pizzorno A, Miorin L, et al. Autoantibodies against type I IFNs in patients with critical influenza pneumonia. *J Exp Med* 2022; **219**(11).
181. Frasca F, Scordio M, Santinelli L, et al. Anti-IFN-alpha/-omega neutralizing antibodies from COVID-19 patients correlate with downregulation of IFN response and laboratory biomarkers of disease severity. *Eur J Immunol* 2022; **52**(7): 1120-8.
182. Hale BG. Autoantibodies targeting type I interferons: Prevalence, mechanisms of induction, and association with viral disease susceptibility. *Eur J Immunol* 2023; **53**(6): e2250164.
183. Zhang X, Bogunovic D, Payelle-Brogard B, et al. Human intracellular ISG15 prevents interferon-alpha/beta over-amplification and auto-inflammation. *Nature* 2015; **517**(7532): 89-93.
184. Lee D, Le Pen J, Yatim A, et al. Inborn errors of OAS-RNase L in SARS-CoV-2-related multisystem inflammatory syndrome in children. *Science* 2023; **379**(6632): eabo3627.
185. Bucciol G, Moens L, Ogishi M, et al. Human inherited complete STAT2 deficiency underlies inflammatory viral diseases. *J Clin Invest* 2023; **133**(12).
186. Gothe F, Stremenova Spegarova J, Hatton CF, et al. Aberrant inflammatory responses to type I interferon in STAT2 or IRF9 deficiency. *J Allergy Clin Immunol* 2022; **150**(4): 955-64 e16.

187. Chen Y, Graf L, Chen T, et al. Rare variant MX1 alleles increase human susceptibility to zoonotic H7N9 influenza virus. *Science* 2021; **373**(6557): 918-22.
188. Crow YJ, Stetson DB. The type I interferonopathies: 10 years on. *Nat Rev Immunol* 2022; **22**(8): 471-83.
189. Aicardi J, Goutieres F. A progressive familial encephalopathy in infancy with calcifications of the basal ganglia and chronic cerebrospinal fluid lymphocytosis. *Ann Neurol* 1984; **15**(1): 49-54.
190. Crow YJ, Hayward BE, Parmar R, et al. Mutations in the gene encoding the 3'-5' DNA exonuclease TREX1 cause Aicardi-Goutieres syndrome at the AGS1 locus. *Nat Genet* 2006; **38**(8): 917-20.
191. Crow YJ, Leitch A, Hayward BE, et al. Mutations in genes encoding ribonuclease H2 subunits cause Aicardi-Goutieres syndrome and mimic congenital viral brain infection. *Nat Genet* 2006; **38**(8): 910-6.
192. Yang YG, Lindahl T, Barnes DE. Trex1 exonuclease degrades ssDNA to prevent chronic checkpoint activation and autoimmune disease. *Cell* 2007; **131**(5): 873-86.
193. Grieves JL, Fye JM, Harvey S, Grayson JM, Hollis T, Perrino FW. Exonuclease TREX1 degrades double-stranded DNA to prevent spontaneous lupus-like inflammatory disease. *Proc Natl Acad Sci U S A* 2015; **112**(16): 5117-22.
194. Mackenzie KJ, Carroll P, Lettice L, et al. Ribonuclease H2 mutations induce a cGAS/STING-dependent innate immune response. *EMBO J* 2016; **35**(8): 831-44.
195. Mackenzie KJ, Carroll P, Martin CA, et al. cGAS surveillance of micronuclei links genome instability to innate immunity. *Nature* 2017; **548**(7668): 461-5.
196. Rice GI, Bond J, Asipu A, et al. Mutations involved in Aicardi-Goutieres syndrome implicate SAMHD1 as regulator of the innate immune response. *Nat Genet* 2009; **41**(7): 829-32.
197. Franzolin E, Pontarin G, Rampazzo C, et al. The deoxynucleotide triphosphohydrolase SAMHD1 is a major regulator of DNA precursor pools in mammalian cells. *Proc Natl Acad Sci U S A* 2013; **110**(35): 14272-7.
198. Maharana S, Kretschmer S, Hunger S, et al. SAMHD1 controls innate immunity by regulating condensation of immunogenic self RNA. *Mol Cell* 2022; **82**(19): 3712-28 e10.
199. Rice GI, Kasher PR, Forte GM, et al. Mutations in ADAR1 cause Aicardi-Goutieres syndrome associated with a type I interferon signature. *Nat Genet* 2012; **44**(11): 1243-8.
200. Pfaller CK, George CX, Samuel CE. Adenosine Deaminases Acting on RNA (ADARs) and Viral Infections. *Annu Rev Virol* 2021; **8**(1): 239-64.
201. Mannion NM, Greenwood SM, Young R, et al. The RNA-editing enzyme ADAR1 controls innate immune responses to RNA. *Cell Rep* 2014; **9**(4): 1482-94.
202. Dias Junior AG, Sampaio NG, Rehwinkel J. A Balancing Act: MDA5 in Antiviral Immunity and Autoinflammation. *Trends Microbiol* 2019; **27**(1): 75-85.
203. Loo YM, Fornek J, Crochet N, et al. Distinct RIG-I and MDA5 signaling by RNA viruses in innate immunity. *J Virol* 2008; **82**(1): 335-45.
204. Rice GI, Del Toro Duany Y, Jenkinson EM, et al. Gain-of-function mutations in IFIH1 cause a spectrum of human disease phenotypes associated with upregulated type I interferon signaling. *Nat Genet* 2014; **46**(5): 503-9.
205. Fremond ML, Hadchouel A, Berteloot L, et al. Overview of STING-Associated Vasculopathy with Onset in Infancy (SAVI) Among 21 Patients. *J Allergy Clin Immunol Pract* 2021; **9**(2): 803-18 e11.
206. Fremond ML, Nathan N. COPA syndrome, 5 years after: Where are we? *Joint Bone Spine* 2021; **88**(2): 105070.
207. Mukai K, Ogawa E, Uematsu R, et al. Homeostatic regulation of STING by retrograde membrane traffic to the ER. *Nat Commun* 2021; **12**(1): 61.
208. Steiner A, Hrovat-Schaale K, Prigione I, et al. Deficiency in coatomer complex I causes aberrant activation of STING signalling. *Nat Commun* 2022; **13**(1): 2321.
209. Deng Z, Chong Z, Law CS, et al. A defect in COPI-mediated transport of STING causes immune dysregulation in COPA syndrome. *J Exp Med* 2020; **217**(11).

210. Toubiana J, Okada S, Hiller J, et al. Heterozygous STAT1 gain-of-function mutations underlie an unexpectedly broad clinical phenotype. *Blood* 2016; **127**(25): 3154-64.
211. Baris S, Alroqi F, Kiykim A, et al. Severe Early-Onset Combined Immunodeficiency due to Heterozygous Gain-of-Function Mutations in STAT1. *J Clin Immunol* 2016; **36**(7): 641-8.
212. Xie Y, Shao F, Lei J, Huang N, Fan Z, Yu H. Case report: A STAT1 gain-of-function mutation causes a syndrome of combined immunodeficiency, autoimmunity and pure red cell aplasia. *Front Immunol* 2022; **13**: 928213.
213. Becker LL, Ebstein F, Horn D, et al. Interferon receptor dysfunction in a child with malignant atrophic papulosis and CNS involvement. *Lancet Neurol* 2022; **21**(8): 682-6.
214. Sullivan KD, Lewis HC, Hill AA, et al. Trisomy 21 consistently activates the interferon response. *Elife* 2016; **5**.
215. Kong XF, Worley L, Rinchai D, et al. Three Copies of Four Interferon Receptor Genes Underlie a Mild Type I Interferonopathy in Down Syndrome. *J Clin Immunol* 2020; **40**(6): 807-19.
216. Malle L, Martin-Fernandez M, Buta S, Richardson A, Bush D, Bogunovic D. Excessive negative regulation of type I interferon disrupts viral control in individuals with Down syndrome. *Immunity* 2022; **55**(11): 2074-84 e5.
217. Ram G, Chinen J. Infections and immunodeficiency in Down syndrome. *Clin Exp Immunol* 2011; **164**(1): 9-16.
218. Araya P, Waugh KA, Sullivan KD, et al. Trisomy 21 dysregulates T cell lineages toward an autoimmunity-prone state associated with interferon hyperactivity. *Proc Natl Acad Sci U S A* 2019; **116**(48): 24231-41.
219. Martin-Fernandez M, Buta S, Le Voyer T, et al. A partial form of inherited human USP18 deficiency underlies infection and inflammation. *J Exp Med* 2022; **219**(4).
220. Alsohime F, Martin-Fernandez M, Temsah MH, et al. JAK Inhibitor Therapy in a Child with Inherited USP18 Deficiency. *N Engl J Med* 2020; **382**(3): 256-65.
221. Misk RA, Qawasme L, Abunejma FM, et al. A Case Report and Literature Review of Pseudo-TORCH Syndrome Type 2 (PTORCH2). *Case Rep Pediatr* 2022; **2022**: 3555532.
222. Hadjadj J, Castro CN, Tusseau M, et al. Early-onset autoimmunity associated with SOCS1 haploinsufficiency. *Nat Commun* 2020; **11**(1): 5341.
223. Michniacki TF, Walkovich K, DeMeyer L, et al. SOCS1 Haploinsufficiency Presenting as Severe Enthesitis, Bone Marrow Hypocellularity, and Refractory Thrombocytopenia in a Pediatric Patient with Subsequent Response to JAK Inhibition. *J Clin Immunol* 2022; **42**(8): 1766-77.
224. Korholz J, Gabrielyan A, Sowerby JM, et al. One Gene, Many Facets: Multiple Immune Pathway Dysregulation in SOCS1 Haploinsufficiency. *Front Immunol* 2021; **12**: 680334.
225. Brehm A, Liu Y, Sheikh A, et al. Additive loss-of-function proteasome subunit mutations in CANDLE/PRAAS patients promote type I IFN production. *J Clin Invest* 2015; **125**(11): 4196-211.
226. Papendorf JJ, Ebstein F, Alehashemi S, et al. Identification of eight novel proteasome variants in five unrelated cases of proteasome-associated autoinflammatory syndromes (PRAAS). *Front Immunol* 2023; **14**: 1190104.
227. Davidson S, Yu CH, Steiner A, et al. Protein kinase R is an innate immune sensor of proteotoxic stress via accumulation of cytoplasmic IL-24. *Sci Immunol* 2022; **7**(68): eabi6763.
228. Akalu YT, Bogunovic D. Inborn errors of immunity: an expanding universe of disease and genetic architecture. *Nat Rev Genet* 2024; **25**(3): 184-95.
229. Gruber C, Bogunovic D. Incomplete penetrance in primary immunodeficiency: a skeleton in the closet. *Hum Genet* 2020; **139**(6-7): 745-57.
230. Kingdom R, Wright CF. Incomplete Penetrance and Variable Expressivity: From Clinical Studies to Population Cohorts. *Front Genet* 2022; **13**: 920390.
231. Rice GI, Park S, Gavazzi F, et al. Genetic and phenotypic spectrum associated with IFIH1 gain-of-function. *Hum Mutat* 2020; **41**(4): 837-49.
232. Crow YJ, group AGS. Clinical Non-penetrance Associated with Biallelic Mutations in the RNase H2 Complex. *J Clin Immunol* 2023; **43**(4): 706-8.

233. Levy DE, Marie IJ, Durbin JE. Induction and function of type I and III interferon in response to viral infection. *Curr Opin Virol* 2011; **1**(6): 476-86.
234. Ali S, Mann-Nuttel R, Schulze A, Richter L, Alferink J, Scheu S. Sources of Type I Interferons in Infectious Immunity: Plasmacytoid Dendritic Cells Not Always in the Driver's Seat. *Front Immunol* 2019; **10**: 778.
235. Shemesh M, Lochte S, Piehler J, Schreiber G. IFNAR1 and IFNAR2 play distinct roles in initiating type I interferon-induced JAK-STAT signaling and activating STATs. *Sci Signal* 2021; **14**(710): eabe4627.
236. Duncan CJA, Randall RE, Hambleton S. Genetic Lesions of Type I Interferon Signalling in Human Antiviral Immunity. *Trends Genet* 2021; **37**(1): 46-58.
237. Goldmann T, Zeller N, Raasch J, et al. USP18 lack in microglia causes destructive interferonopathy of the mouse brain. *EMBO J* 2015; **34**(12): 1612-29.
238. Darnell JE, Jr., Kerr IM, Stark GR. Jak-STAT pathways and transcriptional activation in response to IFNs and other extracellular signaling proteins. *Science* 1994; **264**(5164): 1415-21.
239. Duncan CJA, Thompson BJ, Chen R, et al. Severe type I interferonopathy and unrestrained interferon signaling due to a homozygous germline mutation in STAT2. *Sci Immunol* 2019; **4**(42).
240. Gruber C, Martin-Fernandez M, Ailal F, et al. Homozygous STAT2 gain-of-function mutation by loss of USP18 activity in a patient with type I interferonopathy. *J Exp Med* 2020; **217**(5).
241. Rice GI, Forte GM, Szynkiewicz M, et al. Assessment of interferon-related biomarkers in Aicardi-Goutieres syndrome associated with mutations in TREX1, RNASEH2A, RNASEH2B, RNASEH2C, SAMHD1, and ADAR: a case-control study. *Lancet Neurol* 2013; **12**(12): 1159-69.
242. Leung S, Qureshi SA, Kerr IM, Darnell JE, Jr., Stark GR. Role of STAT2 in the alpha interferon signaling pathway. *Mol Cell Biol* 1995; **15**(3): 1312-7.
243. Li X, Leung S, Kerr IM, Stark GR. Functional subdomains of STAT2 required for preassociation with the alpha interferon receptor and for signaling. *Mol Cell Biol* 1997; **17**(4): 2048-56.
244. Hambleton S, Goodbourn S, Young DF, et al. STAT2 deficiency and susceptibility to viral illness in humans. *Proc Natl Acad Sci U S A* 2013; **110**(8): 3053-8.
245. Backwell L, Marsh JA. Diverse Molecular Mechanisms Underlying Pathogenic Protein Mutations: Beyond the Loss-of-Function Paradigm. *Annu Rev Genomics Hum Genet* 2022; **23**: 475-98.
246. Bousfiha A, Moundir A, Tangye SG, et al. The 2022 Update of IUIS Phenotypical Classification for Human Inborn Errors of Immunity. *J Clin Immunol* 2022; **42**(7): 1508-20.
247. Tangye SG, Al-Herz W, Bousfiha A, et al. Human Inborn Errors of Immunity: 2022 Update on the Classification from the International Union of Immunological Societies Expert Committee. *J Clin Immunol* 2022; **42**(7): 1473-507.
248. Freij BJ, Hanrath AT, Chen R, Hambleton S, Duncan CJA. Life-Threatening Influenza, Hemophagocytic Lymphohistiocytosis and Probable Vaccine-Strain Varicella in a Novel Case of Homozygous STAT2 Deficiency. *Front Immunol* 2020; **11**: 624415.
249. Moens L, Van Eyck L, Jochmans D, et al. A novel kindred with inherited STAT2 deficiency and severe viral illness. *J Allergy Clin Immunol* 2017; **139**(6): 1995-7 e9.
250. Duncan CJA, Hambleton S. Human Disease Phenotypes Associated with Loss and Gain of Function Mutations in STAT2: Viral Susceptibility and Type I Interferonopathy. *J Clin Immunol* 2021; **41**(7): 1446-56.
251. Bogunovic D, Byun M, Durfee LA, et al. Mycobacterial disease and impaired IFN-gamma immunity in humans with inherited ISG15 deficiency. *Science* 2012; **337**(6102): 1684-8.
252. Martin-Fernandez M, Bravo Garcia-Morato M, Gruber C, et al. Systemic Type I IFN Inflammation in Human ISG15 Deficiency Leads to Necrotizing Skin Lesions. *Cell Rep* 2020; **31**(6): 107633.

253. Kang JA, Kim YJ, Jeon YJ. The diverse repertoire of ISG15: more intricate than initially thought. *Exp Mol Med* 2022; **54**(11): 1779-92.
254. Kelley LA, Mezulis S, Yates CM, Wass MN, Sternberg MJ. The Phyre2 web portal for protein modeling, prediction and analysis. *Nat Protoc* 2015; **10**(6): 845-58.
255. Berman HM, Battistuz T, Bhat TN, et al. The Protein Data Bank. *Acta Crystallogr D Biol Crystallogr* 2002; **58**(Pt 6 No 1): 899-907.
256. Kozakov D, Hall DR, Xia B, et al. The ClusPro web server for protein-protein docking. *Nat Protoc* 2017; **12**(2): 255-78.
257. Mitternacht S. FreeSASA: An open source C library for solvent accessible surface area calculations. *F1000Res* 2016; **5**: 189.
258. Delgado J, Radusky LG, Cianferoni D, Serrano L. FoldX 5.0: working with RNA, small molecules and a new graphical interface. *Bioinformatics* 2019; **35**(20): 4168-9.
259. Karczewski KJ, Francioli LC, Tiao G, et al. The mutational constraint spectrum quantified from variation in 141,456 humans. *Nature* 2020; **581**(7809): 434-43.
260. Tonks NK, Diltz CD, Fischer EH. Purification of the major protein-tyrosine-phosphatases of human placenta. *J Biol Chem* 1988; **263**(14): 6722-30.
261. Tonks NK, Diltz CD, Fischer EH. Characterization of the major protein-tyrosine-phosphatases of human placenta. *J Biol Chem* 1988; **263**(14): 6731-7.
262. Barford D, Flint AJ, Tonks NK. Crystal structure of human protein tyrosine phosphatase 1B. *Science* 1994; **263**(5152): 1397-404.
263. Tonks NK. PTP1B: from the sidelines to the front lines! *FEBS Lett* 2003; **546**(1): 140-8.
264. Brown-Shimer S, Johnson KA, Lawrence JB, et al. Molecular cloning and chromosome mapping of the human gene encoding protein phosphotyrosyl phosphatase 1B. *Proc Natl Acad Sci U S A* 1990; **87**(13): 5148-52.
265. Chernoff J, Schievella AR, Jost CA, Erikson RL, Neel BG. Cloning of a cDNA for a major human protein-tyrosine-phosphatase. *Proc Natl Acad Sci U S A* 1990; **87**(7): 2735-9.
266. Guan KL, Haun RS, Watson SJ, Geahlen RL, Dixon JE. Cloning and expression of a protein-tyrosine-phosphatase. *Proc Natl Acad Sci U S A* 1990; **87**(4): 1501-5.
267. Yeh CY, Izaguirre JA, Greisman JB, Willmore L, Maragakis P, Shaw DE. A Conserved Local Structural Motif Controls the Kinetics of PTP1B Catalysis. *J Chem Inf Model* 2023; **63**(13): 4115-24.
268. Denu JM, Dixon JE. Protein tyrosine phosphatases: mechanisms of catalysis and regulation. *Curr Opin Chem Biol* 1998; **2**(5): 633-41.
269. Zahn M, Marienfeld R, Melzner I, et al. A novel PTPN1 splice variant upregulates JAK/STAT activity in classical Hodgkin lymphoma cells. *Blood* 2017; **129**(11): 1480-90.
270. Kamerlin SC, Rucker R, Boresch S. A molecular dynamics study of WPD-loop flexibility in PTP1B. *Biochem Biophys Res Commun* 2007; **356**(4): 1011-6.
271. Brandao TA, Johnson SJ, Hengge AC. The molecular details of WPD-loop movement differ in the protein-tyrosine phosphatases YopH and PTP1B. *Arch Biochem Biophys* 2012; **525**(1): 53-9.
272. Shen R, Crean RM, Olsen KJ, et al. Insights into the importance of WPD-loop sequence for activity and structure in protein tyrosine phosphatases. *Chem Sci* 2022; **13**(45): 13524-40.
273. Liu F, Hill DE, Chernoff J. Direct binding of the proline-rich region of protein tyrosine phosphatase 1B to the Src homology 3 domain of p130(Cas). *J Biol Chem* 1996; **271**(49): 31290-5.
274. Schwarz JJ, Grundmann L, Kokot T, et al. Quantitative proteomics identifies PTP1B as modulator of B cell antigen receptor signaling. *Life Sci Alliance* 2021; **4**(11).
275. Liang F, Lee SY, Liang J, Lawrence DS, Zhang ZY. The role of protein-tyrosine phosphatase 1B in integrin signaling. *J Biol Chem* 2005; **280**(26): 24857-63.
276. Anderie I, Schulz I, Schmid A. Direct interaction between ER membrane-bound PTP1B and its plasma membrane-anchored targets. *Cell Signal* 2007; **19**(3): 582-92.

277. Cortesio CL, Chan KT, Perrin BJ, et al. Calpain 2 and PTP1B function in a novel pathway with Src to regulate invadopodia dynamics and breast cancer cell invasion. *J Cell Biol* 2008; **180**(5): 957-71.
278. Ezumi Y, Takayama H, Okuma M. Differential regulation of protein-tyrosine phosphatases by integrin alpha IIb beta 3 through cytoskeletal reorganization and tyrosine phosphorylation in human platelets. *J Biol Chem* 1995; **270**(20): 11927-34.
279. Frangioni JV, Oda A, Smith M, Salzman EW, Neel BG. Calpain-catalyzed cleavage and subcellular relocation of protein phosphotyrosine phosphatase 1B (PTP-1B) in human platelets. *EMBO J* 1993; **12**(12): 4843-56.
280. Bakke J, Haj FG. Protein-tyrosine phosphatase 1B substrates and metabolic regulation. *Semin Cell Dev Biol* 2015; **37**: 58-65.
281. Liu R, Mathieu C, Berthelet J, Zhang W, Dupret JM, Rodrigues Lima F. Human Protein Tyrosine Phosphatase 1B (PTP1B): From Structure to Clinical Inhibitor Perspectives. *Int J Mol Sci* 2022; **23**(13).
282. Villamar-Cruz O, Loza-Mejia MA, Arias-Romero LE, Camacho-Arroyo I. Recent advances in PTP1B signaling in metabolism and cancer. *Biosci Rep* 2021; **41**(11).
283. Olloquequi J, Cano A, Sanchez-Lopez E, et al. Protein tyrosine phosphatase 1B (PTP1B) as a potential therapeutic target for neurological disorders. *Biomed Pharmacother* 2022; **155**: 113709.
284. Kolodziej-Sobczak D, Sobczak L, Laczkowski KZ. Protein Tyrosine Phosphatase 1B (PTP1B): A Comprehensive Review of Its Role in Pathogenesis of Human Diseases. *International Journal of Molecular Sciences* 2024; **25**(13).
285. van Montfort RL, Congreve M, Tisi D, Carr R, Jhoti H. Oxidation state of the active-site cysteine in protein tyrosine phosphatase 1B. *Nature* 2003; **423**(6941): 773-7.
286. Dadke S, Cotteret S, Yip SC, et al. Regulation of protein tyrosine phosphatase 1B by sumoylation. *Nat Cell Biol* 2007; **9**(1): 80-5.
287. Bandyopadhyay D, Kusari A, Kenner KA, et al. Protein-tyrosine phosphatase 1B complexes with the insulin receptor in vivo and is tyrosine-phosphorylated in the presence of insulin. *J Biol Chem* 1997; **272**(3): 1639-45.
288. Dadke S, Kusari A, Kusari J. Phosphorylation and activation of protein tyrosine phosphatase (PTP) 1B by insulin receptor. *Mol Cell Biochem* 2001; **221**(1-2): 147-54.
289. Tao J, Malbon CC, Wang HY. Insulin stimulates tyrosine phosphorylation and inactivation of protein-tyrosine phosphatase 1B in vivo. *J Biol Chem* 2001; **276**(31): 29520-5.
290. Flint AJ, Gebbink MF, Franza BR, Jr., Hill DE, Tonks NK. Multi-site phosphorylation of the protein tyrosine phosphatase, PTP1B: identification of cell cycle regulated and phorbol ester stimulated sites of phosphorylation. *EMBO J* 1993; **12**(5): 1937-46.
291. Shifrin VI, Davis RJ, Neel BG. Phosphorylation of protein-tyrosine phosphatase PTP-1B on identical sites suggests activation of a common signaling pathway during mitosis and stress response in mammalian cells. *J Biol Chem* 1997; **272**(5): 2957-62.
292. Ravichandran LV, Chen H, Li Y, Quon MJ. Phosphorylation of PTP1B at Ser(50) by Akt impairs its ability to dephosphorylate the insulin receptor. *Mol Endocrinol* 2001; **15**(10): 1768-80.
293. Trumpler A, Schlott B, Herrlich P, Greer PA, Bohmer FD. Calpain-mediated degradation of reversibly oxidized protein-tyrosine phosphatase 1B. *FEBS J* 2009; **276**(19): 5622-33.
294. Kenner KA, Anyanwu E, Olefsky JM, Kusari J. Protein-tyrosine phosphatase 1B is a negative regulator of insulin- and insulin-like growth factor-I-stimulated signaling. *J Biol Chem* 1996; **271**(33): 19810-6.
295. Elchebly M, Payette P, Michaliszyn E, et al. Increased insulin sensitivity and obesity resistance in mice lacking the protein tyrosine phosphatase-1B gene. *Science* 1999; **283**(5407): 1544-8.
296. Zabolotny JM, Bence-Hanulec KK, Stricker-Krongrad A, et al. PTP1B regulates leptin signal transduction in vivo. *Dev Cell* 2002; **2**(4): 489-95.

297. Kaszubska W, Falls HD, Schaefer VG, et al. Protein tyrosine phosphatase 1B negatively regulates leptin signaling in a hypothalamic cell line. *Mol Cell Endocrinol* 2002; **195**(1-2): 109-18.
298. Ozek C, Kanoski SE, Zhang ZY, Grill HJ, Bence KK. Protein-tyrosine phosphatase 1B (PTP1B) is a novel regulator of central brain-derived neurotrophic factor and tropomyosin receptor kinase B (TrkB) signaling. *J Biol Chem* 2014; **289**(46): 31682-92.
299. Xia T, Yi XM, Wu X, Shang J, Shu HB. PTPN1/2-mediated dephosphorylation of MITA/STING promotes its 20S proteasomal degradation and attenuates innate antiviral response. *Proc Natl Acad Sci U S A* 2019; **116**(40): 20063-9.
300. Myers MP, Andersen JN, Cheng A, et al. TYK2 and JAK2 are substrates of protein-tyrosine phosphatase 1B. *J Biol Chem* 2001; **276**(51): 47771-4.
301. Morris R, Keating N, Tan C, et al. Structure guided studies of the interaction between PTP1B and JAK. *Commun Biol* 2023; **6**(1): 641.
302. Li X, Kohn M. Prediction and verification of novel peptide targets of protein tyrosine phosphatase 1B. *Bioorg Med Chem* 2016; **24**(15): 3255-8.
303. Ostergaard M, Mishra NK, Jensen KJ. The ABC of Insulin: The Organic Chemistry of a Small Protein. *Chemistry* 2020; **26**(38): 8341-57.
304. Banting FG, Best CH, Collip JB, Campbell WR, Fletcher AA. Pancreatic Extracts in the Treatment of Diabetes Mellitus. *Can Med Assoc J* 1922; **12**(3): 141-6.
305. Levine R, Goldstein MS, Huddlestun B, Klein SP. Action of insulin on the 'permeability' of cells to free hexoses, as studied by its effect on the distribution of galactose. *Am J Physiol* 1950; **163**(1): 70-6.
306. Freychet P, Roth J, Neville DM, Jr. Insulin receptors in the liver: specific binding of (125 I)insulin to the plasma membrane and its relation to insulin bioactivity. *Proc Natl Acad Sci U S A* 1971; **68**(8): 1833-7.
307. Kasuga M, Zick Y, Blithe DL, Crettaz M, Kahn CR. Insulin stimulates tyrosine phosphorylation of the insulin receptor in a cell-free system. *Nature* 1982; **298**(5875): 667-9.
308. Ebina Y, Ellis L, Jarnagin K, et al. The human insulin receptor cDNA: the structural basis for hormone-activated transmembrane signalling. *Cell* 1985; **40**(4): 747-58.
309. Ullrich A, Bell JR, Chen EY, et al. Human insulin receptor and its relationship to the tyrosine kinase family of oncogenes. *Nature* 1985; **313**(6005): 756-61.
310. Sun XJ, Rothenberg P, Kahn CR, et al. Structure of the insulin receptor substrate IRS-1 defines a unique signal transduction protein. *Nature* 1991; **352**(6330): 73-7.
311. Haeusler RA, McGraw TE, Accili D. Biochemical and cellular properties of insulin receptor signalling. *Nat Rev Mol Cell Biol* 2018; **19**(1): 31-44.
312. Goldstein BJ, Bittner-Kowalczyk A, White MF, Harbeck M. Tyrosine dephosphorylation and deactivation of insulin receptor substrate-1 by protein-tyrosine phosphatase 1B. Possible facilitation by the formation of a ternary complex with the Grb2 adaptor protein. *J Biol Chem* 2000; **275**(6): 4283-9.
313. Klaman LD, Boss O, Peroni OD, et al. Increased energy expenditure, decreased adiposity, and tissue-specific insulin sensitivity in protein-tyrosine phosphatase 1B-deficient mice. *Mol Cell Biol* 2000; **20**(15): 5479-89.
314. Abdelsalam SS, Korashy HM, Zeidan A, Agouni A. The Role of Protein Tyrosine Phosphatase (PTP)-1B in Cardiovascular Disease and Its Interplay with Insulin Resistance. *Biomolecules* 2019; **9**(7).
315. Zhang Y, Proenca R, Maffei M, Barone M, Leopold L, Friedman JM. Positional cloning of the mouse obese gene and its human homologue. *Nature* 1994; **372**(6505): 425-32.
316. Vilarino-Garcia T, Polonio-Gonzalez ML, Perez-Perez A, et al. Role of Leptin in Obesity, Cardiovascular Disease, and Type 2 Diabetes. *Int J Mol Sci* 2024; **25**(4).
317. Chen H, Charlat O, Tartaglia LA, et al. Evidence that the diabetes gene encodes the leptin receptor: identification of a mutation in the leptin receptor gene in db/db mice. *Cell* 1996; **84**(3): 491-5.
318. Lee GH, Proenca R, Montez JM, et al. Abnormal splicing of the leptin receptor in diabetic mice. *Nature* 1996; **379**(6566): 632-5.

319. Allison MB, Myers MG, Jr. 20 years of leptin: connecting leptin signaling to biological function. *J Endocrinol* 2014; **223**(1): T25-35.
320. Zhou Y, Rui L. Leptin signaling and leptin resistance. *Front Med* 2013; **7**(2): 207-22.
321. Delibegovic M, Dall'Angelo S, Dekeryte R. Protein tyrosine phosphatase 1B in metabolic diseases and drug development. *Nat Rev Endocrinol* 2024; **20**(6): 366-78.
322. Liu Z, Xiao T, Liu H. Leptin signaling and its central role in energy homeostasis. *Front Neurosci* 2023; **17**: 1238528.
323. Evans MC, Lord RA, Anderson GM. Multiple Leptin Signalling Pathways in the Control of Metabolism and Fertility: A Means to Different Ends? *Int J Mol Sci* 2021; **22**(17).
324. Colucci-D'Amato L, Speranza L, Volpicelli F. Neurotrophic Factor BDNF, Physiological Functions and Therapeutic Potential in Depression, Neurodegeneration and Brain Cancer. *Int J Mol Sci* 2020; **21**(20).
325. Vieira MN, Lyra ESNM, Ferreira ST, De Felice FG. Protein Tyrosine Phosphatase 1B (PTP1B): A Potential Target for Alzheimer's Therapy? *Front Aging Neurosci* 2017; **9**: 7.
326. Minichiello L. TrkB signalling pathways in LTP and learning. *Nat Rev Neurosci* 2009; **10**(12): 850-60.
327. Jin W. Regulation of BDNF-TrkB Signaling and Potential Therapeutic Strategies for Parkinson's Disease. *J Clin Med* 2020; **9**(1).
328. Ge X, Hu M, Zhou M, et al. Overexpression of forebrain PTP1B leads to synaptic and cognitive impairments in obesity. *Brain Behav Immun* 2024; **117**: 456-70.
329. Hopfner KP, Hornung V. Molecular mechanisms and cellular functions of cGAS-STING signalling. *Nat Rev Mol Cell Biol* 2020; **21**(9): 501-21.
330. Guey B, Ablasser A. Emerging dimensions of cellular cGAS-STING signaling. *Curr Opin Immunol* 2022; **74**: 164-71.
331. David C, Fremond ML. Lung Inflammation in STING-Associated Vasculopathy with Onset in Infancy (SAVI). *Cells* 2022; **11**(3).
332. Xu Q, Xing J, Wang S, Peng H, Liu Y. The role of the cGAS-STING pathway in metabolic diseases. *Heliyon* 2024; **10**(12): e33093.
333. Wang MM, Zhao Y, Liu J, et al. The role of the cGAS-STING signaling pathway in viral infections, inflammatory and autoimmune diseases. *Acta Pharmacol Sin* 2024.
334. Bai J, Liu F. The cGAS-cGAMP-STING Pathway: A Molecular Link Between Immunity and Metabolism. *Diabetes* 2019; **68**(6): 1099-108.
335. Kang J, Wu J, Liu Q, Wu X, Zhao Y, Ren J. Post-Translational Modifications of STING: A Potential Therapeutic Target. *Front Immunol* 2022; **13**: 888147.
336. Zhang C, Shang G, Gui X, Zhang X, Bai XC, Chen ZJ. Structural basis of STING binding with and phosphorylation by TBK1. *Nature* 2019; **567**(7748): 394-8.
337. Wu J, Dobbs N, Yang K, Yan N. Interferon-Independent Activities of Mammalian STING Mediate Antiviral Response and Tumor Immune Evasion. *Immunity* 2020; **53**(1): 115-26 e5.
338. Yamashiro LH, Wilson SC, Morrison HM, et al. Interferon-independent STING signaling promotes resistance to HSV-1 in vivo. *Nat Commun* 2020; **11**(1): 3382.
339. Swiecki M, Colonna M. The multifaceted biology of plasmacytoid dendritic cells. *Nat Rev Immunol* 2015; **15**(8): 471-85.
340. Platanias LC. Mechanisms of type-I- and type-II-interferon-mediated signalling. *Nat Rev Immunol* 2005; **5**(5): 375-86.
341. Gunawardana J, Chan FC, Telenius A, et al. Recurrent somatic mutations of PTPN1 in primary mediastinal B cell lymphoma and Hodgkin lymphoma. *Nat Genet* 2014; **46**(4): 329-35.
342. Zahn M, Kaluszniak B, Moller P, Marienfeld R. The PTP1B mutant PTP1BΔ2-4 is a positive regulator of the JAK/STAT signalling pathway in Hodgkin lymphoma. *Carcinogenesis* 2021; **42**(4): 517-27.
343. Collaborators GBDD. Global, regional, and national burden of diabetes from 1990 to 2021, with projections of prevalence to 2050: a systematic analysis for the Global Burden of Disease Study 2021. *Lancet* 2023; **402**(10397): 203-34.

344. Sacks DB, Arnold M, Bakris GL, et al. Guidelines and Recommendations for Laboratory Analysis in the Diagnosis and Management of Diabetes Mellitus. *Diabetes Care* 2023; **46**(10): e151-e99.
345. Baars DP, Fondevila MF, Meijnikman AS, Nieuwdorp M. The central role of the gut microbiota in the pathophysiology and management of type 2 diabetes. *Cell Host Microbe* 2024; **32**(8): 1280-300.
346. Tan SY, Mei Wong JL, Sim YJ, et al. Type 1 and 2 diabetes mellitus: A review on current treatment approach and gene therapy as potential intervention. *Diabetes Metab Syndr* 2019; **13**(1): 364-72.
347. Marchand L, Kawasaki-Ogita Y, Place J, et al. Long-Term Effects of Continuous Subcutaneous Insulin Infusion on Glucose Control and Microvascular Complications in Patients With Type 1 Diabetes. *J Diabetes Sci Technol* 2017; **11**(5): 924-9.
348. Demir G, Er E, Atik Altinok Y, Ozen S, Darcan S, Goksen D. Local complications of insulin administration sites and effect on diabetes management. *J Clin Nurs* 2022; **31**(17-18): 2530-8.
349. Berger G, Waldhoer T, Barrientos I, et al. Association of insulin-manipulation and psychiatric disorders: A systematic epidemiological evaluation of adolescents with type 1 diabetes in Austria. *Pediatr Diabetes* 2019; **20**(1): 127-36.
350. Lin Y, Shao H, Fonseca V, Shi L. Exacerbation of financial burden of insulin and overall glucose-lowing medications among uninsured population with diabetes. *J Diabetes* 2023; **15**(3): 215-23.
351. Flory JH, Keating S, Guelce D, Mushlin AI. Overcoming barriers to the use of metformin: patient and provider perspectives. *Patient Prefer Adherence* 2019; **13**: 1433-41.
352. Read NE, Wilson HM. Recent Developments in the Role of Protein Tyrosine Phosphatase 1B (PTP1B) as a Regulator of Immune Cell Signalling in Health and Disease. *Int J Mol Sci* 2024; **25**(13).
353. Chen H, Wertheimer SJ, Lin CH, et al. Protein-tyrosine phosphatases PTP1B and syp are modulators of insulin-stimulated translocation of GLUT4 in transfected rat adipose cells. *J Biol Chem* 1997; **272**(12): 8026-31.
354. Lam NT, Covey SD, Lewis JT, et al. Leptin resistance following over-expression of protein tyrosine phosphatase 1B in liver. *J Mol Endocrinol* 2006; **36**(1): 163-74.
355. Lessard L, Stuible M, Tremblay ML. The two faces of PTP1B in cancer. *Biochim Biophys Acta* 2010; **1804**(3): 613-9.
356. Yip SC, Saha S, Chernoff J. PTP1B: a double agent in metabolism and oncogenesis. *Trends Biochem Sci* 2010; **35**(8): 442-9.
357. Wiener JR, Hurteau JA, Kerns BJ, et al. Overexpression of the tyrosine phosphatase PTP1B is associated with human ovarian carcinomas. *Am J Obstet Gynecol* 1994; **170**(4): 1177-83.
358. Wiener JR, Kerns BJ, Harvey EL, et al. Overexpression of the protein tyrosine phosphatase PTP1B in human breast cancer: association with p185c-erbB-2 protein expression. *J Natl Cancer Inst* 1994; **86**(5): 372-8.
359. Hoekstra E, Das AM, Swets M, et al. Increased PTP1B expression and phosphatase activity in colorectal cancer results in a more invasive phenotype and worse patient outcome. *Oncotarget* 2016; **7**(16): 21922-38.
360. Wang Q, Pan Y, Zhao L, Qi F, Liu J. Protein tyrosine phosphatase 1B(PTP1B) promotes melanoma cells progression through Src activation. *Bioengineered* 2021; **12**(1): 8396-406.
361. Dube N, Bourdeau A, Heinonen KM, Cheng A, Loy AL, Tremblay ML. Genetic ablation of protein tyrosine phosphatase 1B accelerates lymphomagenesis of p53-null mice through the regulation of B-cell development. *Cancer Res* 2005; **65**(21): 10088-95.
362. Mei W, Wang K, Huang J, Zheng X. Cell Transformation by PTP1B Truncated Mutants Found in Human Colon and Thyroid Tumors. *PLoS One* 2016; **11**(11): e0166538.
363. Maarouf M, Chen B, Chen Y, et al. Identification of lncRNA-155 encoded by MIR155HG as a novel regulator of innate immunity against influenza A virus infection. *Cell Microbiol* 2019; **21**(8): e13036.

364. Carmichael JC, Yokota H, Craven RC, Schmitt A, Wills JW. The HSV-1 mechanisms of cell-to-cell spread and fusion are critically dependent on host PTP1B. *PLoS Pathog* 2018; **14**(5): e1007054.
365. Yue L, Xie Z, Li H, et al. Protein Tyrosine Phosphatase-1B Negatively Impacts Host Defense against Pseudomonas aeruginosa Infection. *Am J Pathol* 2016; **186**(5): 1234-44.
366. Yue L, Yan M, Tremblay ML, et al. PTP1B negatively regulates nitric oxide-mediated Pseudomonas aeruginosa killing by neutrophils. *PLoS One* 2019; **14**(9): e0222753.
367. Yue L, Yan M, Chen S, Cao H, Li H, Xie Z. PTP1B negatively regulates STAT1-independent Pseudomonas aeruginosa killing by macrophages. *Biochem Biophys Res Commun* 2020; **533**(3): 296-303.
368. Hao Q, Rathinaswamy MK, Klinge KL, et al. Mechanistic insights into a heterobifunctional degrader-induced PTPN2/N1 complex. *Commun Chem* 2024; **7**(1): 183.
369. Tiganis T, Bennett AM. Protein tyrosine phosphatase function: the substrate perspective. *Biochem J* 2007; **402**(1): 1-15.
370. Andersen JN, Mortensen OH, Peters GH, et al. Structural and evolutionary relationships among protein tyrosine phosphatase domains. *Mol Cell Biol* 2001; **21**(21): 7117-36.
371. St-Germain JR, Taylor P, Zhang W, et al. Differential regulation of FGFR3 by PTPN1 and PTPN2. *Proteomics* 2015; **15**(2-3): 419-33.
372. Zhang ZY. Drugging the Undruggable: Therapeutic Potential of Targeting Protein Tyrosine Phosphatases. *Acc Chem Res* 2017; **50**(1): 122-9.
373. Liu Z, Gao H, Zhao Z, Huang M, Wang S, Zhan J. Status of research on natural protein tyrosine phosphatase 1B inhibitors as potential antidiabetic agents: Update. *Biomed Pharmacother* 2023; **157**: 113990.
374. Dong J, Miao J, Miao Y, et al. Small Molecule Degraders of Protein Tyrosine Phosphatase 1B and T-Cell Protein Tyrosine Phosphatase for Cancer Immunotherapy. *Angew Chem Int Ed Engl* 2023; **62**(22): e202303818.
375. Akyol K, Kilic D. Discovery of novel and selective inhibitors targeting protein tyrosine phosphatase 1B (PTP1B): Virtual screening and molecular dynamic simulation. *Comput Biol Med* 2021; **139**: 104959.
376. Keedy DA, Hill ZB, Biel JT, et al. An expanded allosteric network in PTP1B by multitemperature crystallography, fragment screening, and covalent tethering. *Elife* 2018; **7**.
377. Hjortness MK, Riccardi L, Hongdusit A, et al. Evolutionarily Conserved Allosteric Communication in Protein Tyrosine Phosphatases. *Biochemistry* 2018; **57**(45): 6443-51.
378. Dale RC, Brilot F, Fagan E, Earl J. Cerebrospinal fluid neopterin in paediatric neurology: a marker of active central nervous system inflammation. *Dev Med Child Neurol* 2009; **51**(4): 317-23.
379. Sa M, Hacohen Y, Alderson L, et al. Immunotherapy-responsive childhood neurodegeneration with systemic and central nervous system inflammation. *Eur J Paediatr Neuro* 2018; **22**(5): 882-8.
380. Wiesmann C, Barr KJ, Kung J, et al. Allosteric inhibition of protein tyrosine phosphatase 1B. *Nat Struct Mol Biol* 2004; **11**(8): 730-7.
381. Rosenberg BR, Freije CA, Imanaka N, et al. Genetic Variation at IFNL4 Influences Extrahepatic Interferon-Stimulated Gene Expression in Chronic HCV Patients. *J Infect Dis* 2018; **217**(4): 650-5.
382. Kalluri R, Weinberg RA. The basics of epithelial-mesenchymal transition. *J Clin Invest* 2009; **119**(6): 1420-8.
383. Owen KL, Brockwell NK, Parker BS. JAK-STAT Signaling: A Double-Edged Sword of Immune Regulation and Cancer Progression. *Cancers (Basel)* 2019; **11**(12).
384. Brooks AJ, Putoczki T. JAK-STAT Signalling Pathway in Cancer. *Cancers (Basel)* 2020; **12**(7).
385. Jeanpierre M, Cognard J, Tusseau M, et al. Haploinsufficiency in PTPN2 leads to early-onset systemic autoimmunity from Evans syndrome to lupus. *J Exp Med* 2024; **221**(9).
386. Song J, Lan J, Tang J, Luo N. PTPN2 in the Immunity and Tumor Immunotherapy: A Concise Review. *Int J Mol Sci* 2022; **23**(17).

387. Bussieres-Marmen S, Hutchins AP, Schirbel A, et al. Characterization of PTPN2 and its use as a biomarker. *Methods* 2014; **65**(2): 239-46.
388. Wang D, Wang W, Song M, Xie Y, Kuang W, Yang P. Regulation of protein phosphorylation by PTPN2 and its small-molecule inhibitors/degraders as a potential disease treatment strategy. *Eur J Med Chem* 2024; **277**: 116774.
389. Parlato M, Nian Q, Charbit-Henrion F, et al. Loss-of-Function Mutation in PTPN2 Causes Aberrant Activation of JAK Signaling Via STAT and Very Early Onset Intestinal Inflammation. *Gastroenterology* 2020; **159**(5): 1968-71 e4.
390. Awwad J, Souaid M, Yammine T, et al. A homozygous missense variant in PTPN2 with early-onset Crohn's disease, growth failure and dysmorphic features in an infant: a case report. *J Genet* 2023; **102**.
391. Thaventhiran JED, Lango Allen H, Burren OS, et al. Whole-genome sequencing of a sporadic primary immunodeficiency cohort. *Nature* 2020; **583**(7814): 90-5.
392. Heinonen KM, Nestel FP, Newell EW, et al. T-cell protein tyrosine phosphatase deletion results in progressive systemic inflammatory disease. *Blood* 2004; **103**(9): 3457-64.
393. Spalinger MR, Manzini R, Hering L, et al. PTPN2 Regulates Inflammasome Activation and Controls Onset of Intestinal Inflammation and Colon Cancer. *Cell Rep* 2018; **22**(7): 1835-48.
394. Svensson MN, Doody KM, Schmiedel BJ, et al. Reduced expression of phosphatase PTPN2 promotes pathogenic conversion of Tregs in autoimmunity. *J Clin Invest* 2019; **129**(3): 1193-210.
395. Todd JA, Walker NM, Cooper JD, et al. Robust associations of four new chromosome regions from genome-wide analyses of type 1 diabetes. *Nat Genet* 2007; **39**(7): 857-64.
396. Hitomi Y, Ueno K, Aiba Y, et al. A genome-wide association study identified PTPN2 as a population-specific susceptibility gene locus for primary biliary cholangitis. *Hepatology* 2024; **80**(4): 776-90.
397. Marcil V, Mack DR, Kumar V, et al. Association between the PTPN2 gene and Crohn's disease: dissection of potential causal variants. *Inflamm Bowel Dis* 2013; **19**(6): 1149-55.
398. Pike KA, Tremblay ML. TC-PTP and PTP1B: Regulating JAK-STAT signaling, controlling lymphoid malignancies. *Cytokine* 2016; **82**: 52-7.
399. Wiede F, Shields BJ, Chew SH, et al. T cell protein tyrosine phosphatase attenuates T cell signaling to maintain tolerance in mice. *J Clin Invest* 2011; **121**(12): 4758-74.
400. Pike KA, Hatzihristidis T, Bussieres-Marmen S, et al. TC-PTP regulates the IL-7 transcriptional response during murine early T cell development. *Sci Rep* 2017; **7**(1): 13275.
401. Wiede F, Dudakov JA, Lu KH, et al. PTPN2 regulates T cell lineage commitment and alphabeta versus gammadelta specification. *J Exp Med* 2017; **214**(9): 2733-58.
402. Wiede F, La Gruta NL, Tiganis T. PTPN2 attenuates T-cell lymphopenia-induced proliferation. *Nat Commun* 2014; **5**: 3073.
403. Flosbach M, Oberle SG, Scherer S, et al. PTPN2 Deficiency Enhances Programmed T Cell Expansion and Survival Capacity of Activated T Cells. *Cell Rep* 2020; **32**(4): 107957.
404. Spalinger MR, Kasper S, Chassard C, et al. PTPN2 controls differentiation of CD4(+) T cells and limits intestinal inflammation and intestinal dysbiosis. *Mucosal Immunol* 2015; **8**(4): 918-29.
405. Bothur E, Raifer H, Haftmann C, et al. Antigen receptor-mediated depletion of FOXP3 in induced regulatory T-lymphocytes via PTPN2 and FOXO1. *Nat Commun* 2015; **6**: 8576.
406. LaFleur MW, Nguyen TH, Coxe MA, et al. PTPN2 regulates the generation of exhausted CD8(+) T cell subpopulations and restrains tumor immunity. *Nat Immunol* 2019; **20**(10): 1335-47.
407. Wiede F, Lu KH, Du X, et al. PTPN2 phosphatase deletion in T cells promotes anti-tumour immunity and CAR T-cell efficacy in solid tumours. *EMBO J* 2020; **39**(2): e103637.
408. Martin-Granados C, Prescott AR, Le Sommer S, et al. A key role for PTP1B in dendritic cell maturation, migration, and T cell activation. *J Mol Cell Biol* 2015; **7**(6): 517-28.
409. Heinonen KM, Dube N, Bourdeau A, Lapp WS, Tremblay ML. Protein tyrosine phosphatase 1B negatively regulates macrophage development through CSF-1 signaling. *Proc Natl Acad Sci U S A* 2006; **103**(8): 2776-81.

410. Traves PG, Pardo V, Pimentel-Santillana M, et al. Pivotal role of protein tyrosine phosphatase 1B (PTP1B) in the macrophage response to pro-inflammatory and anti-inflammatory challenge. *Cell Death Dis* 2014; **5**(3): e1125.
411. Lu X, Malumbres R, Shields B, et al. PTP1B is a negative regulator of interleukin 4-induced STAT6 signaling. *Blood* 2008; **112**(10): 4098-108.
412. Morita M, Stamp G, Robins P, et al. Gene-targeted mice lacking the Trex1 (DNase III) 3'-->5' DNA exonuclease develop inflammatory myocarditis. *Mol Cell Biol* 2004; **24**(15): 6719-27.
413. Maelfait J, Bridgeman A, Benlahrech A, Cursi C, Rehwinkel J. Restriction by SAMHD1 Limits cGAS/STING-Dependent Innate and Adaptive Immune Responses to HIV-1. *Cell Rep* 2016; **16**(6): 1492-501.
414. Bustamante J, Boisson-Dupuis S, Abel L, Casanova JL. Mendelian susceptibility to mycobacterial disease: genetic, immunological, and clinical features of inborn errors of IFN-gamma immunity. *Semin Immunol* 2014; **26**(6): 454-70.
415. Sacco KA, Milner JD. Gene-environment interactions in primary atopic disorders. *Curr Opin Immunol* 2019; **60**: 148-55.
416. Pattanaik A, Bhandarkar BS, Lodha L, Marate S. SARS-CoV-2 and the nervous system: current perspectives. *Arch Virol* 2023; **168**(6): 171.
417. Haidar MA, Shakkour Z, Reslan MA, et al. SARS-CoV-2 involvement in central nervous system tissue damage. *Neural Regen Res* 2022; **17**(6): 1228-39.
418. Salzer U, Grimbacher B. TACI deficiency - a complex system out of balance. *Curr Opin Immunol* 2021; **71**: 81-8.
419. Del Pino-Molina L, Rodriguez-Ubreva J, Torres Canizales J, et al. Impaired CpG Demethylation in Common Variable Immunodeficiency Associates With B Cell Phenotype and Proliferation Rate. *Front Immunol* 2019; **10**: 878.
420. Rodriguez-Cortez VC, Del Pino-Molina L, Rodriguez-Ubreva J, et al. Monozygotic twins discordant for common variable immunodeficiency reveal impaired DNA demethylation during naive-to-memory B-cell transition. *Nat Commun* 2015; **6**: 7335.
421. Jordan W, 3rd, Rieder LE, Larschan E. Diverse Genome Topologies Characterize Dosage Compensation across Species. *Trends Genet* 2019; **35**(4): 308-15.
422. Ahluwalia JK, Hariharan M, Bargaje R, Pillai B, Brahmachari V. Incomplete penetrance and variable expressivity: is there a microRNA connection? *Bioessays* 2009; **31**(9): 981-92.
423. Luo J, Zheng M, Jiang B, et al. Antidiabetic activity in vitro and in vivo of BDB, a selective inhibitor of protein tyrosine phosphatase 1B, from Rhodomela confervoides. *Br J Pharmacol* 2020; **177**(19): 4464-80.
424. Qian S, Zhang M, He Y, Wang W, Liu S. Recent advances in the development of protein tyrosine phosphatase 1B inhibitors for Type 2 diabetes. *Future Med Chem* 2016; **8**(11): 1239-58.
425. Krishnan N, Koveal D, Miller DH, et al. Targeting the disordered C terminus of PTP1B with an allosteric inhibitor. *Nat Chem Biol* 2014; **10**(7): 558-66.
426. Ito M, Fukuda S, Sakata S, Morinaga H, Ohta T. Pharmacological effects of JTT-551, a novel protein tyrosine phosphatase 1B inhibitor, in diet-induced obesity mice. *J Diabetes Res* 2014; **2014**: 680348.
427. Sharma S, Skaist Mehlman T, Sagabala RS, Boivin B, Keedy DA. High-resolution double vision of the allosteric phosphatase PTP1B. *Acta Crystallogr F Struct Biol Commun* 2024; **80**(Pt 1): 1-12.
428. Pettersen EF, Goddard TD, Huang CC, et al. UCSF ChimeraX: Structure visualization for researchers, educators, and developers. *Protein Sci* 2021; **30**(1): 70-82.
429. Guerois R, Nielsen JE, Serrano L. Predicting changes in the stability of proteins and protein complexes: a study of more than 1000 mutations. *J Mol Biol* 2002; **320**(2): 369-87.
430. Subramanian A, Tamayo P, Mootha VK, et al. Gene set enrichment analysis: a knowledge-based approach for interpreting genome-wide expression profiles. *Proc Natl Acad Sci U S A* 2005; **102**(43): 15545-50.

431. Liberzon A, Birger C, Thorvaldsdottir H, Ghandi M, Mesirov JP, Tamayo P. The Molecular Signatures Database (MSigDB) hallmark gene set collection. *Cell Syst* 2015; **1**(6): 417-25.